Pre-clinical treatment of prostate cancer using targeted oncolytic viral therapy

by

Maryam Moussavi

A THESIS SUBMITTED IN PARTIAL FULFILLMENT OF THE REQUIREMENTS FOR THE DEGREE OF

DOCTOR OF PHILOSOPHY

in

THE FACULTY OF MEDICINE

(Experimental Medicine)

THE UNIVERSITY OF BRITISH COLUMBIA

(Vancouver)

April 2011

Abstract

Prostate cancer is the most prevalent non-skin malignancy and the second leading cause of cancer-related mortality in North American men. Current therapies for patients with locally advanced or metastatic prostate cancer are largely palliative and non-curative. Oncolytic viral-therapy provides a new approach to efficiently target and kill cancer cells while sparing normal cells. Vesicular Stomatitis Virus (VSV) is an oncolytic virus, which can infect and kill cells that have defects in their cellular anti-viral interferon (IFN) response. In this study, enhanced IFN-sensitive VSV(AV3) strain was intra-prostatically injected into two different transgenic mouse models ($PTEN^{-/-}$ and TRAMP) and monitored for infectivity, apoptosis, and innate-immune response. Viral spread and load were monitored by bioluminescence and plaque analysis over 96h time period. It was determined that viral spread begins as early as 3-6h post-viral administration and persisted >72h in prostates of tumour-bearing mice compared to control. Plaque assay provided a similar pattern, with much higher concentrations of replicating virus in prostates and metastatic lymph nodes of tumour-bearing mice compared to control. TUNEL staining of paraffin-embedded prostates and enlarged lymph nodes demonstrated VSV(AV3)'s ability to selectively infect and kill malignant cells while sparing normal cells. This tumour-selective cell death was attributed to a disrupted IFN response in the prostates of tumour-bearing transgenic mice. However, evidence of activated IFN response in the enlarged lymph nodes was observed. To augment the safety of future oncolytic viral-therapies alternate targeting strategy based on tumour-specific over-expression of eIF4E was employed. Three different length of 5'UTRs, which require abundant levels of eIF4E for translation, derived from either fibroblast growth factor-2 (FGF-2) or ornithine decarboxylase were inserted downstream of ubiquitin promoter in a lentiviral-plasmid. Expression of each plasmid was tested *in vitro* using prostate cancer and control cell lines, and *in vivo* using $PTEN^{-/-}$ and control mice. Immunofluorescence and Western blot analysis determined FGF-2-5'UTR to be most sensitive to eIF4E levels. Results suggested that control of locally advanced and metastatic prostate cancer may be achievable through intra-prostatic injection and amplification of a safe oncolytic virus, such as VSV(AV3). Also, judicious selection of a complex 5'UTR can enhance viral-based targeted-therapies for prostate cancer.

Preface

A version of **Chapter 2** has been published in journal of Cancer research. **Maryam Moussavi**, Fazl,i L., Tearle, H., Guo, Y., Cox, M.E., Bell, J.C., Ong, C., Jia, W., Rennie, P.S.. Oncolysis of prostate cancers induced by vesicular stomatitis virus in PTEN knockout mice. Cancer Research. 2010 Feb 15;70(4):1367-76. The experiments were designed, conducted and analyzed by myself, Maryam Moussavi, and my supervisor Dr. Paul S. Rennie. Drs. W. Jia and C. Ong are my PhD committee members and were also involved in fine tuning of experimental design. Dr. Ladan Fazli is the resident pathologist at the prostate center, she has scored each pathological slide. MPPK-1 cell lines were a gift from Drs. M. Cox and Y. Guo. Mr. H. Tearle was involved in animal breading and teaching of animal surgery and techniques. Dr. J.C. Bell has provided material (such as antibodies and virus) as our collaborator.

A version of **Chapter 3** will be submitted. **Maryam Moussavi**, Tearle, H., Fazli, L., Bell, J.C., Jia, W., Rennie, P.S. Detection of metastatic lesions in the transgenic adenocarcinoma of mouse prostate (TRAMP) model using Vesicular Stomatitis Virus. The experiments were designed, conducted and analyzed by myself, Maryam Moussavi, and my supervisor Dr. Paul S. Rennie. Dr. W. Jia is my PhD committee member and has been involved in fine tuning of experimental design. Dr.L. Fazli as our resident pathologist has scored the pathological slides. Mr. H. Tearle was involved in animal breading and helping in surgical removal of lymph-nodes from the mice.

A version of **Chapter 4** has been submitted and is currently under consideration. **Maryam Moussavi,** Moshgabadi, N., Fazli, L., Leblanc, E., Jia,W., and Rennie, P.S. Viral targeting of prostate cancer in human prostatic cells and prostate-specific $PTEN^{-/-}$ transgenic mice using fibroblast growth factor and ornithine decarboxylase 5'UTRs. The experiments were designed, conducted and analyzed by myself, Maryam Moussavi, and my supervisor Dr. Paul S. Rennie. Dr. W. Jia is my PhD committee member and has been involved in fine tuning of

experimental design. Dr.L. Fazli as our resident pathologist has scored the pathological slides. Ms. N. Moshgabadi, helped with preparation of Western blot analysis. Dr. E. Leblanc helped in manuscript revision.

Please check the first pages of these chapters to see footnotes with similar information.

Table of Contents

List of Tables

List of Figures

List of Abbreviations

4EBP	eIF4E Binding Protein
5-FC	F-Fluorocytosine
5'UTR	5'Untranslated Region
ACTH	Adernocorticotropic Hormone
ADT	Androgen-Deprivation Therapy
Akt/PKB	Serine/Threonine Protein Kinase
AP	Anterior Prostate
AR	Androgen Receptor
ARE	Androgen-Responsive Element
ATP	Adenosine Triphosphate
AUA	American Urologic Association
BPH	Benign Prostatic Hyperplasia
CD4/8	Cluster of Differentiation 5/8
CK	Cytokeratine
CRH	Corticotropin Releasing Hormone
CRPC	Castration-Resistant Prostate Cancer
CYP17A1	17α-hydroxylase/17,20 lyase/17,20 desmolase
CZ	Central Zone
DHEA	Dehydroepiandrosterone
DHT	Dihydrotestostrone
DLP	Dorso-Lateral Prostate
DNA	Deoxyribonucleic acid
DP	Dorsal Prostate
DRE	Digital Rectal Exam
EBRT	External Beam Radiation Therapy
eIF4A	Initiation Factor 4A
eIF4E	Initiation Factor 4E
eIF4G	Initiation Factor 4G
ERG	ETS-Regulated Gene

ERK	Extracellular-signal-Regulated Kinases
ETS	E-Twenty six
FGF-2	Fibroblast Growth Factor-2
FSH	Follicle Stimulating Hormone
GCV	Ganciclovir
gD	Glycoprotein D
GnRH	Gonadotropin Releasing Hormone
H&E	Haematoxylin and Eosin
HDAC	Histone Deacetylases
Her2/neu	Human Epidermal Growth factor Receptor 2
HPC1	Hereditary Prostate Cancer gene 1
HSP	Heat Shock Protein
HSV-1	Herpes Simplex Virus 1
ICP	Infected Cell Protein
IFN	Interferon
IFNR1	Interferon Receptor type 1
IRF	Interferon Response Factor
JNK	c-Jun N-terminal kinase
LHRH	Leutenizing Hormone Releasing Hormone
LP	Lateral Prostate
MAPK	Mitogen-Activated Protein Kinase
Met-51	Methionine 51
MMP	Matrix Metalloproteinase
mRNA	messenger RNA
mTOR	Mammalian Target of Rapamycin
ODC	Ornithine Decarboxylase
PAP	Prostatic Acid Phosphatase
PCR	Polymerase Chain Reaction
PDK1	3-Phosphoinositide-Dependent Kinase 1
Pfu	Plaque Forming Unit

PI3 Kinase	Phosphoinositide 3-kinase
PIN	Intraepithelial neoplasia
PIP3	Phsphatidylinositol-3,4,5-triphosphate
PKR	Protein Kinase R or Protein Kinase RNA-activated
PSA	Prostate Specific Androgen
PTEN	Phosphatase and Tensin homolog
PZ	Peripheral Zone
qPCR	Quantitative real-time PCR
Ras	Rat Sarcoma
RNA	Ribonucleic Acid
ss	Single-Stranded
SV40	Simian Virus 40
TK	Thymidine Kinase
TNM	Tumour Lymph node and metastasis classification
TRAMP	Transgenic Adenocarcinoma of the Mouse Prostate
TRUS	Transrectal Ultrasound
TSC1/2	Tuberous Sclerosis protein 1/2
TUNEL	Terminal deoxynucleotidyl transferase dUTP Nick End Labelling
TURP	Transurethral Resection of the Prostate
TZ	Transitional Zone
UK	United Kingdom
UVI	Ultra Violet Inactivated
VEGF	Vesicular Endothelial Growth Factor
VP	Ventral Prostate
VSV	Vesicular Stomatitis Virus
VSV G-protein	Glycoprotein D
VSV L and P proteins	Polymerase Proteins
VSV M-protein	Matrix Protein
VSV N-protein	Nucleocapsid Protein

Acknowledgements

I offer my gratitude to the faculty, staff and my fellow students at the Prostate Centre and UBC's department of Experimental Medicine, who have inspired me to continue my work in this field. I owe particular thanks to my mentor, and thesis supervisor Dr. Paul S. Rennie, for giving me the opportunity to explore the world of oncolytic viral therapy. I would like to thank him for his guidance and constant encouragement of my thesis projects. I especially wanted to thank him for his continued support and his encouragement of my research and life pursuits. I thank Dr. William Jia and Dr. Christopher Ong, my supervisory committee members, for lending their expertise in development of this thesis. I particularly wanted to thank them for their patience to my never-ending questions.

I thank the people working at the prostate center, in particular the Rennie lab (Latif Wafa, Eric Leblanc, Helen Cheng, and Fariba Ghaedi) for their support and advice during completion of this thesis. I would particularly like to thank Dr. Latif Wafa, for his never ending support, his detailed reading and critiquing of this thesis and the papers which have resulted from this thesis, all during his own medical school training, have been priceless. In short his friendship is truly appreciated. I would like to thank Dr. Eric Leblanc, for his help on preparation of papers. I would also like to thank the following people for their expertise and help and their direct involvement in helping me generate this thesis: Dr. Ladan Fazli, Ms. Estelle Li, Ms. Noushin Moshgabadi, and Mr. Howard Tearle.

I would also like to acknowledge that funding for this research was provided by the Terry Fox Foundation, the National Cancer Institute of Canada (Canadian Cancer Society Research Institute) and the Prostate Cancer Research Foundation of Canada. A pre-doctoral training award for prostate cancer research was provided by the U.S. Department of Defence.

Most importantly I would like to thank my family. I specially would like to thank my parents, Ezzat Tehrani and Hassan Moussavi, and my brothers, Maysam and Pedram

Moussavi, for their constant emotional support, for believing in me, encouraging me, and teaching me to never give up. I would also like to thank my new parents, Cindy and Bob McGlashan, for their support and listening to my stories. Last but not least, I would like to thank my loving husband, Brent, whose full unwavering emotional support has enabled me to conduct and complete this thesis.

To my loving husband and best friend

Brent I. McGlashan

1. Introduction

1.1 Prostate gland

1.1.1 Prostate structure and regulation

The prostate is the largest male accessory gland and plays an important role in male reproduction. Typically it weighs a few grams at birth and grows to approximately 20 g by age 20 (1). The prostate gland requires stimulation by male sex hormones (androgens) and growth factors for its growth and development (1-4). The prostate is an exocrine gland, which after puberty produces various enzymes and proteins, such as prostate specific antigen (PSA) and prostatic acid phosphatase (PAP) into seminal fluid. Within the prostate gland testosterone is converted to a more potent form, dihydrotestostrone (DHT), which controls glandular growth (1).

Anatomically, the prostate surrounds the urethra, sitting inferior to the bladder, posterior to pubic symphysis and anterior to the rectum. The prostate is surrounded by a thin fibro-elastic tissue layer, which gives rise to septa that extends inwards and subdivides the prostate into five lobes: anterior, posterior, medial and two lateral lobes.

Histologically, the prostate can be divided into two major zones that have distinct pathological features (5). The central zone (CZ) encompasses approximately 25% of the normal prostate gland and surrounds the ejaculatory ducts (6). The peripheral zone (PZ) comprises of about 70% of the normal prostate tissue. The PZ is located at the sub-capsular portion of the posterior aspect of the prostate and surrounds the urethra. The remaining 5% of the prostate tissues is comprised of the transitional zone (TZ) and the anterior fibro-muscular zone otherwise known as the prostate stroma (4). The TZ surrounds the proximal urethra and is capable of growing throughout life (5). The stroma is composed of muscle and fibrous tissue.

1.1.2 Cellular components of the prostate

The prostate gland is comprised of both an epithelial component, in the form of epithelial cells lining multiple secretory acini, and a stromal element that consists of smooth muscle cells,

fibroblasts and endothelial cells, which surround the secretory acini. The epithelial element is separated from the stroma *via* basement membrane. In addition, these granular acini drain into epithelial ducts and eventually into the prostatic urethra (7).

Locally, the fibromuscular stroma plays an important role by controlling the epithelial microenvironment, since nutrients such as, androgens and gases, from blood have to pass through it before reaching the epithelial cellular component (8). Also, through this mass musculature the prostate participates in both the control of urine output from the bladder and seminal fluid during ejaculation (1). The epithelial element of the prostate consists of basal, luminal, and neuroendocrine cells. The basal cells, which sit beneath the luminal cells are the proliferative component of the prostate epithelium and thus responsible for prostate self-renewal. They are androgen-independent and can be characterized by the expression of cytokeratin (CK) 5 and 14 (9, 10). In contrast, luminal cells are mature epithelial cells that require the presence of androgens for survival and can be characterized through expression of CK 8 and CK 18 (9, 10). The primary function of luminal cells is to produce PSA and PAP, which are key contributors of the prostatic secretion to seminal fluid (11, 12). Finally, neuroendocrine cells are terminally differentiated androgen-independent prostate cells that are thought to be involved in the regulation of growth and differentiation of the prostate (13). These cells are typically scattered throughout both the basal and luminal layers. They are most often characterized by the expression of chromogranin A and serotonin (13, 14). Based on their morphology, two types of prostatic neuroendocrine cells have been described; the “open” cell type has long processes that stretch through both basal and luminal layers in order to reach the lumen, and the “closed” cell types do not have luminal extensions. Both open and closed cells have irregular dendritic processes which extend through the neighbouring cells (15, 16). **Figure 1.1** illustrates the cellular compartments of the prostate gland.

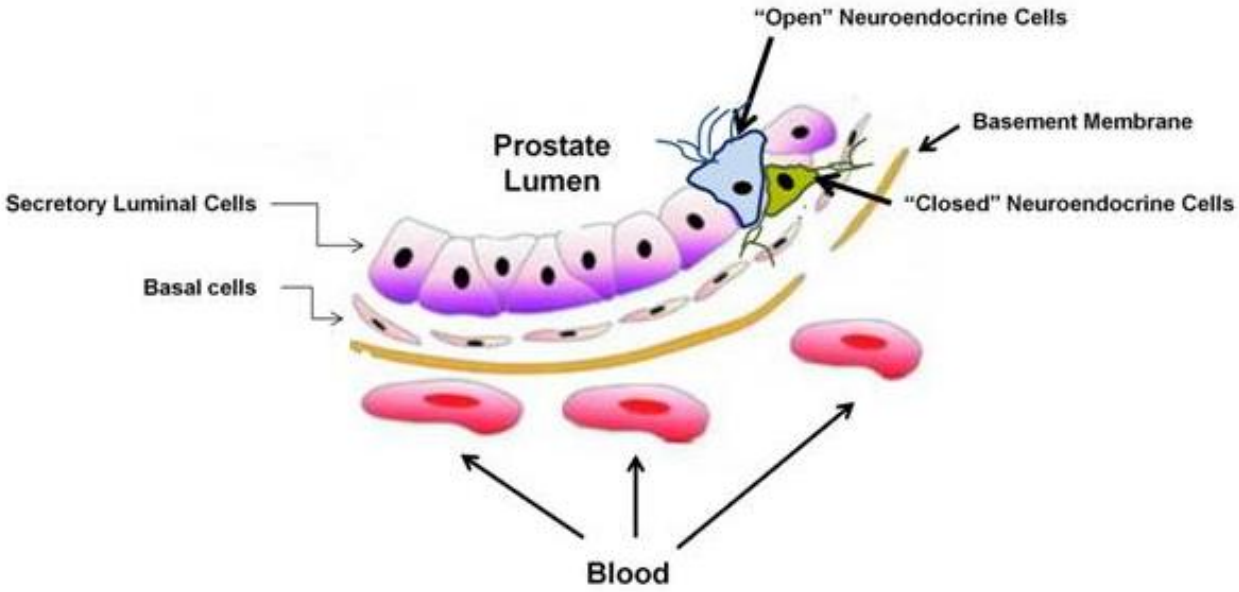

Figure 1.1 Cellular components of the prostate gland.

The prostate epithelial compartment consists of basal, luminal and neuroendocrine cells. The epithelial layer is separated from the stroma component by a basement membrane.

Modified from http://endotext.com/male/index.htm.

1.1.3 Hormonal regulation of the prostate

The prostate gland is one of the target organs of androgens. Androgen signalling is regulated through the hypothalamus-pituitary-gonadal hormone axis (17). This pathway begins in the hypothalamus with the production and excretion of two hormones; 1) Leutenizing Hormone Releasing Hormone (LHRH), otherwise known as the Gonadotropin Releasing Hormone (GnRH), and 2) Corticotropin Releasing Hormone (CRH). GnRH and CRH traveling through portal blood system reach the anterior pituitary, where GnRH stimulates the release of both lutenizing hormone (LH) and follicle stimulating hormone (FSH), while CRH leads to production and release of adrenocorticotropic hormone (ACTH) into the blood stream (18). Circulating LH target the Leydig cells in the testes and stimulate production of testosterone. The testes are responsible for production of approximately 95% of circulating testosterone. Circulating FSH targets Sertoli cells in the testes leading to spermatogenesis. Similarly, circulating ACTH targets and stimulates the adrenal gland which leads to production of androstenedione and dehydroepiandrosterone (DHEA).These androgens travel to the prostate. The prostate is capable of using both of these steroids and coverts them into highly active androgens such as dihydrotestosterone, DHT (19, 20). Serum testosterone regulates the hormonal axis through a feedback loop at the hypothalamus and pituitary axis **(Figure 1.2)**. Ablation of the hypothalamus-pituitary-gonadal axis has been the main therapeutic approach for prostate cancer patients, which will be discussed further in section 1.3.4.

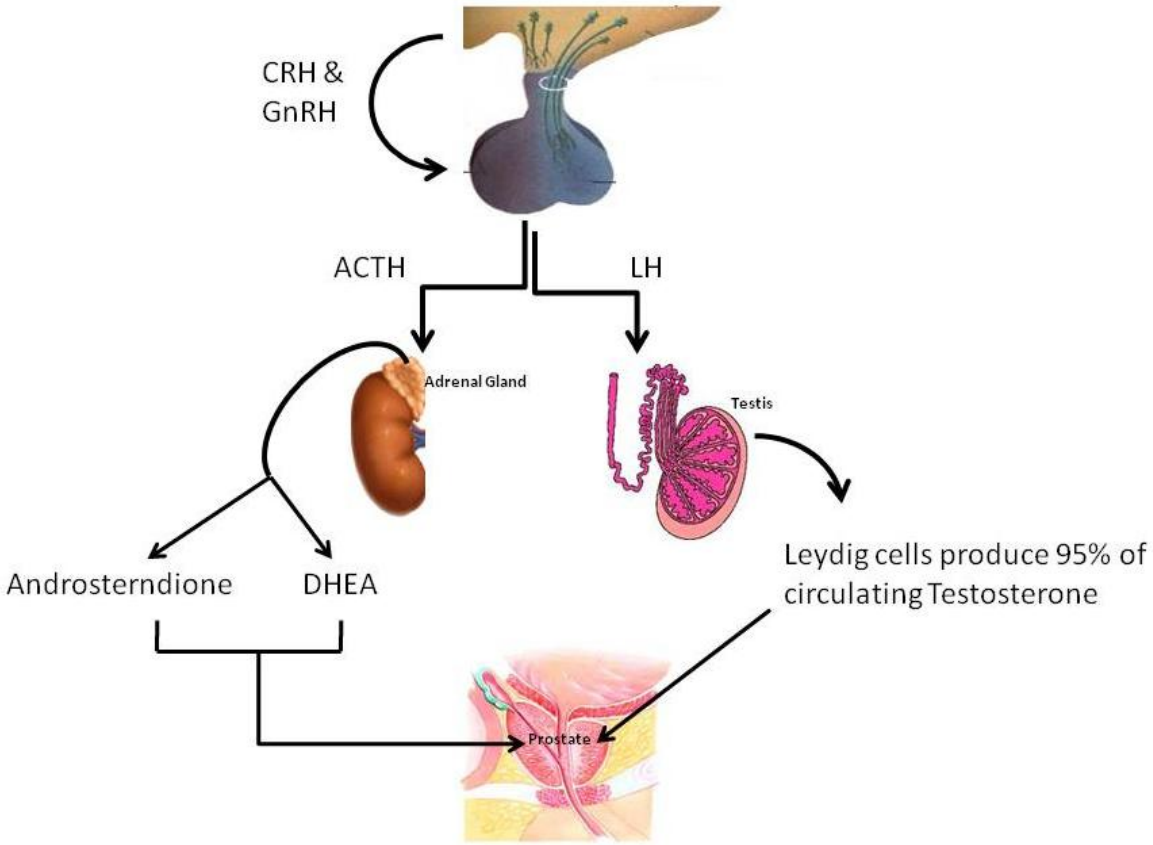

Figure 1.2 Hypothalamus-Pituitary-Gonadal hormonal Axis

Hormones produced from the organs involved in the hypothalamus-pituitary-gonadal axis, along with adrenal androgens, contribute to androgen biosynthesis and ultimately prostate growth and development.

1.2 Prostate disorders

Diseases of the prostate gland can include prostatitis, benign prostatic hyperplasia (BPH), and prostate cancer. Prostatitis is the inflammation of the prostate that may be due to bacterial infection, typically treated through antibiotics, or chronic prostatitis which can occur in the absence of bacterial infection. The cause of non-bacterial chronic prostatitis is not currently known. Benign prostatic hyperplasia is an age-related progressive neoplastic condition, which if left untreated may lead to stasis of bacteria in the bladder that can cause bladder, kidney, or urinary tract infections. Previous studies have demonstrated that testosterone levels are very high in the blood entering the prostate, which stimulate proliferation and enlargement of the prostate gland (21, 22). In patients suffering from BPH, it has been shown that the one-way valves in the spermatic veins are destroyed over time, thus causing leakage of high levels of testosterone into the prostate tissues (23). Current treatment for BPH ranges from life-style and diet changes, to drugs, such as α1-androgenic receptor antagonists (e.g. doxazosis) and 5α-reductase blockers (e.g. finasteride), to surgical intervention, such as transurethral resection of the prostate (TURP). TURP is currently the gold standard of prostate procedures for patients with BPH. It involves surgical removal of parts of the enlarged prostate through the urethra. In cases where TURP cannot be used (e.g. excessive prostate enlargement), open surgery is performed. In recent years, laser surgery has been used as an alternative option. Laser surgery is similar to TURP except lasers are used to vaporize obstructing prostate tissue (24). The third common prostate disease is prostate cancer, which is discussed in detail in section 1.3.

1.3 Prostate cancer

Prostate cancer is the second leading cause of cancer related mortality in North American men (25). In Canada, it is estimated that 24,600 men will be diagnosed with prostate cancer in 2010 and approximately 4,300 will die from this disease (26). Patients with localized disease are often treated by surgery or radiation therapy, though almost half of these patients

are not cured (27). Prostate cancer is a multistep disease that progresses from benign prostatic epithelium to formation of prostatic intraepithelial neoplasia (PIN), to locally invasive disease and ultimately metastatic disease (28-31). The majority of prostate cancer related mortality is due to advanced and metastatic disease. Although most patients with advanced metastatic disease initially respond to androgen-ablation therapies, over time their tumours become unresponsive and progress to castration-resistant prostate cancer (CRPC), resulting in a typical median life expectancy of ~18 months (32-35). The high incidence of prostate cancer in the North American population and its ability to evolve and become resistant to treatment highlights the urgent need to develop alternative therapeutic options.

1.3.1 Prostate cancer epidemiology

Prostate cancer rates vary across the globe, with studies showing it to be most prevalent in the Western society. Risk factors such as genetic background, age, and diet have been implicated in the development and progression of prostate cancer (36, 37). Studies have demonstrated that genetic background contributes to prostate cancer development. Men with one first degree relative with prostate cancer have a two-fold increase chance of developing prostate cancer (38, 39). To date there are a variety of genes that have been implicated in prostate cancer development and progression. An example of hereditary prostate cancer is a rare autosomal dominant high-risk gene, known as RNaseL, which is part of the Hereditary Prostate cancer gene 1 (HPC1) family (40). RNaseL is an enzyme which plays an important role in the interferon (IFN) pathway (41). Also, genetic mutations of the androgen and the vitamin D receptors have been associated with prostate cancer development (42). Recent discoveries have demonstrated involvement of fusion genes, such TMPRSS2-ERG in the propagation of prostate cancer (43). Involvement of androgens in regulation on TMPRSS2 mediated over-expression of ERG (an E-twenty six (ETS)-regulated gene) is seen in approximately 90% of prostate cancer patients and in 41% of lymph node metastatic cancers (43-45). Other genetic factors such as loss of cancer suppressor genes are often seen in early stages of prostate

carcinogenesis. PTEN alterations or deletions have been observed in approximately 79% of CRPC samples (46, 47). Other tumour suppressors such as P53 have been shown to be mutated specifically in late-stage prostate cancers (48).

Epidemiological investigations support the role of diet and lifestyle factors as contributors to clinical presentation of prostate cancer (49, 50). Studies have demonstrated that prevalence of prostate cancer in Asian men living in Asia is very low. However, Asian immigrants in North America have a higher incidence of prostate cancer. This marked disparity between geographical incidences of prostate cancer highlights the importance of environmental factors (51). Possible protective roles of dietary Vitamin B6 (52), selenium, vitamin E (53), lycopene (54) and soy foods (55-57) have been reported. However, there are conflicting studies on which dietary supplements have preventative effects on prostate cancer development. For example, one study showed that diets rich in crucifers (vegetables that include broccoli) reduced cancer incidence, while four other studies revealed that crucifers have no cancer preventative properties (39, 58). In another set of trials conducted by the National Prevention of Cancer, it was demonstrated that men who took selenium supplements daily reduced the probability of developing prostate cancer by half (59). In a disappointing follow-up trial, SELECT (Selenium and Vitamin E Cancer Prevention Trial), lack of any benefits of combination of selenium and vitamin E supplementation were reported (60). These results demonstrated that further clinical analysis on the effects of nutrient supplements and prostate cancer are required.

1.3.2 Prostate cancer screening and diagnosis

Approximately 70% of early stage prostate cancer is not detected (61). Typically early stage prostate adenocarcinomas are asymptomatic because malignant cells arise in the prostate's peripheral zone, furthest from urethra and bladder. As the cancer progresses, it invades into the urethra and the bladder neck, causing blockage of the urinary tract leading to urinary symptoms such as dysuria. To date, early stage prostate cancer screening relies heavily on two clinical examinations; the digital rectal exam (DRE), and a blood PSA test (61). DRE is typically

used to assess the shape, symmetry and nodulation of the prostate. Although there are reports that indicate 14-30% of early stage prostate cancers have been detected using DRE, the examination itself depends on the experience of the examiner, and thus has a low reproducibility rate (61). Therefore, the DRE is normally used in conjunction with blood PSA testing.

PSA is an androgen-regulated serum protease which is produced by the prostate epithelial cells (62). Studies have determined that serum PSA levels increase and decrease proportionally with changes in tumour burden (**Figure 1.3**) (63). Although PSA elevation is a good indicator of presence of prostate cancer, PSA increase has also been correlated with other prostate conditions such as prostate enlargement and BPH (61). Traditionally, if serum PSA levels increase above the acceptable 4 ng/ml range, prostate biopsies are performed. However, it has been found that measurement of total blood PSA lacks sensitivity and specificity, thus resulting in high numbers of either false negative or false positive results (64, 65). Therefore variations of the PSA test have evolved including looking at PSA density, velocity, and percentage of free unbound PSA compared to total PSA. PSA density test, measures the ratio of PSA level to the volume the prostate, which is measured through transrectal ultrasound (TRUS). PSA velocity looks at the rate of increase of PSA over time. Therefore, it is now accepted that serum PSA testing should only be used as part of a risk assessment. Regardless of the inconsistencies in PSA testing, the combination of DRE and PSA screening have dramatically increased detection rates of early stage organ confined prostate cancer (64, 65).

Currently the Gleason grading system for prostatic carcinoma is the best histological standard for diagnosis and prognosis of prostate cancer patients. The Gleason score was first described by Gleason and Mellinger in 1974 (66). The Gleason grading system is based on the staining of glandular architecture of the two most prevalent histological sections of prostate

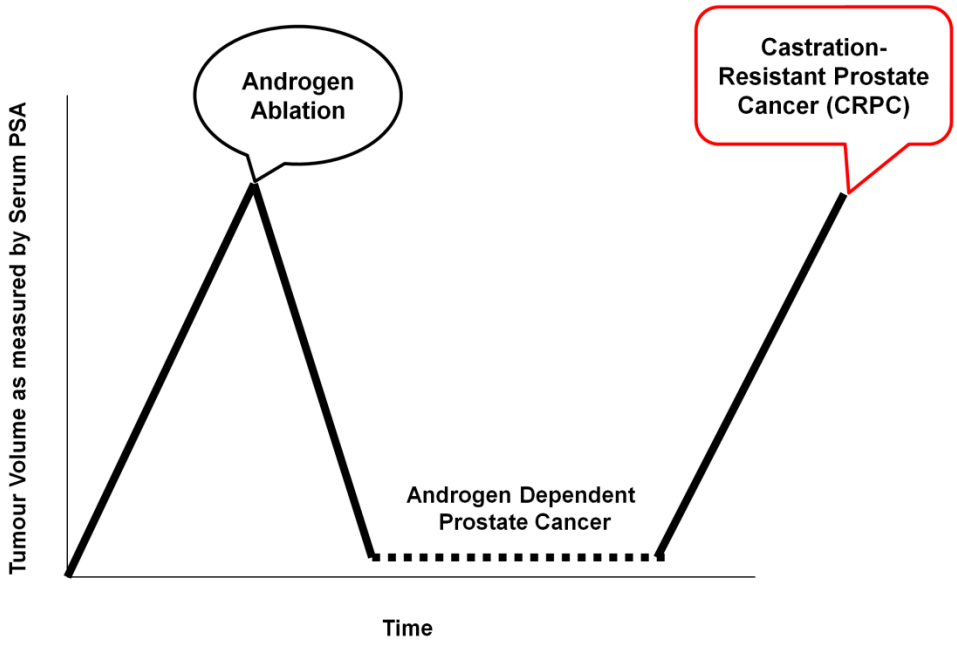

Figure 1.3 Progression of prostate cancer from Androgen dependent to Castration-Resistant Prostate cancer

Prostate growth is monitored through PSA secretion. Elevated PSA levels directly correlate with increase in prostate tumour burden. Upon introduction of androgen-ablation therapy the PSA levels in patients drastically drops and the tumour regresses due androgen dependency of the prostate adenocarcinoma cells. However, a portion of the tumour cells survive through bypassing their need for external androgens and therefore transition to castration-resistant prostate cancer (CRPC) disease.

tumours. Gleason grade uses a scoring system of 1 to 5, which is assigned to the two most predominant haematoxylin and eosin (H&E) stained patterns. The sum of these two grades is referred to as the Gleason Score which ranges from 2 to 10. A low Gleason Score of 2 to 4 is typically given to well-differentiated tumours, and as the tumours become more moderately differentiated they are scored between 5 to 7. A high Gleason score of 8 to 10 is reserved for poorly differentiated tumours, wherein the glandular structure of prostate is no longer recognizable and is usually equated to poor clinical prognosis for the patients, along with a greater risk of metastatic disease.

The TNM (tumour, lymph node, and metastasis) classification system is another method used to determine the stage of prostate cancer. Where T describes the size of the tumour and whether it has invaded nearby tissue, N describes the involvement of regional lymph nodes, and M describes spread of cancer to distant regions. A primary tumour is often evaluated through clinical examination, imaging, endoscopy, biopsy, and biochemical tests. Lymph node involvement is based on clinical examination and imaging. Finally, the M designation is based on clinical examination, imaging, skeletal studies, and biochemical testes to detect metastatic lesions (67).

1.3.3 Androgen receptor and its involvement in prostate cancer development

The androgen receptor (AR) is located on the X chromosome q11-12. AR is a 110 kilodalton (kDa) nuclear receptor protein that upon binding to androgens such as testosterone or DHT, homodimerizes and trans-locates to the nucleus (68). Once in the nucleus, AR binds to the androgen-responsive elements (ARE), and mediates transcription of target genes that modulate growth and differentiation of prostatic epithelial cells. AR signalling is crucial for prostate growth and development **(Figure 1.4)**. Mice with mutations in the AR harbour genetic defects that lead to poor development of the prostate or prostate cancer (69, 70). The prostate's dependency on AR for its function is evident in the progression of prostate cancer. This was highlighted in the Huggins and Hodges study, which demonstrated that prostate cancer

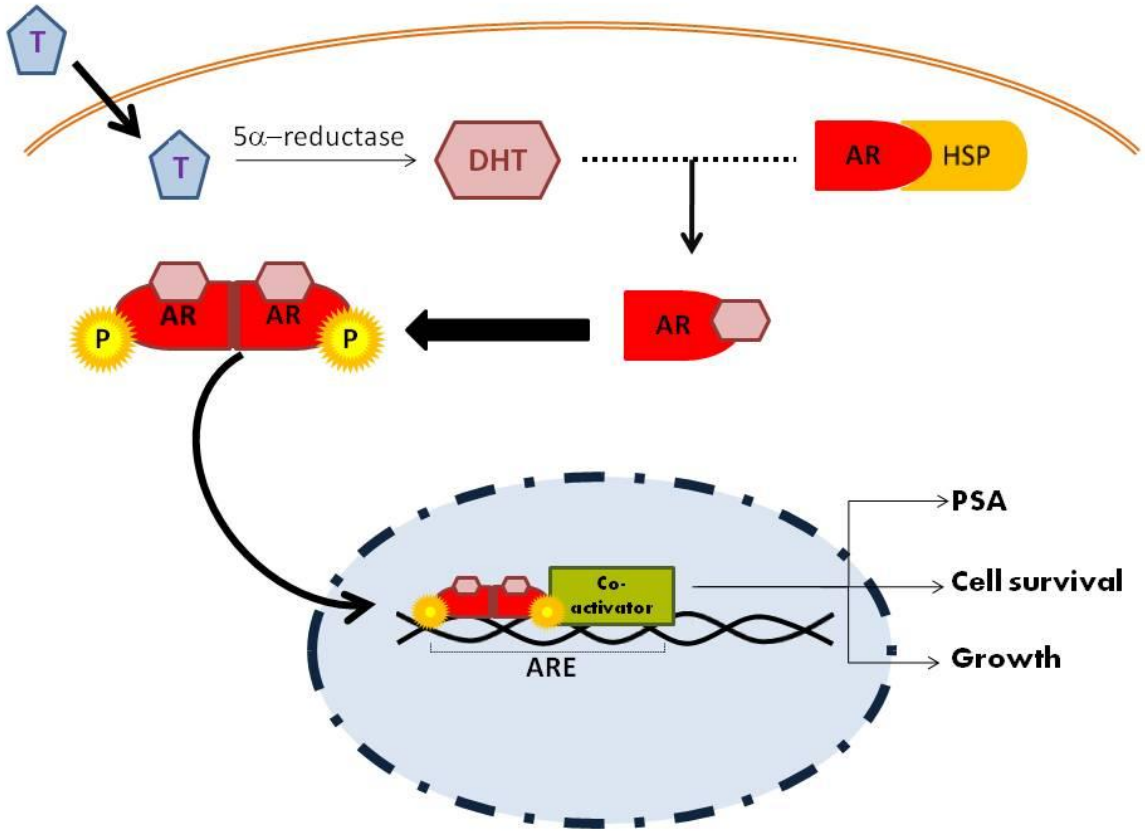

Figure 1.4 Androgen receptor signalling

Upon entering a prostate luminal cell, 5-α-reductase converts testosterone (T) to dihydrotestostrerone (DHT). Androgen receptor (AR) has a high affinity for DHT. DHT activates the AR by binding to its ligand binding domain. AR is released from the heat shock protein (HSP), chaperone proteins that sequester AR in the cytoplasm. The DHT bound AR, undergoes a series of transformations such as phosphorylation (P) and homodimerization which enable AR to translocation to the nucleus. Once in the nucleus, the dimerized AR binds to the DNA at the Androgen Response Element (ARE) sequence, and along with assistance of co-activators it leads to transcription of various genes such as PSA.

Modified from Feldman and Feldman (2001) (71).

regressed in patients that had undergone orchiectomy (72-74). Although hormone-ablation therapy is the gold standard for treatment of advanced and metastatic prostate cancer, it has been shown that tumour regression in most cases is temporary with some tumour cells transitioning to become androgen-independent and thus resistant to therapy. An increase in serum PSA is observed in prostate cancer as the disease moves towards CRPC **(Figure 1.3)**. Numerous studies have demonstrated that as the disease progresses towards CRPC, the AR signalling pathway is still active in the absence of androgens. Thus, new strategies for targeting the AR signalling pathway as a treatment option of CRPC are currently being studied.

1.3.4 Current therapies

There are a variety of treatment options available for patients with localized prostate cancer, including active surveillance, radical prostatectomy, radiation therapy, and cryotherapy (75). This variety of treatment options often provides a challenge for choosing the best treatment for the newly diagnosed patient. Active surveillance and watchful waiting for localized disease is growing in popularity as it lacks active intervention. Active surveillance typically involves periodic follow-up examination of blood PSA levels, repeated biopsies, and is prescribed for patients who either have a life expectancy of less than 10 years, or for healthy men of 65 years with both low tumour volume and low grade prostate cancer. The main concern and challenge with active surveillance treatment is insufficient sampling and inadequate mapping of the cancer volume present (75, 76).

Radical prostatectomy is another option available to patients with confined prostate cancer. The main advantage of radical prostatectomy over other treatments is the precise pathologic staging of the cancer. Roughly a third of patients undergoing prostatectomy discover a significant upgrade of their Gleason score. Prostatectomy also has the added benefit of an unambiguous interpretation of post-operative PSA levels (PSA ≤ 0.2 ng/ml) (77, 78). However, the main limitations of radical prostatectomy are the post-operative complications, such as

incontinence (up to 20%), erectile dysfunction (up to 50%), bladder neck contractures (up to 3%), and in rare cases rectal injuries (75, 76).

The field of radiation therapy is constantly improving and undergoing optimizations for delivery to localized prostate tumours. Radiation therapy is typically administered either through external beam radiation therapy (EBRT), interstitial brachytherapy or as a combination of the two. In EBRT, an external linear accelerator is used to produce high-energy x-rays which are directed as a beam towards the prostate. There are various benefits reported with EBRT, such as long term cancer control and very low possibility of incontinence in comparison to other therapeutic options. Some of the main limitations to EBRT are; possibility of erectile dysfunction in up to 50% of patients during a 5-year period, no post-treatment staging information, and the radiation treatment is a daily procedure over a 6-8 week period, typically causing fatigue after each treatment. Additionally, between 5-10% of patients report bowl/rectal problems such as urgency, pain, diarrhea, or bleeding. In higher risk tumours, EBRT is typically combined with androgen-deprivation therapy (ADT); this combination of therapies for prostate cancer patients with advanced tumours has proven beneficial and is supported by data from multiple randomized clinical trials (79, 80). Another popular radiation therapy treatment is brachytherapy. Brachytherapy involves insertion of approximately 100 small seeds of radioactive material, such as palladium-103 or iodine-125, into the tumour. These seeds emit lower energy x-rays that travel a short distance. It is a convenient treatment, with minimal surgical risks and delivers high dose of radiation to the prostate itself and low dose to surrounding tissues. However, this type of radiotherapy is recommended for men with low grade prostate cancer and although the risk of exposure to others is considered low, patients are encouraged to take precautions when around children and pregnant women (75, 76, 81).

Although cryotherapy was first introduced in 1850's by Dr. James Arnot for treatment of surgical lesions, it wasn't until 1996 that it was recognized as a treatment for prostate cancer by the American Urologic Association (AUA) (82). In this method, under ultrasound guidance, metal

rods are inserted through the skin at the perineum into the prostate and then purified Argon gas is used to cool the rods to freeze the surrounding tissue at -186˚C. Cryotherapy has a 10-year biochemical disease-free rate which is superior to all other treatments including radical prostatectomy and radiation therapies. The main limitation of cryotherapy is in the number of available facilities that perform this type of therapy (75, 83).

Even though early stage prostate cancer is frequently curable through the above discussed methods of treatments, advanced, recurrent and metastatic disease have fewer curative treatment options with median life expectancy of less than 3 years (84, 85). The primary treatment for advanced prostate cancer is androgen-ablation therapy either by chemical castration using LHRH agonists or surgical castration. However, despite initial response to ADT, almost all patients advance to an androgen-independent or castration-resistant prostate cancer (CRPC), which is correlated with an increase in blood PSA levels (Figure 1.3) (86). Docetaxel chemotherapy treatment of CRPC is relatively ineffective with marginal increase of patient survival of approximately 10-12 months (87). Interestingly, while a small minority of CRPC cases bypass AR requirement for growth, the vast majority retains its dependence on AR signalling for growth and proliferation of prostate tumours.

The recent discoveries of new mechanisms that enhance AR signalling in the presence of low serum androgens in CRPC, has led to novel therapeutic strategies (3, 88). Current therapies for CRPC disease range from antiandrogen therapies, androgen lowering therapies, heat shock protein 90 (HSP90) inhibitors, histone deacetylases (HDAC) inhibitors, and kinase inhibitors all aiming to abrogate androgen signalling at different steps (3). Antiandrogens, such as flutamide and bicalutamide, typically act by inhibiting AR signalling by mimicking androgens. However, they have been shown to also act as a weak agonist in some CRPC cases with mutated AR. MDV-3100 is a new antiandrogen which has been designed based on AR crystal structure and has been shown to bind AR at 10-fold higher affinity then bicalutamide. Currently MDV-3100 is being tested in phase III clinical trials (89-91).

Androgen lowering therapies are based on targeting enzymes involved in steroid synthesis pathways. It has been demonstrated that up-regulation of steroid synthesis in the adrenal gland or intracrine androgen synthesis in prostate tumours can lead to increase of androgen levels, which may be sufficient to promote CRPC in patients on ADT. Thus, inhibitors of steroid synthesis pathway, such as Abiraterone, a high affinity inhibitor of the P450 enzyme, CYP17, can be used to abrogate residual serum androgens, as well as up-regulated intracrine androgen synthesis. P450 (CYP17) enzyme is implicated in steroid synthesis and testosterone production in both adrenal and intracrine prostate tumour signalling. Currently, an international randomized Phase III trial comparing Abiraterone to placebo in patients with CRPC, who have progressed on docetaxel, is being conducted (91, 92).

Although there are some positive clinical responses observed with both antiandrogen and androgen lowering therapies, other therapeutic targets such as HSP90 inhibitors, HDAC inhibitors and kinase inhibitors are still evolving. HSP90 is a molecular chaperone that plays a crucial role in folding of proteins such as AR. The geldanamycin family of antibiotics have been shown to bind to the ATP binding pocket of HSP90 to inhibit its function and therefore causing degradation of HSP90's client proteins such as AR. 17-AAG is a geldanamycin derivative, which has been shown to inhibit growth of AR positive prostate cancer cells in xenografts without causing toxicity to the host (93).

Histone deacetylases (HDAC) are enzymes involved in deacetylating histone proteins, which are bound by the DNA. HDAC enzymes allow for gene transcription and complex interplay between transcription factors such as AR and chromatin. Thus, inhibition of HDAC inhibits AR activity. HDAC inhibitors, such as suberoylanilide hydroxamic acid (SAHA), have been shown to have anti-proliferative effects on AR positive prostate cancer cells in comparison to AR negative counterparts. However, Phase I/II clinical trials with HDAC inhibitors have not been successful. This sub-optimal inhibition of CRPC progression is thought to be due to dosing problems, as low concentrations may inadvertently increase AR activity (3, 94).

Agents targeting kinase activities of EGFR, Her2, PI3K, including small molecules kinase inhibitors (e.g. geftinib), and monoclonal antibodies (e.g.trastuzumab) have been extensively studies in CRPC. However, clinical trials using kinase inhibitors have largely resulted in disappointing results (3, 95, 96).

Another approach for treatment of CRPC in patients has been through immunotherapy. The main goal of immunotherapy is to activate and attract T-cells towards the tumour site, to attack and kill cancer cells (97). Various therapeutic approaches have been implemented, which have lead to clinical trial testing of new agents. Three of these agents, Sipuleucel-T (98, 99), ProstVac (100, 101), and prostate GVAX (102) have progressed to clinical trial testing and are currently phase II, and III clinical trials. Although these agents have significantly increased life expectancy of CRPC patients, they have not been able to establish their primary end point (time to tumour progression) and abrogate tumour progression (97).

Up to now the treatment modalities for CRPC has been palliative and not curative. Therefore, there is a clear need for an alternate therapeutic option that is more effective than the current therapies. Oncolytic viral therapy is an attractive, non-conventional approach for treatment of prostate cancer and is the focus of this thesis; hence it is discussed in depth under section 1.4.

1.4 Oncolytic viral therapy

Oncolytic viral therapy uses replication-competent viruses in order to selectively infect and kill cancer cells while sparing non-malignant cells **(Figure 1.5)**. In recent years, oncolytic viruses have been tested in various clinical trials for their antitumor targeting capabilities, as they are often able to exploit tumour-specific defects (103-105). Although the use of viruses in the clinic is not a new concept for cancer treatment, it is only recently that oncolytic viruses have been perceived as a therapeutic option for treatment of prostate cancer. Prostate cancer is a suitable target for oncolytic viral therapy since the prostate gland is easily accessible for

inoculating viruses through the perineal, trans-urethral or trans-rectal routes. Oncolytic viruses can be divided into three categories:

1) First generation oncolytic viruses are naturally occurring and have inherited tumour-specific properties. Examples include Newcastle disease virus, Vesicular Stomatitis virus (VSV) and reovirus.

2) Second generation oncolytic viruses, includes viruses which through mutations of their essential genes have been synthetically modified to become more selective for malignant cells. Adenovirus Onyx-015 and herpes virus G207, and VSV(AV3) are examples of second generation viruses.

3) Third generation oncolytic viruses, include viruses that have been engineered to contain tissue-specific genes and elements. H101 and Onyx015 are two of the most established third generation examples (106).

Sections 1.4.1 discusses various methods for virus engineering in order to produce second and third generation synthetic oncolytic viruses. Section 1.4.2 will discuss current clinical trials conducted using oncolytic viral therapy for treatment of prostate cancer in patients.

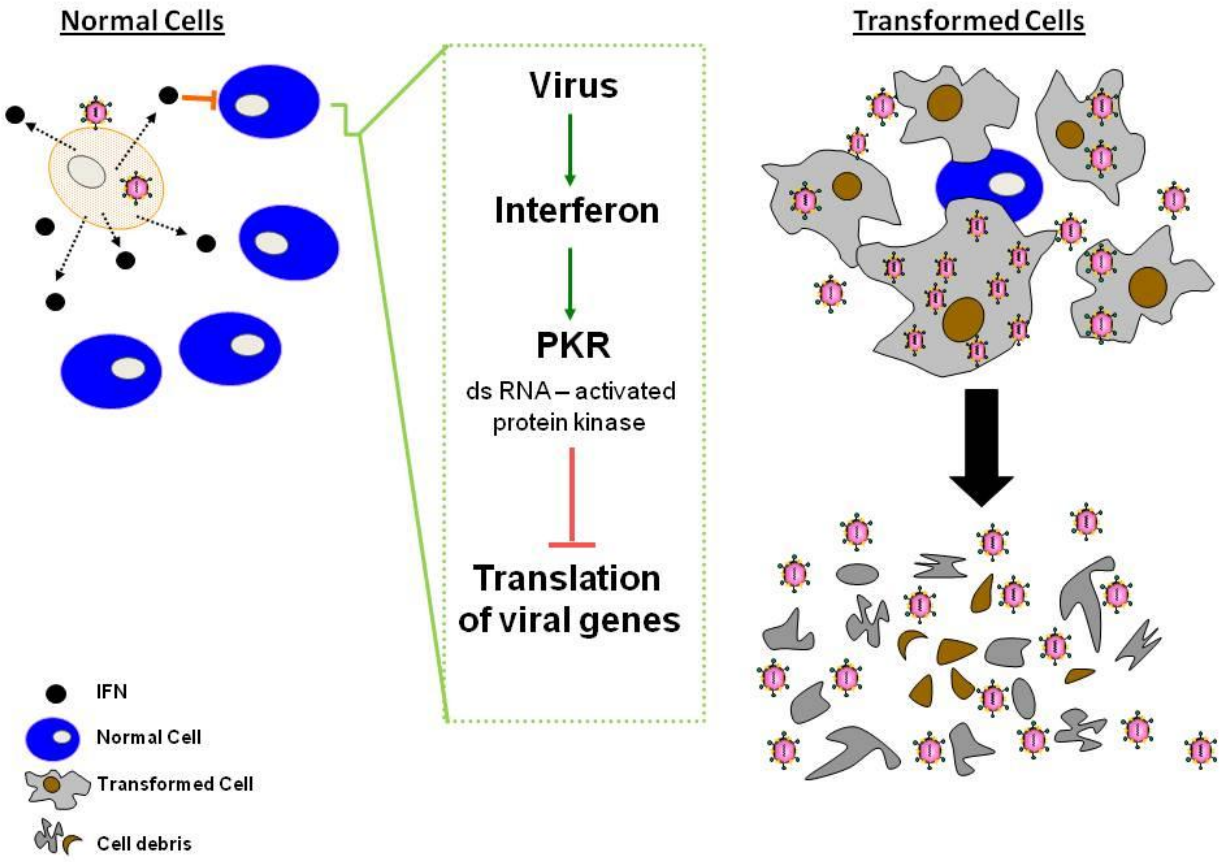

Figure 1.5 Mechanism of viral oncolysis.

This is a schematic representation demonstrating selective replication of an oncolytic virus in transformed cells. In normal cells upon viral infection, cells undergo an anti-viral response, such as production of interferons (IFN). The secreted IFN by the host cell alerts the neighbouring cells to the presence of virus. Thus normal neighbouring cells will protect themselves from potential viral infection by producing enzymes and proteins (such as PKR) that inhibit viral translation. However, transformed cells lack the ability to signal, or to receive signal, from other transformed cells.

1.4.1 Viral engineering

1.4.1.1. Attenuation of virus to generate cancer-specific viral mutants

One of the targeting strategies for viral therapy is to delete viral genes that are required for efficient replication in normal cells but are unnecessary for replication in tumour cells. An example of this strategy is adenovirus Onyx-015, the first oncolytic virus used in the clinic. The E1B gene in Onyx-015 has been deleted, thus allowing for the virus to selectively replicate in p53 deficient cancer cells. E1B gene encodes for a 55 kDa protein which through interactions with another adenoviral product, E4ORF6, is capable of inactivating p53. Deletion of this gene is a safety feature that limits the virus to replicate in absence of p53 (107). This is an appealing quality given that approximately 40% of human cancers contain p53 mutations (108). Onyx-015 has been extensively studied and it has been shown that administration of 10^{11} plaque forming unit (pfu) of virus daily for 5 consecutive days was well tolerated by patients with no evidence of toxicity. However, long term survival outcomes were marginal. Combination of Onyx-015 with chemotherapy proved effective (109, 110). In November 2005 China licensed adenovirus H101 (Shanghai Sunway Biotech), which is almost identical to Onyx-015, as the first oncolytic viral therapy for treatment of head and neck cancers (111, 112). However, outside of China the emergence of various reports challenging Onyx-015's p53 selectivity as well as financial burden of conducting these clinical trials have slowed the interest of the clinical use of Onyx-015 (112).

Another example of an attenuated virus is the herpes simplex virus 1 (HSV-1) G207. G207 is derived from wild-type HSV-1 F strain (113). This agent is a multi-mutated virus in which both copies of Infected Cell Protein (ICP) 34.5 gene have been deleted. In addition the ICP6 gene has been rendered inactive due to a LacZ gene insertion. ICP34.5 gene products block the host's ability to shut off its protein synthesis; this is done through inhibition of Protein Kinase R (PKR) (114, 115). PKR is part of host cells anti-viral response which typically malfunctions in cancer cells. Deletion of ICP34.5 is a safety feature which ensures lack of neurovirulence thus

limiting the virus to only replicate in tumour cells. Inactivation of ICP6 offers additional targeting to tumour cells with defects in tumour suppressor p16 (116). Initial studies of G207 in animal models of malignant glimoa demonstrated efficacy and safety of the virus. Subsequent studies in other solid tumour models were conducted showing tumour regression (117). It is thought that G207 may illicit tumour-specific systemic immune and cytotoxic T lymphocyte (CTL) responses in addition to its viral cytopathic effects (118, 119). A phase I clinical trial demonstrated that patients safely tolerated doses of up to $3x10^9$ pfu inoculations into brain tumours (120). A subsequent phase 1b clinical trial demonstrated that multiple dose (10^9 pfu) deliveries of G207 can be safely tolerated when virus is inoculated directly into surrounding brain tissue (121).

An example of an attenuated RNA virus is the AV3 strain of VSV. VSV is a single-stranded RNA virus which as noted above (section 1.4), is a first generation oncolytic virus and thus exhibits oncolytic activity in a wild-type format. The AV3 strain of VSV is an attenuated form of the virus (second generation oncolytic virus), which contains a deletion of methionine 51 of the matrix (M) protein. This deletion of Met-51 of M protein ablates the virus's ability to infect normal tissue while retaining its ability to replicate in tumour cells (122). This virus will be discussed in more detail in section 1.5.

1.4.1.2. Altering viral tropism to target transformed tissue

Non-specific infection of normal tissues, such as liver, presents as a problem in systemic delivery of oncolytic viruses. Therefore, by changing viral tropism so that it directs viral infection towards targeted tissue may improve efficacy and eliminate needless toxicity. One method to alter viral tropism is through modification of viral coat proteins. In 2003 Wickham *et al* added a short peptide sequence to the C-terminal end of the coat protein of adenovirus and successfully changed viral tropism (123). Another study demonstrated that insertion of a single-chained antibody against the human epidermal growth factor receptor 2 (Her2/neu) into HSV-1 viral envelop protein, gD, altered viral tropism so that the virus was capable of only infecting HER2/neu positive cells (124). More recently, trastuzumab antibody bound to lentivirus, pseudo-

typed with an engineered Sindbis virus envelope protein, was demonstrated to target prostate cancer cells both *in vitro* and *in vivo* (125). These studies indicate that alteration of viral tropism can direct and limit viral infection into tumour cells. However, viral targeting through altering viral tropism is limited by production of low titers of these viruses (126) .

1.4.1.3. Transcriptional targeting

Transcriptional targeting is another targeting strategy in which tissue-specific promoters are placed up-stream of either suicide genes or attenuated viral genes to increase anti-cancer specificity of the viral therapy. This is yet another safety mechanism which allows for tissue-specific expression of the virus (e.g. tissue-specific promoters, such as PSA and probasin are expressed only in prostate tissue, and hence can be used to target prostate specific expression, sparing other tissues such as liver). This strategy was initially implemented in adenovirus CV706 (127). CV706 is a conditionally-replicating adenovirus that contains a prostate-specific promoter (PSA) driving expression of the E1A gene. E1A is the first early gene expressed by the virus and is responsible for inactivation of host proteins such as retinoblastoma, causing for further propagation of viral particles. The incorporation of a PSA promoter upstream of E1A limits viral propagation in PSA over-expressing prostate cells (127, 128). Similarly, adenovirus CG7870 has the probasin promoter driving the E1A gene and a PSA promoter driving the E1B gene, thus making the virus prostate-specific leading to increased cell death (129, 130). Similar targeting strategies have been implemented using HSV-1 oncolytic viruses. Recently, Lee *et al.* (2010) demonstrated that insertion of probasin promoter upstream of ICP27 gene leads to inhibition of tumour growth in the prostate cancer LNCaP xenograft model (131). These preclinical data capitalize on use of tissue-specific promoters to enhance viral targeting.

1.4.1.4. Translational targeting

In addition to transcriptional targeting, oncolytic viruses can be engineered to interfere and target cancer cells at the translational level. Translation of mRNA plays an important role in

cell growth, proliferation, and differentiation. Translation is divided into three distinct steps; initiation, elongation, and termination. Typically eukaryotic cells cope with this funnel by having a reservoir of mRNAs ready to start translation upon receiving activation signal. The initiation phase of translation is the rate-limiting step of this process, wherein initiation factor 4E (eIF4E) has a key role. The role of eIF4E is discussed in detail under sections 1.4.1.4.1 to section 1.4.1.4.4.

1.4.1.4.1. eIF4E

In eukaryotes, most mRNAs are blocked at their 5' ends by a cap structure M^7GpppN (where N is any nucleotide) (132). The role of the mRNA cap structure is to enhance translational efficiency and mRNA stability. It is also involved in RNA splicing and nuclear transport. The mRNA cap binding protein eIF4E is a 24 kDa protein that exists as both a free form or part of a multiprotein complex called eIF4F. In addition to eIF4E, the eIF4F complex consists of eIF4A, an ATP-dependent helicase, and eIF4G, which is a large scaffolding protein (133). eIF4E binds to the 5'cap 7-methylguanosine (M^7GpppN), which is present on all nuclear transcribed mRNAs, and with help of eIF4A it unwinds the secondary structures within the 5'untranlated region (5'UTR) to assist in stacking the 40S ribosomal subunit onto mRNA. EIF4F assembly is inhibited by a family of proteins called eIF4E binding proteins (4EBP) (134, 135). 4EBPs (4E-BP1, 4E-BP2 and 4E-BP3) regulate eIF4E through phosphorylation. Upon mitogenic activation, 4E-BP is phosphorylated by either PI3 kinase/Akt or by ras-ERK signalling pathway and dissociates from eIF4E (136, 137). eIF4E is then free to bind mRNA along with the rest of eIF4F complex and initiate translation. Therefore, eIF4E is the rate-limiting protein involved in translation. In non-neoplastic cells there is a limited amount of free eIF4E available in the cytoplasm causing competition between available mRNAs to gain access to the eIF4F complex (138). Typically mRNAs that contain short unstructured 5'UTRs (e.g. housekeeping genes) bind more efficiently to the eIF4F complex and can be translated with ease in low level eIF4E environments. In contrast, mRNAs with lengthy 5'UTRs (e.g. growth factors or proto-

oncogenes), which contain extensive secondary hairpin structures due to rich G+C regions, require a high level eIF4E environment in order to recruit sufficient eIF4F complex to initiate translation (139).

1.4.1.4.2. Upstream effectors of eIF4E

Mitogens, growth factors, and hormones activate the phophatidylinositol 3-kinase (PI3K) mammalian Target of Rapamyciyn (mTOR) pathway. Activation of PI3K initiates a signalling cascade in which 3-phosphoinositide-dependent kinase 1 (PDK1) is activated through phosphorylation. Tumour suppressor phosphatase and tensin homolog (PTEN) negatively regulates AKT by de-phosphorylating PI3K to phosphatidylinositol-3,4,5-triphosphate (PIP3) (140). PDK1 then signals to downstream AKT, which upon activation destabilizes TSC1/TSC2 protein complex by phosphorylating TSC2 (141). Activation of TSC2 ultimately leads to activation of mTOR which by phosphorylating 4E-BPs allows for dissociation of eIF4E, thus allowing it to bind to the eIF4F complex to initiate translation (139, 142). Other pathways such as RAS and stress-activated JNKK also lead eIF4E activation. **Figure 1.6** illustrates a schematic representation of the eIF4E pathway.

1.4.1.4.3. eIF4E in Cancer

Several groups have investigated the role of eIF4E in cellular transformation. It was hypothesized that eIF4E over-expression could lead to deregulation of translation. This hypothesis was based on low levels of eIF4E in non-transformed cells in comparison to other initiation factors (143). Through a series of experiments in transformed cell lines, it was observed that over-expression of eIF4E promoted tumourigenesis (139). Subsequent studies demonstrated that eIF4E is over-expressed in many solid tumours, such as colon, breast, bladder, lung, prostate, gastrointestinal tract, head and neck, Hodgkin's lymphoma, and neuroblastoma (139, 144-146). This observation lead to further investigations, which demonstrated that eIF4E elevation causes over-expression of oncogenic protein translations;

such as c-myc, cyclin D1, vascular endothelial growth factor (VEGF), matrix metalloproteinase (MMP), fibroblast growth factors (FGF) and ornithine decarboxylase (ODC) (139). This is in light of the fact that the mRNA of these oncogenic proteins typically displays a complex 5' UTR. Thus, excess levels of eIF4E leads to translation of these proteins.

1.4.1.4.4. Selecting eIF4E with 5'UTR

With the understanding that malignant cells display a higher level of eIF4E compared to normal cells, in 2002 DeFatta and colleagues designed a series of experiments that targeted malignant cells based on elevated levels of eIF4E (147). They postulated that placement of a complex 5'UTR, originated from FGF-2, upstream of HSV-1 derived thymidine kinase (TK) cDNA would restrict translation of TK mRNA to cells with high levels of eIF4E. Therefore, malignant cells expressing TK would be susceptible to the pro-drug ganciclovir (GCV) (148). Systemic delivery of this plasmid using liposome as a vehicles, demonstrated up to >90% reduction in subcutaneous breast tumours and lung metastasis. This translational targeting

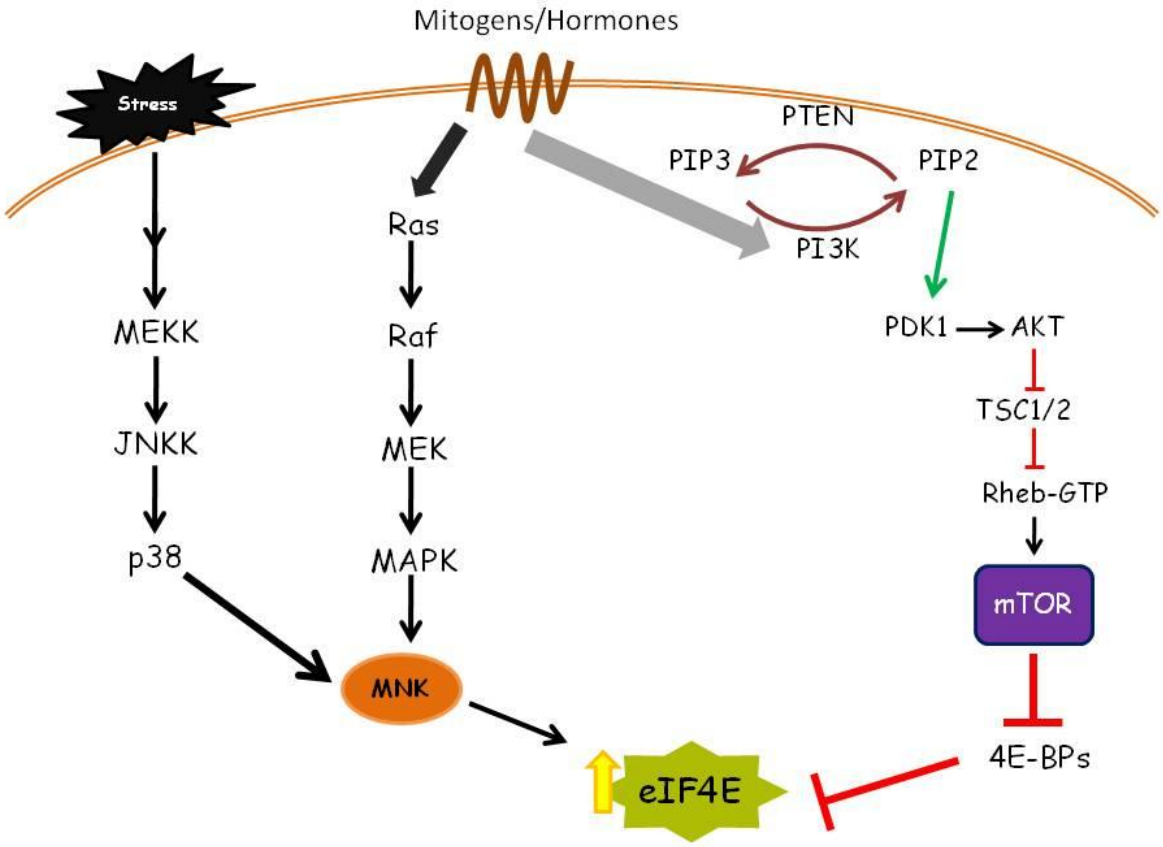

Figure 1.6 eIF4E signalling pathway

The above is a schematic representation of upstream effectors in the eIF4E pathway. The diagram emphasizes the links between PTEN/PI3K/mTOR up to the activation of eIF4E translational initiation pathway.

system was later implemented in prostate cancer wherein prostate-specific probasin promoter and FGF-2 derived 5'UTR were placed upstream of the TK gene in a lentiviral vector. In this method *Yu et al.* (2006) have combined transcriptional tissue-specific targeting along with translational targeting to direct viral therapy towards prostate cancer (33). In a more recent study, LNCaP tumour xenograft models were treated using HSV-1 virus which had been modified to include a probasin promoter upstream of FGF-2 derived 5'UTR driving the ICP27 gene. This study demonstrated that the efficacy of virus was increased with insertion of 5'UTR compared to probasin prostate-specific promoter alone (131). These preclinical data have capitalized on use of both tissue-specific promoters along with targeting elevated eIF4E through 5'UTR insertion, to enhance viral targeting.

1.4.2 Current clinical trials

Due to promising advances in recent years, treatment of cancer with viral agents has become a real possibility. The first oncolytic viral therapy (H101) for head and neck cancer treatment was approved and licensed in 2005 in China. Over the past decade, a series of clinical trials using oncolytic viral therapy for treatment of prostate cancer have been conducted (129). Recent randomized clinical trials using reovirus for treatment of prostate cancer have debuted in Canada (106, 149). The following section summarizes the results of completed clinical trials using predominantly adenovirus and reovirus **(Table 1.1)**.

1.4.2.1. Adenovirus-Mediated Clinical Trials for Prostate Cancer

To date three clinical trials using adenovirus targeting prostate cancer have been conducted. CV706 and CG7870 adenoviruses were tested in patients with recurrent local prostate disease. CV706 adenovirus was directly injected into the prostates of 20 patients following primary radiotherapy. DeWeese *et al* (2001) demonstrated a dose-dependent reduction in PSA levels with CV706 administration (128). CG7870 was delivered intravenously to 23 prostate cancer patients suffering from advanced metastatic, hormone refractory disease.

However, at high doses of CG7870, thrombocytopenia and mild liver inflammation was observed. Five patients showed between 25% to 49% decrease in blood PSA levels. This virus is now in two phase II trials, one in combination with radiotherapy and another in combination with taxane-based chemotherapy (129, 130).

The third adenovirus currently being tested in clinical trials is Ad5-CD/TKrep. Ad5-CD/TKrep is an adenovirus that has two suicide genes embedded in its backbone, cytosine deaminase (CD) and HSV-1 thymidine kinase (TK), which causes malignant cells to be sensitive to specific pharmacological agents; 5-fluorocytosine (5-FC) and ganciclovir (GC), respectively (150). Ad5-CD/TKrep was injected into prostates of 16 patients using ultrasound guidance. These patients were diagnosed with local recurrent prostate cancer and had undergone radiation therapy previous to injection with Ad5-CD/TKrep. Two days post viral injection patients were given a cocktail of 5-fluorocytsoine and ganciclovir (5-FC/GC) pro-drug therapies for 1 or 2 weeks. Approximately 44% of the patients demonstrated a 25% reduction in serum PSA levels, while 19% of the patients demonstrated upto 50% reduction in serum PSA. Moreover, patients treated with viral therapy displayed a marked increase in their PSA doubling-time from a mean of 17 to 31 months observed at the 5-year follow-up (109, 129).

In a second trial, Ad5-CD/TKrep was administered intra-prostatically into 15 patients. Patients were then administered between 1-3 weeks of 5-FC/GC pro-drug therapy and three-dimensional confocal radiotherapy. There was no significant adverse effects or dose-limiting toxicities observed in these patients. Additionally at a median follow-up of 9 months, 50% of the patients not treated with ADT achieved a serum PSA level of less than or equal to 0.5 ng/mL (110). A third trial with Ad5-CD/TKrep was conducted, wherein intensity-modulated radiotherapy (IMRT) IMRT was given during administration of 5-FC/GC pro-drugs. This therapy was also associated with low toxicity and there were no dose-limiting toxicities and treatment-related adverse events. The result of the last two trails were combined and it was observed that

approximately 22% of patients had visible adenocarcinoma in their last biopsies, which is a significant improvement over the expected >40% for this group of patients (129, 151) .

1.4.2.2. Reovirus-Mediated Clinical Trials for Prostate Cancer

Reovirus is a non-attenuated, double stranded RNA virus which is able to exploit deviant signalling pathways causing selective cytotoxicity. In recent years reovirus has been used as a potential treatment for prostate cancer. To date two clinical trials using reovirus have been reported. In a UK phase I trial, reovirus (Reolysin- type 3 reovirus) was administered intravenously in patients with solid prostate tumours. A reduction in the serum PSA levels (from 100 to 50 ng/ml) was observed in patients. A phase II trial was carried out in patients with stage T2 (organ confined) prostate cancer, where a single intra-prostatic injection was given 3 weeks prior to prostatectomy. No significant toxicity was observed in patients and immune cell infiltration was minimized to the tumour (129, 152).

In a separate study conducted in Canada, reovirus (Reolyisn) was administered to 6 patients displaying organ-confined prostate cancer with Gleason score ranging from 3 to 5 (149). Patients were intra-prostatically injected with reovirus (Reolysin) with the help of transrectal ultrasound. A small group of patients reported flu-like symptoms. There was no evidence of viral shedding in stool, urine or serum samples collected from each patient. Patients underwent prostatectomy three weeks post-viral injection. Histological staining of each prostate tumour demonstrated an increase in apoptotic cell death in reovirus treated patients. An increase in T-lymphocyte (CD8) infiltration into tumour sites post-reovirus treatment was also observed. Although, it is controversial whether T-cell infiltration into tumour correlates with tumour regression, it is possible that reovirus infection can lead to immune therapy (149). Results from the above clinical trials (section 1.4.2) demonstrated that these oncolytic viral therapies were in fact well tolerated by most patients and tumour selectivity was demonstrated. However, anti-tumour potency is still limited especially in cases of virus therapy acting alone as opposed to reported combination therapies. In contrast to the above

Virus	Doses (pfu)	Delivery	Pro-drug or combination therapy	Cancer Type	Anti-tumour activity
CV706	10^{11}-10^{13}	Intra-prostate	Ø	Local recurrence of prostate cancer after radiation (n=20 patients)	> 50% PSA reduction in 5/20 patients and >25% PSA reduction in 13/20 patients
CG7870	$1x10^{11}$ - $6x10^{12}$	Intravenous	Ø	Castration-resistant metastatic prostate cancer (n=23 patients)	> 25% PSA reduction in 5/23 patients
Ad5-CD/Tkrep	10^{10} - 10^{12}	Intra-prostate	5FC/GC	Local recurrence of prostate cancer after radiation (n=16 patients)	> 50% PSA reduction in 3/16 patients and > 25% PSA reduction in 7/16 patients
Ad5-CD/Tkrep	$1x10^{12}$	Intra-prostate	5FC/GC +3D Confocal radiotherapy	Newly diagnosed prostate cancer (n=15 patients)	PSA <0.5 ng/mL for 9 months in 5/10 patients and >25% PSA reduction in 15/15 patients
Ad5-CD/Tkrep	$1x10^{11}$ - $6x10^{12}$	Intra-prostate	5FC/GC + IMRT	Newly diagnosed prostate cancer (n=12 patients)	0/12 patients were positive for cancer at biopsy and > 25% PSA reduction in 8/9 patients
Reolysin	up to $3x10^{10}$	Intravenous	Ø	Patients with solid tumours including organ confined prostate cancer (n=33 patients)	PSA reduction from 100 to 50 ng/mL in one patient
Reolysin	$1x10^{7}$	Intra-prostate	Ø	Organ confined prostate cancers with Gleason Score ranging from 3 to 5 (n=6 patients)	Increase apoptosis and T-lymphocyte infiltration into all 6 patients prostates

Table 1.1 Summary of results from closed oncolytic virus clinical trials for prostate cancer

The table lists each virus used in the clinic with the route and titre administered. Some viruses were combined with other pro-drug therapy. Anti-tumour activity was mainly analysed by serum PSA levels.

This table was adapted from Fukuhara *et.al* (2010) (129).

combination therapies, a viable alternative viral therapy that may increase both tumour selectivity and anti-tumour potency is through use of VSV. Since this specific virus is the major component of study in this thesis, VSV has been discussed more comprehensively under section 1.5.

1.5 Vesicular stomatitis virus

Vesicular stomatitis virus (VSV) is a small, bullet-shaped, enveloped, negative stranded RNA virus belonging to the *Rhabdoviridae* family **(Figure 1.7)** (153, 154). VSV's RNA genome is approximately 11kB in length which encodes for five proteins referred to as nucleocapsid (N), polymerase proteins (L and P), matrix protein (M) and surface glycoprotein (G) (155). In nature, VSV is transmitted by insects infecting livestock that typically leads to a self-limiting disease, which manifest as vesicular lesions around the mouth. Rare accounts of human infection with VSV have been reported. Infection symptoms range from asymptomatic infection to mild flu-like disease (156, 157). VSV lends itself to be a great candidate for oncolytic viral therapy due to the following characteristics: 1) lack of pre-existing immunity to VSV in the general human populations, 2) ease of genetic manipulation of VSV's genome, 3) VSV contains robust gene expression and is known to infect a wide range of cell types and finally (158), and 4) relative ease of *in vitro* propagation of VSV (154). It has been estimated that 1 L of cultured VSV is sufficient to vaccinate up to one billion people (159, 160).

1.5.1 VSV structure and replication

Similar to other members of *Rabdoviridae* family, VSV is an enveloped virus. VSV's envelop consists of trimers of the viral glycoprotein (G protein). G protein plays a crucial role in initial steps of viral infection. G protein is responsible for viral attachment to host by binding to cell surface receptors. The nature of the receptor that binds to G protein remain elusive and although there are studies indicating that it is a phosphatidylserine (161), recent results negate this probability (162). After binding of virus to cell membrane, a drop in the pH within the

A)

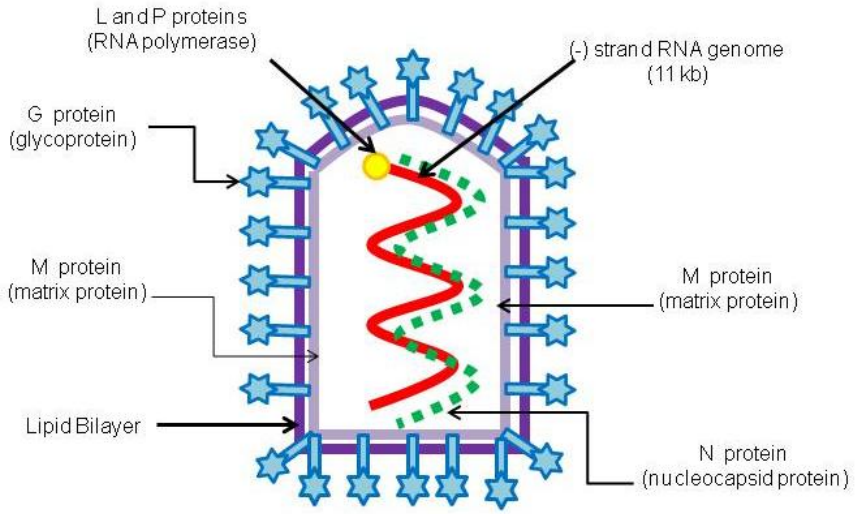

B)

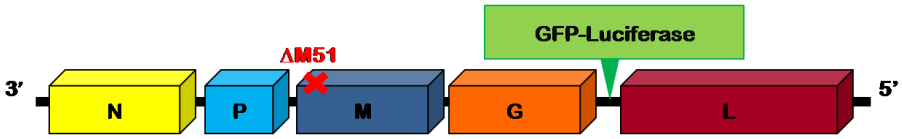

Figure 1.7 Structure of vesicular stomatitis virus

(A) A schematic representation of VSV structure. Viral glycoproteins cover the outer layer of the virus. A lipid bilayer protects the negative single-stranded RNA viral genome. The viral genome is surrounded by the viral nucleocapsid and matrix proteins. Each VSV viral particle is equipped with a viral RNA polymerase that allows transcription of the viral genes upon entering the host.

(B) Genomic representation of VSV(AV3) negative ssRNA strain. The amino acid methionine at position 51 of the M protein has been deleted. A GFP-luciferase fusion gene has been inserted between the viral genes G and L, allowing for visualization of virus.

endosome induces membrane fusion and allows for insertion of the viral core in to the cytoplasm (155, 163-165). The viral core consists of viral RNA, polymerase proteins, nucleoprotein and matrix proteins. Viral polymerase protein L binds to the 3' end of the viral RNA and initiates transcription of the five individual mRNAs encoding for N, P, M, G, and L. Therefore viral mRNA synthesis begins at the 3'-end of the N-mRNA and carries on until it reaches stop codon ($AUACUUU_7$) sequence. At this point, transcriptase stutters and either falls off the RNA and restarts to transcribe from the beginning or continues to transcribe, for this reason there is a gradient in amounts of mRNA available in the following descending order, N > P > M > G > L. VSV-encoded mRNAs are capped and polyadenylated (155, 160). Although not entirely clear how the viral polymerase switches from transcription of viral mRNAs to replication of viral genome, it is thought that excess N protein is responsible for this switch to genome replication. After generation of viral protein and negative-sense viral RNA, N protein aids in its encapsulation by forming ribonucleocapsid particles (RNP) along with P and L proteins. The viral core is further condensed by M protein present at the plasma membrane. G protein is also present on the plasma membrane and coats the progeny virions as they lyse out of the host cell. The M protein plays an important role in control of VSV replication and pathogenesis (160). During the last stages of infection, accumulation of M protein catalyzes the generation of inactive RNP cores, preparing them for packaging into virions. At the later stages of viral infection, M protein aids in viral budding by binding to cellular TSG101 protein. In addition to aiding with viral budding, M protein helps VSV to avoid cellular antiviral detection by, interrupting host nuclear cytoplasm interaction, disrupting antiviral cell signalling pathways and ultimately causing apoptosis (160). Deletion of methionine 51 of the M protein disables VSV's ability to inhibit the interferon (IFN) response (166). These mutants allow activation of TLR-7 which leads to activation of the IFN response (167). **Figure 1.8** depicts VSV replication cycle (160). Over the past decade a series of elegant studies have demonstrated that defects in the antiviral immune

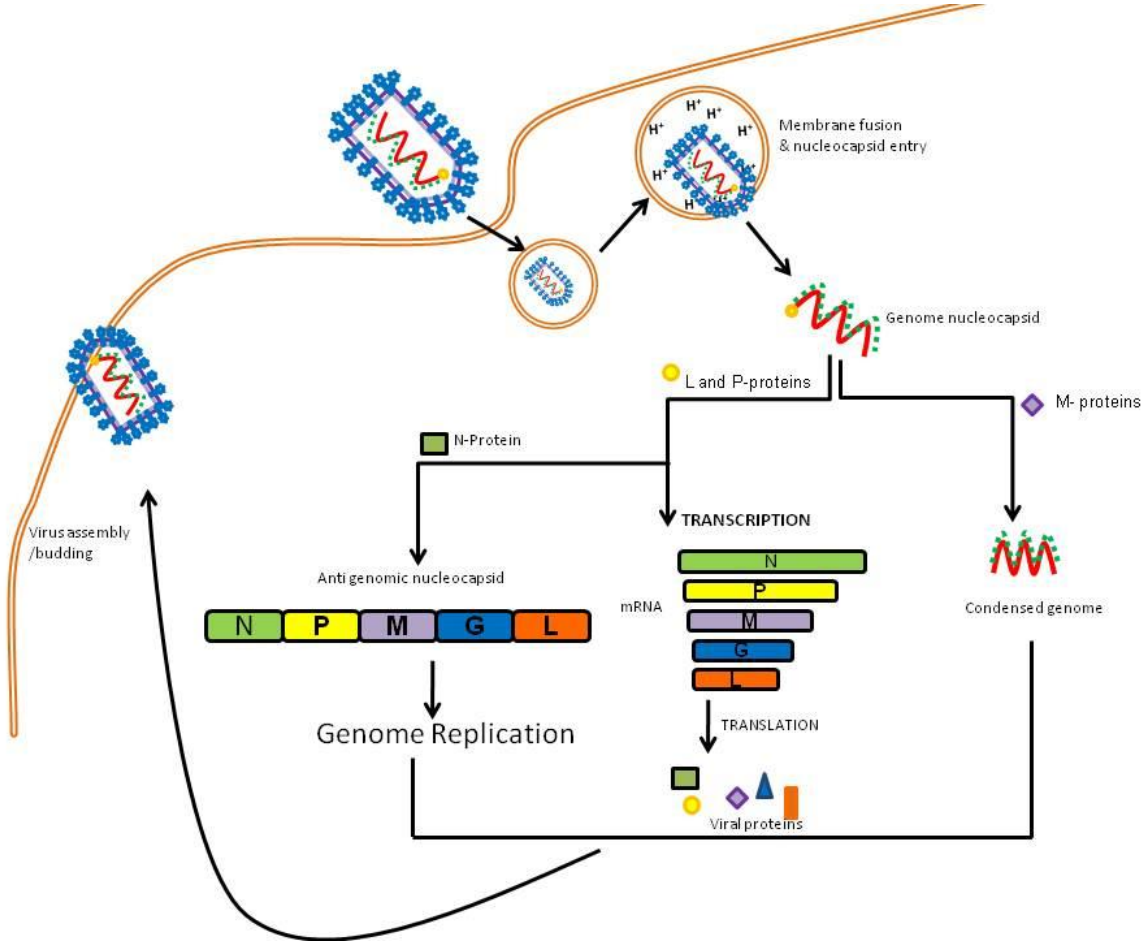

Figure 1.8 VSV replication

VSV binds to cellular membrane components through its surface G-glycoprotein and enters the host cell by endocytosis. Due to a drop in pH in the endosome, the RNA genome nucleocaspsid is released into the hosts' cytoplasm. Viral RNA-polymerase helps in transcription of the viral genes. Viral mRNA expression decreases as each subsequent gene is transcribed (N>P>M>G>L). All viral mRNAs are translated into proteins that are assembled in a bullet shaped virion with help of M- protein, and subsequently lyse the host cell in order to find new cells to infect.

response, specifically the IFN response plays a prominent role in enhancing VSV replication discussed bellow in section 1.5.2.

1.5.2 Interferon response

Interferons are cytokines which were fist discovered in 1958, and have since been divided into three groups: type I (IFN α/β), type II (IFNγ) and type III (IFNλ) (168). Induction of type I IFN is the hallmark response to viral infection. Type I IFNs induce an anti-viral state in cells, which make them resistant to viral infections (169, 170). However, majority of tumours contain a faulty IFN response and in the case of prostate cancer, recent studies have shown up to 30% down-regulation of IFN inducible genes. VSV is very sensitive to IFN antiviral properties, thus making it a good selective oncolytic viral candidate (171, 172).

The type I IFNs are located on chromosome 9. They consist of several short α genes and one β gene and are induced by most cell types (170). The type I IFN signalling pathway is initiated with the presence of foreign viral genome which is recognized by toll-like receptors (TLRs) in the host cytoplasm. Upon activation of TLRs, adapter molecules such as MyD88 relay the signal to the nucleus to produce interferon stimulating genes (ISGs), such as interferon response factor 3 (IRF-3), 7 (IRF-7), IFNα/β, and PKR. This activation leads to intracrine or paracrine signalling that enhances presence of ISGs such as RNaseL, which leads to degradation of the viral genome and thus inhibition of viral propagation **(Figure 1.9)** (173-175).

As previously stated VSV-M protein is crucial in averting the host IFN response. M protein interrupts cellular transcription pathways in addition to blocking mRNA export from the nucleus thus upsetting host IFN response. Recent studies have demonstrated that presence of mutations and or deletions in the VSV-M protein, in particular at methionine 51 position, renders the virus more susceptible to the host antiviral response. Mutant viruses fail to block export and translation of IFN mRNAs (122, 160, 176).

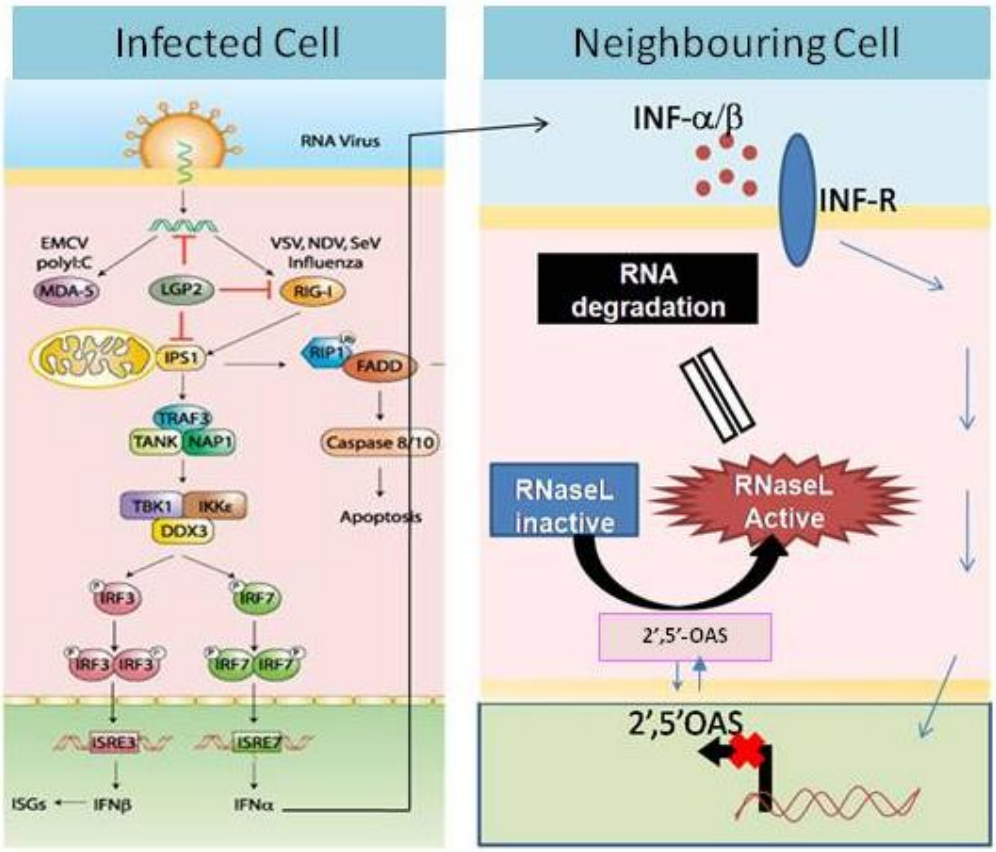

Figure 1.9 The interferon (IFN) signalling pathway

A schematic representation of signalling cascade that leads to IFN activation due to viral infection. The cell on the left is a schematic representation of the original infected cell, while the cell on the right represents a neighbouring cell. Upon detection of presence of viral RNA, interferon response factors (IRF) 3 and 7 undergo a conformational change by phosphorylation, resulting in dimerization and nuclear transportation. Once in the nucleus both IRF-3 and IRF-7 bind to the DNA, initiating IFNα/β production. IFNα/β signals neighbouring cells and alerts them of viral presence. The neighbouring cells activate enzymes such as RNaseL, through production of its substrate 2'5' oligoadenylate synthase (OAS) which in turn degrade viral doubles stranded RNA. Modified from InvivoGen website (177).

1.6 Mouse models of prostate cancer

To increase our understanding of prostate carcinogenesis and test the use of oncolytic viruses (such as VSV) in a pre-clinical setting, different animal models are available. Historically, mouse xenograft models with either primary or genetically altered cell lines derived from localised and metastatic disease have been utilized. However, more recently, use of transgenic mice to study prostate cancer progression and treatment has grown in popularity. Some of the main advantages of using transgenic mice for pre-clinical testing of viral therapy are; 1) cancer arises *in situ* within the appropriate microenvironment, 2) these mice have intact immune systems, 3) cancers are frequently heterogeneous and by arising *de novo* neoplastic progression is similar to human cancer (178).

These transgenic mouse models are complicated and no one model represents the entire spectrum of the disease. A solution to this problem is to use multiple transgenic models. This thesis has utilized both the prostate-specific PTEN knockout mouse model (section 1.6.2) and the transgenic adenocarcinoma of the mouse prostate (TRAMP) (section 1.6.3) model. Though transgenic mice are very attractive models for researchers, the similarities and differences between both gross anatomy and microanatomy of mice versus human prostates must be considered in order to make conclusions across species.

1.6.1 Comparison of mouse to human prostate

Both human and mouse prostates have similar epithelial cell types, such as luminal, basal and neuroendocrine, presumed to have the same functions. However, the ratios of these cells vary between the two species. For example, the basal cells form a continuous layer in the human prostate while in mouse they are scant with discontinuous layers surrounding each acini (179). However, neuroendocrine cells are rare and scattered in both mouse and human prostate glands (180). The main histological difference between mouse and human prostate is in the stroma. The human prostate has a predominant fibromuscular stroma, while in a mouse the

stroma is a minor component. Anatomically, there are obvious differences between human and mouse prostates. Human prostate is not divided into obvious lobes and typically is situated postero-inferior to the bladder surrounding the urethra (section 1.1.1). Mouse prostate is comprised of four well-defined paired lobes that are located inferior to the bladder and incompletely surround the urethra. The mouse prostate is divided into anterior (AP), dorsal (DP), lateral (LP), and ventral (VP) prostate compartments. Typically, the dorsal and lateral prostates are referred to in combination as dorso-lateral prostate (DLP) (181). The mouse DLP lobe is considered to be analogous to the human PZ, from which the majority of prostate carcinomas arise (182). A schematic representation of the mouse prostate is depicted in **figure 1. 10**.

Since mice are not prone to spontaneous development of prostate cancer, genetic manipulation of their prostates are required to recapitulate disease progression as seen in human (181). Here we discuss the generation of two different prostate cancer mouse models.

1.6.2 Prostate specific PTEN$^{-/-}$ transgenic mice

Tumour suppressor gene, phosphatase and tensin homologue on chromosome 10 (PTEN), is frequently mutated in a variety of tumours (46). PTEN deletion or mutations lead to dysregulation of the PI3K-AKT pathway and up-regulation of survival pathways, which leads to continuous activation of translational machinery (**Figure 1.6**). PTEN has been implicated in prostate cancer (46). The *Pten* gene is frequently lost in prostate cancer cell lines and PTEN mutations have been reported in approximately 30% (183) of localized and 63% of metastatic prostate tumours in the clinic (184). Biologically PTEN is an essential genes and loss of PTEN is embryonically lethal (181, 185). Conditional deletion of PTEN in the mouse prostate results in invasive carcinoma between 12-15 weeks. These prostate-specific PTEN knockout (PTEN$^{-/-}$) mice were generated by crossing a mouse harbouring floxed alleles of *Pten* gene to another mouse harbouring *Cre* gene linked to probasin promoter (186). Homozygous mice with PTEN deletion exhibit enlarged prostate glands. PIN formation is evident in the DLP

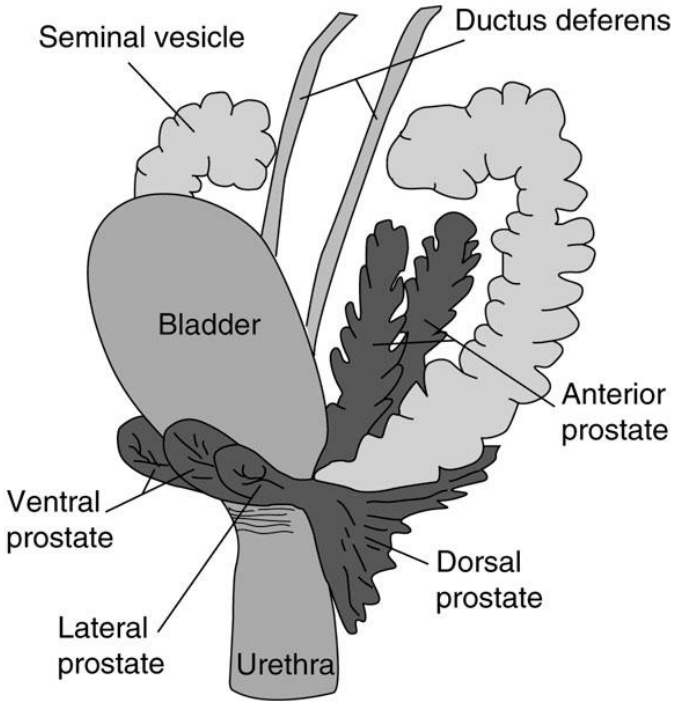

Figure 1.10 Adult mouse prostate

A schematic lateral view of adult mouse urogenital tract. The multi-lobular prostate is presented in dark gray color.

Picture reproduced with permission (187).

and VP of PTEN$^{-/-}$mice from by 4-6 weeks. All PTEN$^{-/-}$ mice exhibit adenocarcinoma by 10-12 weeks of age (188, 189). A summary of onset and disease progression in PTEN$^{-/-}$ mice is depicted in **Figure 1.11**. The advantage of this model is that it recapitulates disease progression as seen in clinic leading to development of prostate adenocarcinoma. However, this model is limited by lack of consistent metastatic lesions. In the clinic the majority of metastatic lesions occur in the bone. In PTEN$^{-/-}$ mice despite evidence of bone remodelling activity in mature mice, they do not present with such metastatic lesions (186, 190).

1.6.3 TRAMP transgenic mouse model

The transgenic adenocarcinoma of the mouse prostate (TRAMP) model is the most established prostate cancer transgenic model. This model uses minimal rat probasin (-426/+28 bp) promoter to direct expression of the early tag (T, t) antigens of simian virus 40 (SV40) in the terminally differentiated tall columnar (luminal) epithelial cells of the prostate (191, 192). Expression of tag (T, t) antigens, abrogate p53 and retinoblastoma (Rb) protein expression, therefore causing malignant transformation. The male progeny develop invasive disease that morphs into metastatic disease (178). Probasin-derived Tag expression is evident between 4 to 6 weeks of age, consequently mice develop mild to severe hyperplasia by week 12. By week 24 approximately 100% of the mice exhibit poorly differentiated and invasive tumours with metastasis observed predominantly in lymph nodes and lung (**Figure 1.12**). Castration of TRAMP mice at 12 weeks causes initial regression of the prostate, indicating androgen sensitivity. Approximately 20% of castrated mice are cured of their prostate cancer, the rest progress to poorly differentiated CRPC disease (192). The main benefits of using the TRAMP model are that it recapitulates disease progression, as seen in clinic from PIN to invasive carcinoma. This model produces reproducible metastatic lesions in proportion of the progeny (193). A characteristic of a T-antigen driven neoplastic model, such as TRAMP, is that they progress to a neuroendocrine phenotype. Extensive multi-focal neuroendocrine tumours are

A)

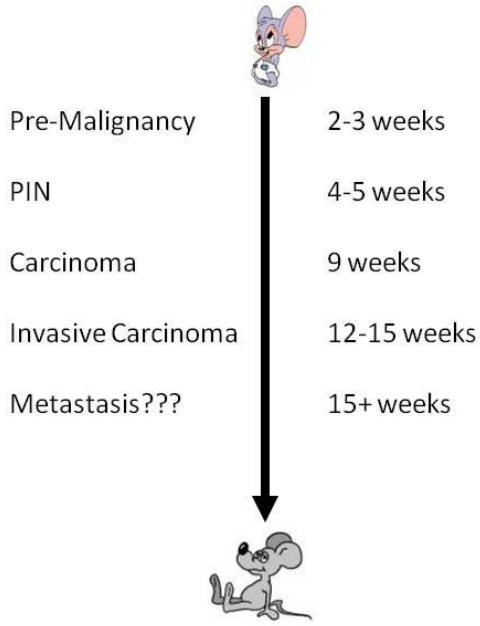

B)

Figure 1.11 Disease progression in PTEN$^{-/-}$ mice

(A) Summary of progression of prostate cancer in prostate specific PTEN$^{-/-}$ mice. Diagram is adapted from Wang *et.al* 2003) (189).

(B) Comparison of prostate size between two 15 week old mice. The left prostate is a representative picture of a control mouse PTEN$^{+/+}$, the right prostate is a representative picture of prostate-specific tumour-bearing PTEN$^{-/-}$ mice.

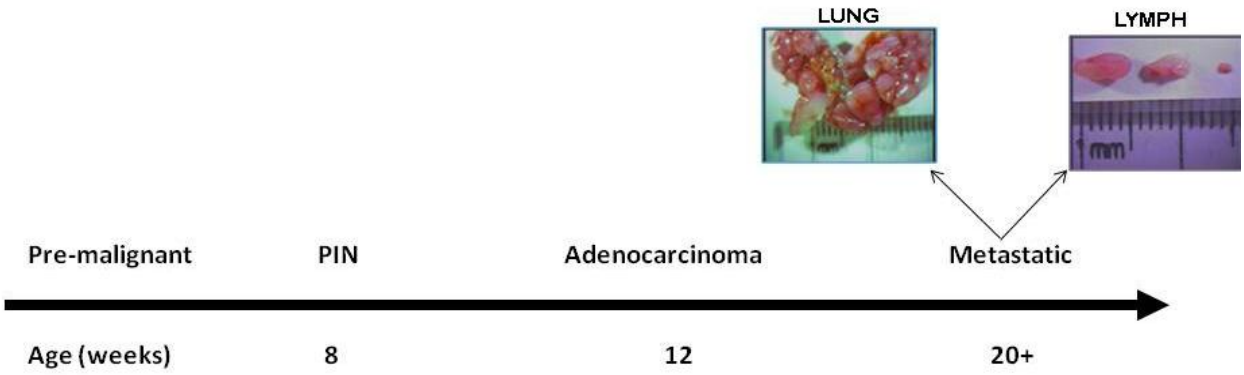

Figure 1.12 Disease progression in TRAMP mice

Prostate cancer disease progression is summarized from PIN formation to onset of metastatic lesions in TRAMP mice. Diagram is adapted from Varghese *et al.* 2007(194) .

rare in humans, and constitute 5-10% of all prostate cancers (195). This neuroendocrine phenotype has been associated with more advanced cancer (196).

1.7 Thesis rationale and objectives

Prostate cancer remains a significant health issue for Canadian men. The Canadian Cancer Society predicts 1 in 7 men will develop prostate cancer throughout his life time (26). Although there are curative treatment options for localized disease, almost half of these men will not be cured through common treatments such as radiotherapy or surgery (27). Our current treatment options for patients with metastatic and advanced prostate cancer are largely palliative and non-curative. Patients with advanced metastatic disease on average have a life expectancy of ~18 months (32, 34, 35, 197). These staggering statistics highlight the importance of research for alternative treatment options such as use of viral therapy. Given the location of the prostate and the various routes to access this gland, it lends itself as a good candidate for viral gene therapy. Recently, oncolytic viruses have been tested for their anti-tumour targeting capabilities, and series of clinical trials for treatment of prostate cancer have been conducted (129). Results of these trials have indicated that while viral delivery is relatively easy, viral efficacy remains limited. Moreover, the animal models used in previous studies (109, 110, 130, 151, 198-200) included predominantly xenografts tumour-bearing mice; these models do not mimic organ-based prostate cancer as it develops in humans. It is hence important to use animal models that develop prostate cancer in an organ-confined manner (e.g. TRAMP, prostate-specific $PTEN^{-/-}$). Thus, the overall objective of this thesis is to test the efficacy of a previously unused oncolytic virus (VSV) in targeting and destroying malignant cells, while sparing normal cells in prostates tumours of transgenic mice.

The hypothesis to be tested in this thesis is that viral gene therapy can be utilized as a reliable method of treating advanced prostate carcinoma in pre-clinical animal models. More specifically, the use of VSV oncolytic virus can efficiently and selectively kill prostate adenocarcinoma cells over normal cells in mouse models that mimic human

prostate cancer development. Accordingly, in order to test this hypothesis, the following specific objectives were devised:

Aim 1: To determine whether VSV (AV3) can infect and selectively kill the prostate tumors of PTEN$^{-/-}$ mice while sparing control prostates tissue (Chapter 2).

Aim 2: To determine whether VSV (AV3) can find and infect metastatic cancer cells using the Transgenic Adenocarcinoma Mouse Prostate cancer model (TRAMP) (Chapter 3).

In addition a third aim was devised for future use in enhancement of efficacy of oncolytic viruses:

Aim 3: To construct and test (*in vitro* and *in vivo*) novel viral vectors containing complex 5'UTR sequences to target prostate tumour cells with elevated eIF4E levels, so that these vectors maybe used in the future for selectively destroying malignant cells *in vivo* (Chapter 4).

The first objective of this project was completed by injecting enhanced interferon-sensitive VSV(AV3), intra-prostatically into tumour-bearing PTEN$^{-/-}$ and control mice and then monitoring for infectivity, apoptosis, and immune response. Bioluminescence analysis showed that VSV(AV3) dispersed throughout the body of each group after only 3 h, and persisted at high levels > 72 h in PTEN$^{-/-}$ mice but at relatively low levels and for only ~48 h in controls. Plaque assay provided a similar pattern, with much higher concentrations of replicating virus in prostates of PTEN$^{-/-}$ mice than in controls. Apoptotic analyses by TUNEL staining revealed that VSV(AV3) was able to selectively infect and kill prostate cells in PTEN$^{-/-}$ mice, while sparing normal cells in control mice. These results suggested that control of locally advanced prostate cancer may be achieved through intra-prostatic injection and amplification of a safe oncolytic virus, such as VSV(AV3).

The second objective was completed through intra-prostatic injection of VSV(AV3) into both control mice and the TRAMP metastatic prostate cancer model. Distribution, infectivity,

apoptosis, and status of the innate immune response were evaluated at the site of viral injection (prostate) and in the metastatic lesions (lymph nodes). Bioluminescence analysis showed that VSV(AV3) persisted in the prostate region of TRAMP at high levels up to 96 h but at relatively low levels and only for 48 h in controls. Plaque analysis depicted a similar viral distribution, with higher concentration of live virus found in TRAMP prostates compared to control. Additionally, an abundance of live virus was discovered in the lymph nodes and lung tissues, both of which are reported sites of metastatic lesions in TRAMP mice, while no virus was seen in the control mice (178). These data were corroborated by immunohistochemical staining of prostate and lymph node tissues with VSV antibody. Apoptotic analyses by TUNEL staining revealed that VSV(AV3) was able to infect and kill metastatic cells in the lymph nodes of TRAMP mice, while sparing normal cells in control mice. However, there was evidence of IFN activation in the metastatic lymph nodes. Overall, these results suggested that intra-prostatic injections of VSV(AV3) may be used for treatment of advanced metastatic prostate cancer.

The third aim was constructed to test possibility of using over-expression of eIF4E in prostate cancer cells. Three different lengths of 5'-untranslated regions (5'UTRs) derived from either fibroblast growth factor-2 (FU-FGF2-GW) or ornithine decarboxylase (FU-ODC_{149}-GW and $FUODC_{274}$-GW) were inserted upstream of the enhanced green florescence protein gene (GFP) in a lentiviral backbone. Both non-malignant control (PNT1B and BPH-1) and neoplastic (LNCaP, C4-2, DU145 and PC-3) prostate cell lines were transfected with each plasmid alone or in the presence of siRNA against eIF4E and their expression was monitored via GFP protein levels. Two 5'UTRs (FU-FGF2-GW and FU-ODC-GW) were selected as being most sensitive to eIF4E status. Lentiviruses containing these sequences were injected directly into the prostates of $PTEN^{-/-}$ (tumour-bearing) and control mice. Immunofluorescence data and Western blot analyses determined that a lentivirus containing a 5'UTR derived from FGF-2 was the best candidate for directing selective gene expression in the prostate tumours of $PTEN^{-/-}$ mice *in vivo*. This study demonstrated that judicious selection of a complex 5'UTR can enhance

selective targeting of viral-based gene therapies for prostate cancer. In the future, the FGF-2 derived 5'UTR can be inserted into viral genome of VSV(AV3) to enhance targeted killing of *in vivo* prostate adenocarcinomas.

Overall, this thesis demonstrates that VSV(AV3) is able to selectively target and kill prostate cancer cells in $PTEN^{-/-}$ mice. Thus, suggesting that intra-prostatic injection of VSV(AV3) can be used for control of locally advanced human prostate cancer. In addition, VSV(AV3) is capable of finding, infecting, and killing metastatic lesions found in the TRAMP mice. However, it is evident that some malignant cells are capable of mounting an innate immune response against VSV(AV3) through production of IFNs. Therefore, other markers of malignancy, such as over-expression of eIF4E, can be used in future to further harness toxicity of VSV(AV3) to cancer cells.

2. Oncolysis of prostate cancer induced by vesicular stomatitis virus in PTEN knockout mice[1]

2.1 Introduction

The high incidence of prostate cancer in men over 50, coupled with the rapidly aging North American male demographic, highlight the need for better management and treatment of this cancer (25). Although there are some curative treatment options for early staged non-invasive prostate cancer, not all patients are cured. Moreover, the majority of treated patients suffer from side effects that seriously compromise their quality of life (27, 201-204). In recent years the use oncolytic viral therapy has become a valid treatment option for prostate cancer and a series of clinical studies have been conducted. To broaden our preclinical understanding and increase the variety of oncolytic viruses for prostate cancer treatment, we have conducted series of experiments using Vesicular Stomatitis Virus (VSV).

VSV is an oncolytic virus which can infect and kill cells that have defects in their cellular anti-viral, namely the IFN, response. The use of this virus is advantageous since, large titres of VSV can easily be generated. The majority of the human population does not have neutralizing antibodies against VSV and rare cases of human infection have been either asymptomatic or accompanied with mild flu-like symptoms. Previous studies have demonstrated VSV's preference for infection of tumour cells compared to normal cells. It has been shown that deletion of methionine at position 51 in the matrix (M) protein of VSV renders it more susceptible to the host innate immune response (160). This deletion causes the virus to be safely cleared from normal cells, while maintaining its ability to destroy malignant cells, thereby making VSV(AV3) more cancer specific (122, 160, 205, 206). Recent findings have demonstrated that IFN-response genes are involved in the pathogenesis of prostate cancer, such that down

[1] A version of chapter 2 has been published. Moussavi M, Fazli L, Tearle H, Guo Y, Cox M, Bell J, Ong C, Jia W, Rennie PS. (2010). Oncolysis of prostate cancers induced by vesicular stomatitis virus in PTEN knockout mice Cancer Research. Feb 15; 70(4):1367-76.

regulation of IFN-inducible genes were observed in approximately 30% of clinical samples (171, 172).

Transplantable human xenografts and transgenic mouse tumour models can be used to test new strategies for the treatment of prostate cancer. While use of xenografts are limited by the necessity of using immunecompromised animals and need for surgical implantation at orthotropic or subcutaneous sites, transgenic mouse tumour models offer several key advantages for pre-clinical testing, including: the cancer arises *in situ* in the target tissue with the appropriate microenvironment, mice possess an intact immune system, cancers are frequently heterogeneous, and by arising *de novo*, undergo neoplastic progression similar to that seen in human cancers (178, 188, 189). One such transgenic model for prostate cancer is the pbARR2x $PTEN^{fl/fl}$ mouse or prostate-specific PTEN null mice ($PTEN^{-/-}$), which leads to *de novo* formation of prostate tumours. The disease progression of $PTEN^{-/-}$ mice to prostate cancer is similar to that seen in humans (188, 189). Deletion or mutation of the tumour suppressor PTEN gene has been implicated in many human cancers and has been seen in up to 30% of primary prostate cancers and over 64% of prostate metastases, making PTEN an important candidate gene for prostate cancer development and progression (188, 189, 207, 208).

The goal of this study was to determine whether VSV (AV3) can differentially infect and kill the prostate tumours that arise in the $PTEN^{-/-}$ mouse. Our results indicate that this virus is able to selectively infect, replicate, and increase apoptosis in malignant tissue while sparing normal tissue, due to a faulty IFN response. Furthermore, cell death is not a by-product of neutrophil infiltration as previously reported in other cancer models (209)

2.2 Material and methods

2.2.1 Cell culture

RWPE-1, LNCaP, PC-3 and Vero cells were purchased from the American Type Culture Collection. RWPE-1 was maintained in keratinocyte serum-free medium (K-SFM) (Invitrogen) supplemented with bovine pituitary extract and human recombinant epidermal growth factor. LNCaP, PC-3 cells were maintained in RPMI, while Vero cells were maintained in DMEM medium (Invitrogen). All cell lines were supplemented with 10% fetal bovine serum (FBS) (Invitrogen) and 100 units/ml penicillin/streptomycin. MPPK-1 cells are prostate epithelial cells derived from $PTEN^{-/-}$ mice (**Figure 2.1**).

2.2.2 Viral propagation

VSV(AV3), a recombinant IFN-inducing mutant of the Indiana serotype , was propagated in Vero cells. VSV(AV3) was constructed to express the GFP-firefly luciferase fusion gene as previously described (122). Virons were collected and purified as previously described (210). Plaque forming units (pfu) were counted and used for calculating infectious titres (122, 209, 210).

2.2.3 *In vitro* cell proliferation assay

Briefly, RWPE-1, LNCaP and MPPK-1 cells were plated into 96-well plates at a 1 x 10^4 cells/well density. Cells were grown for 24 h, stimulated with universal type I IFN (PBL Biomedical Laboratories) for 16 h and then challenged with VSV(AV3) at multiplicity of infection (MOI)= 1.0 pfu/Cell for LNCaP and MPPK-1 and MOI= 100 pfu/Cell for RWPE-1. MTS[3-(4,5-dimethylthiaol-2-yl)5-(3-carboxymethoxyphenyl)-2-(4-sulphophenyl)-2H-tetrazolium (250µg/ml) inner salt] (Promega) and 20 µg of PMS (Gibco) solutions were mixed together and added to each well for 2 h. Colorimetric analysis was carried out using an ELISA plate reader at an absorbance of 490 nm (211).

2.2.4 Western blot analysis

Cell lysates, prepared in a lysis buffer (50 mM Tris HCI, pH 7.5,150 mM NaCl, 1% NP40 and 5 mM EDTA) in the presence of a protease and phosphatase inhibitor cocktail (Sigma, St Louis, MO),containing equivalent amounts of protein (60 µg), were resolved using 10% SDS–PAGE and transferred on to a nitrocellulose membrane using Bio-RAD transblot apparatus at 350 mA for 90 min. The nitrocellulose membrane (Gibco) was then blocked with Odyssey blocking buffer for 45 min and stained with primary antibodies to PARP (Cell Signalling), Caspase 3 (Cell Signalling), PTEN (Cell Signalling), E-Cadherin (Cell Signalling), N-Cadherin (Cell Signalling), Androgen Receptor (AR) (Santa Cruz), Actin (Cell Signalling), and Vinculin (Cell Signalling) at a dilution of 1:1000. Protein expression was shown by IRDye 800CW goat anti-mouse or goat anti-rabbit IgG and scanned on an Odyssey scanner (LI-COR Biosciences, Lincoln, NE).

2.2.5 Prostate-specific PTEN$^{-/-}$ mouse tumour model

To generate prostate specific PTEN$^{-/-}$ mice, the ARR2probasin-Cre transgenic line, a gift from Dr. P. Roy-Burman (University of Southern California) (188), were crossed in-house with PTEN $^{flox/flox}$ mice from Dr. Tak Mak (University of Toronto) (212). To confirm PTEN deletion in the offspring mice, genomic DNA was removed from tail clips of F2 offspring and tested by PCR using PTEN^{flox} and Cre specific primers. For this study, all mice used were 15 weeks of age.

2.2.6 *In vivo* studies

A small incision was made in the abdomen of PTEN$^{-/-}$ male mice and 100 µl of VSV(AV3) at 5 x 10^8 pfu/ml was delivered by intra-prostate injection. For quantification of viral uptake and distribution, animals were injected through the intra-peritoneal (i.p.) route with 150 mg/kg luciferin (Xenogen) at 3, 6, 24, 48, 72 and 96 h post-viral inoculation and imaged with an IVIS100 Imaging System (Xenogen). Data was analyzed using Living Image 2.50 (Xenogen) software. At least three mice per group were sacrificed at indicated time points. Organs (kidney,

liver, lung, prostate and spleen) were extracted and either fixed in 10% buffered formalin and paraffin-embedded or snap-frozen in liquid nitrogen. Animal procedures were performed according to the Canadian Council on Animal Care guidelines and approved by local (University of British Columbia) Animal Care Committee.

2.2.7 Titration of VSV from infected tissue

Tissues were removed at indicated time points, weighed and homogenized in 1ml PBS using a Polytron homogenizer. Serial dilutions were prepared in serum-free media and added to confluent Vero cells for 60 min. Cells were subsequently overlaid with 1% methyl cellulose (Sigma) and plaques were grown for 48 h. Infected Vero cells were then fixed in 4% formaldehyde and stained with crystal violet. Plaques were counted by visual inspection, and titers were calculated as pfu/ml (213, 214).

2.2.8 Immunohistochemical staining

Five micrometer sections were prepared from paraffin-embedded tissues and tissues were extracted from paraffin as described previously (215). TUNEL (Terminal deoxynucleotidyl transferase dUTP nick end labelling) assays were performed according to company instructions (ROCHE). Tissues were stained with primary antibody at the following dilutions Ki67 (1:100), IRF-3 (1:50), IRF-7 (1:75), IFNR1 (1:1000), RNaseL (1:1000), neutrophil (1:50) and CD68 (1:100). All antibodies were purchased from abcam with exception of IFNR1 which was purchases from PBL. All sections were reviewed by a pathologist and scored blinded.

2.2.9 Quantitative real-time PCR

Total RNA from mouse tissue was isolated using the Trizol method (Invitrogen), and reverse transcribed and amplified with IFN-α/β primers (174) on an Applied Biosystems 7900HT Fast Real-time PCR System following the SYBR Green PCR Master Mix protocol. Relative quantification of gene expression was performed using ribosomal RNA as control.

2.2.10 Statistical analysis

GraphPad InStat 3 was used for all statistical analyses. Results are expressed as mean ± standard deviation unless otherwise noted. $P < 0.05$ was considered statistically significant. To measure statistical differences between mice stained tissues, the non-parametric Wilcoxon-rank test was used, as there was no assumption of a normal distribution of scores.

2.3 Results

2.3.1 VSV(AV3) cytotoxicity in prostate cells in vitro

MTS assay was used to assess the effect of VSV(AV3) infection on the viability of prostate cells propagated *in vitro*. Two human cell lines representing normal prostate epithelial (RWPE-1) and prostate cancer cells (LNCaP) were tested, as well as a mouse cell line (MPPK-1) (**Figure 2.1**) derived from prostatic tissue of $PTEN^{-/-}$ mice (**Figure 2.2**). The results demonstrated that there was an approximate parallel relationship between cell death and increasing viral titer over a 24 h period for all three cell lines. However, VSV(AV3)'s induction of cell death at a given viral titer was significantly higher in MPPK-1 and LNCaP cells compared to RWPE-1 normal prostate epithelial cells ($p < 0.05$), suggesting that there was preferential killing of cancer cells by this virus (**Figure 2.2A**). In addition, Western blot analysis of control, RWPE-1, and prostate cancer, MPPK-1, cell lines has shown that treatment with VSV(AV3) led to reduction of pro-caspase 3 and pro-PARP proteins in MPPK-1 cells, which further demonstrates that these cells undergo apoptotic cell death (**Figure 2.3**).

VSV is known to be sensitive to IFN and the mutant AV3 strain has been shown to be even more IFN-sensitive (122, 205, 206). To test this in our system, LNCaP, RWPE-1 and MPPK-1 cells were pre-incubated for 16 h with increasing doses of universal type I IFN prior to being challenged with VSV(AV3). Pre-incubation of cells with (10,000 IU/ml) IFN led to increased cell viability in the RWPE-1 cells. However, in $PTEN^{-/-}$ derived MPPK-1 and LNCaP prostate cancer cells, there was no significant difference in cell death followed pre-treatment with IFN (**Figure 2.2B**). This demonstrated that the VSV(AV3) strain is highly sensitive to IFN response in normal prostate epithelial cells (RWPE-1), and only partially in MPPK-1 cells (**Figure 2.4**).

2.3.2 Viral distribution after intra-prostatic injections of VSV(AV3) virus into PTEN$^{-/-}$ and control mice

In vivo studies were performed to determine VSV(AV3) distribution in both prostate-specific PTEN$^{-/-}$ transgenic mice and control mice. PTEN$^{-/-}$ and normal control mice were injected intra-prostatically with 100 µl of 5x10^{8} pfu/ml of VSV(AV3) or UV-inactivated virus (UVI) (209, 216). Viral distribution was monitored by i.p. injection of luciferin followed by bioluminescence measurement over a 3-96 h time period (**Figure 2.5**). Initially after VSV(AV3) infection, viral distribution was seen in the lung and abdomen regions, indicating viral spread in the body. The strongest prostate – localized signal was detected at 3 h post-inoculation with a 6-fold increase in bioluminescence detected in PTEN$^{-/-}$compared to control mice. In control mice, the prostate-localized signal decayed approximately 40% at 24 h post injection and only trace amounts of bioluminescence were detected at > 48 h (**Figure 2.5 A and C**). However, in PTEN$^{-/-}$ mice, a substantial bioluminescence signal was sustained 72 h post injection, with 18-fold higher bioluminescence intensity measured in comparison to control mice (**Figure 2.5 B and C**). These results demonstrate that there was a higher initial expression and a greater persistence of VSV(AV3) in the tumour-bearing PTEN$^{-/-}$ relative to control mice.

After administration of the same amount of VSV(AV3) by the intra-venous (i.v.) route, the virus was diluted and not clearly detectable. In all cases, VSV(AV3) was sequestered to the spleens of both control and PTEN$^{-/-}$ mice, with only a small amount of bioluminescence detected in ~50% of the prostates of PTEN$^{-/-}$ animals (data not shown). Hence, by injecting virus directly into the prostates of PTEN$^{-/-}$ mice, there was an apparent amplification of viral load which led to a distribution of virus throughout the body.

2.3.3 Presence of live virus in prostatic tissue of PTEN$^{-/-}$ mice

To determine whether the observed bioluminescence data correlated with the presence of infectious virus, at 3-96 h post-injection PTEN$^{-/-}$ and control mice were sacrificed and their

organs (prostate, spleen, lung, liver, and kidney) were harvested and frozen. Homogenized tissues were titrated by plaque assay (209) to quantify viral delivery and replication within various tissues. Within 3 h after VSV(AV3) injection in PTEN$^{-/-}$ mice (**Figure 2.6A**), viral titre was highest in prostate (13.0±1.5 Log pfu/g) followed by spleen (4.3 ± 0.7 Log pfu/g) and lung (2.3 ± 0.3 Log pfu/g), with no virus detected in liver and kidney. Live virus in the lung reached its highest point (3.7 ± 0.9 Log pfu/g) at 24 h post intra-prostatic injection, while in the spleen the viral titer declined and was no longer detectable by 48 h. By comparison, viral titer in the prostate at 24 h was slightly reduced (11.7 ± 0.9 Log pfu/g) but dramatically increased at 48 h (30.3 ± 1.5 Log pfu/g), suggesting viral replication and amplification in the prostate tissue of these mice. After 72 h, there was a marked decline of live virus (1.30 ± 0.33 Log pfu/g) in the prostate. In liver and kidney, there was no virus detected at any time, suggesting that these organs were not readily infected or able to support live virus.

In control mice (**Figure 2.6B**), VSV(AV3) was present in both prostate (9.5 ± 0.9 Log pfu/g) and spleen (8.7 ± 1.7 Log pfu/g) at 3 h after injection, but not in the liver or kidneys. By 24 h, this initial level of virus was maintained in the prostate (9.1 ± 1.8 Log pfu/g), but declined at 48h (4.4 ± 1.2 Log pfu/g) and at 72h (1.9 ± 0.9 Log pfu/g) until eventually no virus was detected. This decline in prostate virons is seen earlier in control mice in comparison to PTEN$^{-/-}$ mice. These results demonstrate that there was enhanced amplification, viral spread, tissue distribution, and persistence of high levels of prostatic VSV(AV3) infection in PTEN$^{-/-}$ mice prostates relative to control animals. Also, there was a higher level of VSV(AV3) detected initially (3 h) in the spleen of control (8.67 ± 1.67 Log pfu/g) mice in comparison to PTEN$^{-/-}$ mice (4.3 ± 0.9 Log pfu/g), possibly indicating that the control mice sequester the virus for clearance in their spleen. This difference is no longer detectable by 24 h post-infection with (1.67 ± 0.9 Log pfu/g) in control mice compared to (1.7 ± 0.3 Log pfu/g) in PTEN$^{-/-}$ mice. The plaque assay was validated using real time quantitative PCR analysis of viral RNA in the organs of both PTEN$^{-/-}$and control mice relative to UVI VSV(AV3)-treated tissues (**Table 2.1**).

2.3.4 VSV(AV3) causes preferential killing of prostate cancer cells *in vivo* while sparing normal prostate tissue

The difference between viral levels and persistence in the prostates of PTEN$^{-/-}$ and control mice led us to assess whether the virus was preferentially infecting and killing tumour cells. To test this, VSV(AV3) infected prostate tissue from both PTEN$^{-/-}$ and control mice were collected at various time points, embedded in paraffin and evaluated for apoptosis by TUNEL assay (**Figure 2.7A**). There was a substantial increase in apoptotic cell bodies observed in the prostates of VSV(AV3)-treated PTEN$^{-/-}$ mice compared to virus treated controls, where virtually no change in apoptosis was observed (**Figure 2.7B**).

To see the effect of VSV(AV3) infection on cell proliferation, prostate tissues were stained with Ki67 (proliferation marker) and positive cells were counted (**Figure 2.7C and D**). Although there was consistently higher proliferation seen in PTEN$^{-/-}$ prostates compared to control, there was no significant difference in proliferation detected post VSV(AV3) infection. This increase in apoptosis and lack of difference in proliferation in the tumour-bearing mice correlated with the increased viral titre previously noted (**Figure 2.6B**); indicating that active infection of tumour cells with VSV(AV3) is the cause of this increased apoptosis.

2.3.5 Viral-induced cell death *in vivo* is not associated with neutrophil infiltration in the PTEN$^{-/-}$ tumour model

Previous reports on VSV infection using a non-transgenic mouse model indicated that viral delivery was blocked by vasoconstriction and that cell death was associated with neutrophil infiltration (209, 217), implying that tumour cell death was a consequence of a neutrophil-mediated immune response rather than direct viral oncolysis. To test whether this was also the prevalent cell-death mechanism in the endogenous, non-transplanted tumours that arise in our PTEN$^{-/-}$ model, prostate tissue was collected post-VSV(AV3) infection at various time points, stained for the presence of a repertoire of host immune cells, and then evaluated by a

pathologist. **Figure 2.8** shows that in both PTEN$^{-/-}$ and control mice prostates, there was an initial rise in neutrophil cells as compared to untreated and UVI treated prostates. However, this peak in neutrophil penetration at the 6 h time point was not significantly different ($p > 0.05$) between tumour-bearing (23 ± 6 cells/time point) and control mice (30 ± 7 cells/time point) and this peak quickly diminished by 24 h in both and PTEN$^{-/-}$ mice (10 ± 6 cells/time point) and controls (8 ± 4 cells/time point). These results suggest that the differences seen in apoptosis (**Figure 2.7**) are not correlated with neutrophil infiltration (**Figure 2.8A**).

When prostate tissues of PTEN$^{-/-}$ and control mice were stained for the presence of macrophages, which like neutrophils are phagocytic, there was a marked increase in their number at 24 h (79 ± 21 cells/time point) and at 72 h (72 ± 28 cells/time point) in PTEN$^{-/-}$ mice, but almost undetectable and unchanged number of macrophages was seen in the control prostate tissue (**Figure 2.8B**). This macrophage increase may reflect a response to the increasing number of apoptotic tumour cells for which macrophages are recruited to carry out phagocytosis.

2.3.6 Effects of VSV(AV3) on IFN pathway *in vivo*

Since VSV infection leads to activation of the IFN response pathway expression, prostates of control and PTEN$^{-/-}$ mice challenged with VSV(AV3) infection were stained for various components of the IFN pathway such as interferon receptor-1 alpha (IFNR-1α) , ribonuclease L (RNase L) , interferon regulatory transcription factors 3 (IRF-3) and 7 (IRF-7) (**Figure 2.9A**). Immunohistochemical analysis of the prostates of control mice post VSV(AV3) injection demonstrates an increase in staining of all of the mentioned IFN pathway components, demonstrating that there is an intact initial IFN response towards the virus in the prostate tissues of control mice. However, in PTEN$^{-/-}$ prostates, there was no change observed over time in any of the IFN pathway components as scored by a pathologist. This correlates with the

increase propagation of virus as seen over time in prostate tumours of PTEN$^{-/-}$ mice (**Figure 2.6A**).

Additionally, mRNA levels of IFN-α present in prostate tissues of VSV(AV3) infected PTEN$^{-/-}$ and control mice were checked and compared by qPCR analysis. **Figure 2.9B** demonstrates that in control prostates treated with VSV(AV3), there is an approximately 500-fold increase in IFN-α mRNA levels by 48 h. However, in PTEN $^{-/-}$ prostates treated with virus at the same time point there is only an approximately 40-fold increase in IFN-α mRNA levels. These data suggest that there is a partial IFN response to viral infection in PTEN$^{-/-}$ mice that permits further viral infection and oncolysis of tumour cells (**Figure 2.6A**).

2.4 Discussion

The goal of any viral therapy for treatment of cancer is to efficiently kill primary and metastatic cancer cells, while sparing normal cells (218, 219). Prostate cancer is a good candidate for viral therapy since there are various technically easy routes (e.g. trans-urethral, trans-perineal and trans-rectal) for viral delivery (220). Here the effect of oncolytic virus VSV(AV3), which replicates in IFN defective cells, has been studied in the prostate-specific $PTEN^{-/-}$ mice model (189). Studies show approximately 75% of tumour cells and 30% of prostate cancer tumours have a defective IFN response, making VSV a useful tumour-selective therapy (172, 221, 222). Additionally, since the primary hosts of VSV are rodents, cattle, horses and swine, patients living in non-endemic areas do not have neutralizing antibody titres to the virus. VSV rarely infects humans and, in rare cases of infection, presents mild flu-like symptoms, making VSV (AV3) a relatively safe therapeutic agent (223, 224).

To show that VSV(AV3) was able to infect human and mouse prostate cell lines, three cell lines representing normal prostate epithelial cells (RWPE-1), human prostate cancer cells (LNCaP) and mouse prostate cancer cells, (MPPK-1) were tested. As shown in **Figure 2.2**, there was a direct correlation between increased viral titre and decreased cell survival in $PTEN^{-/-}$ derived cell lines (**Figure 2.1**) compared to non- neoplastic control cells. These results are consistent with the findings of others (210, 225), although the effects of VSV(AV3) on RWPE-1 and MPPK-1 cells have not been previously shown. Furthermore, the lack of dose response seen post viral infection may be a result of rapid viral replication, which can lead to the presence of an excess amount of virus, even in conditions with a low MOI of 0.001 at 24 h.

An underlying assumption for using VSV(AV3) for viral therapy is that tumour cells have a defective antiviral host response, specifically in activation of the interferon pathway. To test this, both prostate cancer cell lines (LNCaP and MPPK-1) and non-cancerous prostatic cells (RWPE-1) were pre-treated with IFN. Our results (**Figure 2.2B**) indicated that due to a defective IFN response, there was no change in the death of prostate cancer cells (LNCaP and

MPPK-1), whereas pre-treatment of RWPE-1 normal prostate epithelial cells with IFN led to an increase in cell survival. These results confirm previous reports that the mutated M(matrix)-protein in VSV can restrict its infectivity to cancer cells with a malfunctioning IFN response (122, 225).

It was evident from bioluminescence data that, after *in vivo* administration of VSV(AV3) via direct injection into the prostate, the virus is quickly distributed throughout the body (**Figure 2.5**). This phenomenon is seen in both control and PTEN$^{-/-}$ mice and, as expected, there is a higher viral infection in the prostate by 24 h, the original site of viral injection. Based on both luminescence and plaque assay data (**Figures 2.5 and 2.6**) the level of VSV(AV3) infection and replication in PTEN$^{-/-}$ mice is higher than that of non tumour-bearing control mice, with an amplification of viral load detected between 24-48h in PTEN$^{-/-}$ mice.

TUNEL staining of paraffin-embedded prostate tissue from control and PTEN$^{-/-}$ mice post-infection indicated high levels of apoptosis in tumour-bearing mice, with very low levels of apoptosis observed in control mice (**Figure 2.7**). Presence of apoptotic cells in control prostate at earlier time points may be due to a low level of viral killing (225) or the trauma of the injection process. The apoptotic cell count peaked at 48 h post infection in the prostates of PTEN$^{-/-}$ mice. Interestingly, by 96 h after infection, there was a decrease in apoptotic cells, together with morphological changes in the prostate tissue suggesting cell loss through apoptosis (**Figure 2.7**).

It has previously been reported that intra-tumour injection of VSV(AV3) in BALB/c mice with subcutaneous tumours leads to tumour cell death through an indirect mechanism, which was linked to neutrophil infiltration (209). Neutrophils originate from white blood cells, are phagocytic, and typically act as a first response to pathogens (226). To test this in our model, prostate tissues from both control and PTEN$^{-/-}$ mice, at various times following VSV(AV3) injection, were stained for neutrophils. Our results (**Figure 2.8A**) show that although there was some initial neutrophil infiltration in prostates of control and tumour-bearing mice, there is no evidence that

this increase in neutrophil presence correlated with an increase in cell death observed in PTEN$^{-/-}$ prostates. This indicates that neutrophil infiltration did not play a major role in VSV-mediated tumour cell death in the PTEN$^{-/-}$ model. However, with respect to other immune system parameters such as macrophages, there was a significant difference detected after VSV(AV3) injection (**Figure 2.8B**). Previous studies have shown that macrophages play an inhibitory role in viral replication by direct phagocytic clearance of viruses (227, 228). In the PTEN$^{-/-}$ model, an increase in macrophage infiltration occurred after a surge of viral replication, which takes place at 3 h and then again at 48 h after viral administration (**Figure 2.6A**), coincident with maximum apoptosis. Since one of the main functions of macrophages is to remove dead cells, this likely explains the increase in macrophage count between 48-72h post viral infection in these prostate tumours.

VSV infection of normal cells leads to production of IFN-α/β, a primary host innate defence system. IRF-3 and IRF-7 play key roles in transcription of IFN-α/β which upon production, signals neighbouring cells through IFN-R α/β (229). Binding of IFN-α/β to its receptor activates a new chain of reactions where eventually RNaseL is activated. Activated RNaseL degrades all RNA, thus causing inhibition of viral replication. Therefore, an increase in RNaseL, IRF-3, IRF-7 and IFN-Rα upon VSV infection was anticipated and confirmed in the case of control mice injected with VSV(AV3). This was further confirmed through qPCR analysis, demonstrating an increase in IFN-α mRNA levels (**Figure 2.9**). Conversely in tumour-bearing mice, there was no change detected in the IFNR-α, IRF-3, IRF-7, and RNaseL protein or IFN-α transcription levels upon viral infection. Thus, due to a disrupted IFN response in the PTEN$^{-/-}$ prostates, VSV(AV3) is able to infect cells and increase cell death (**Figure 2.7**).

In conclusion, we have found that in an immunocompetent host, intra-prostatic tumour VSV(AV3) injection enables viral replication and amplification sufficient to selectively kill cancer cells while sparing normal cells. The primary mechanism for cell kill is apparently apoptotic

oncolysis due to a defective IFN response, as opposed to neutrophil invasion as has been reported using xenograft models (209). These results suggest that control of locally advanced prostate cancer in humans (230) may be achievable through injection of a safe oncolytic virus, such as VSV(AV3), directly into a patient's prostate tumour.

2.5 Figures

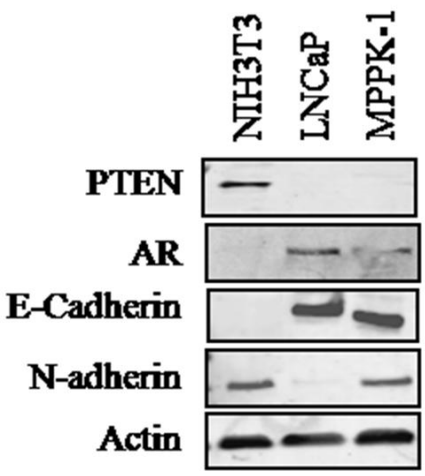

Figure 2.1 Characterization of MPPK-1 cells

60μg of whole cell lysates from NIH3T3, LNCaP and MPPK-1 cells were separated on SDS-page gel. Western blot analysis demonstrated that MPPK-1 cells lack PTEN, but are positive for AR, E and N-Cadherin, indicative that these are $PTEN^{-/-}$ derived mouse prostate neoplastic cells.

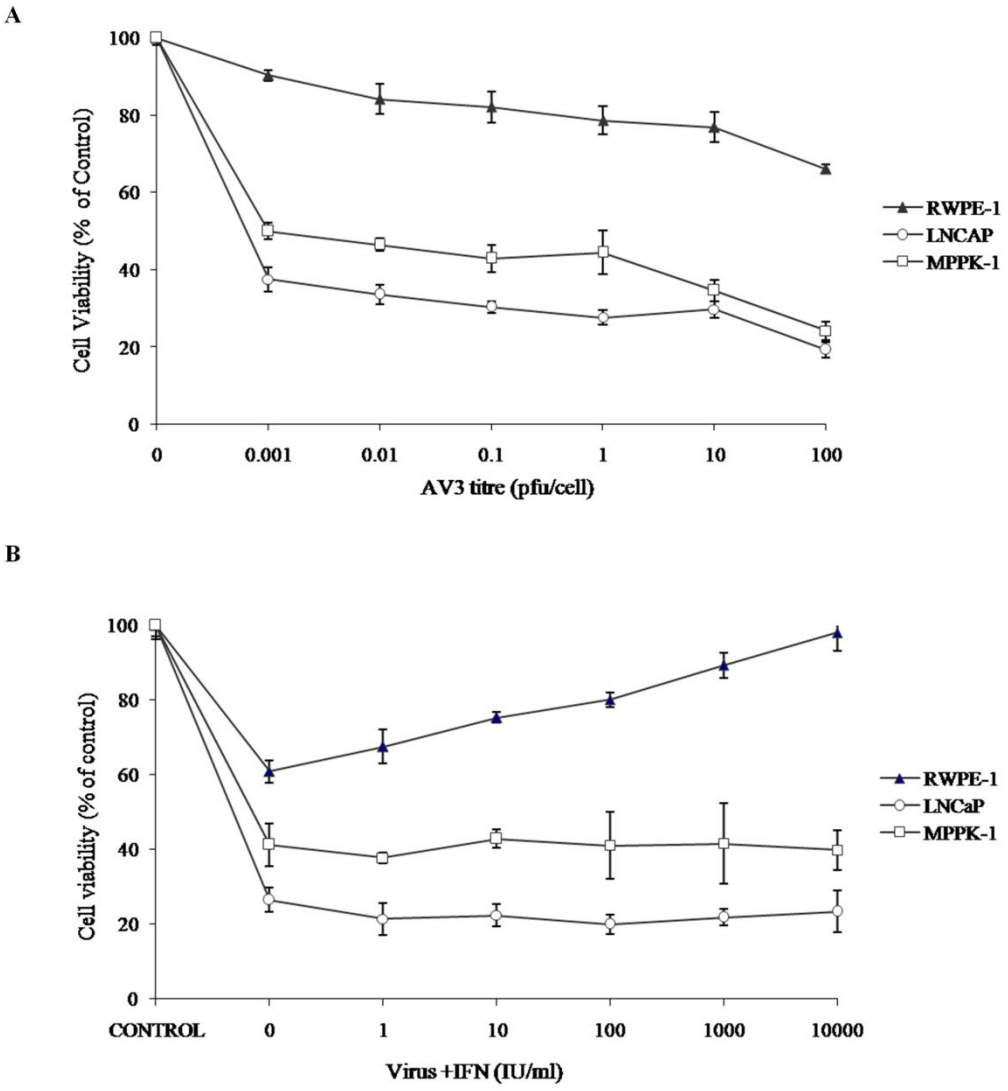

Figure 2.2 Effects of VSV(AV3) infection and IFN treatment on cell survival

(A) Cells were infected with increments of viral titre from MOI of 0-100 pfu/cell and MTS assays were performed 24 h after viral infection.

(B) Cells were pre-incubated with increasing concentrations of IFN (0-10,000 IU/ml) for 16 h and then challenged with VSV(AV3) at MOI of 1 (LNCaP and MPPK-1) and MOI of 100 (RWPE-1) for 24 h. Cell viability was measured by MTS assays 24 h post infection. Control represents untreated cells. Each graph is representative of three independent experiments with five replicates.

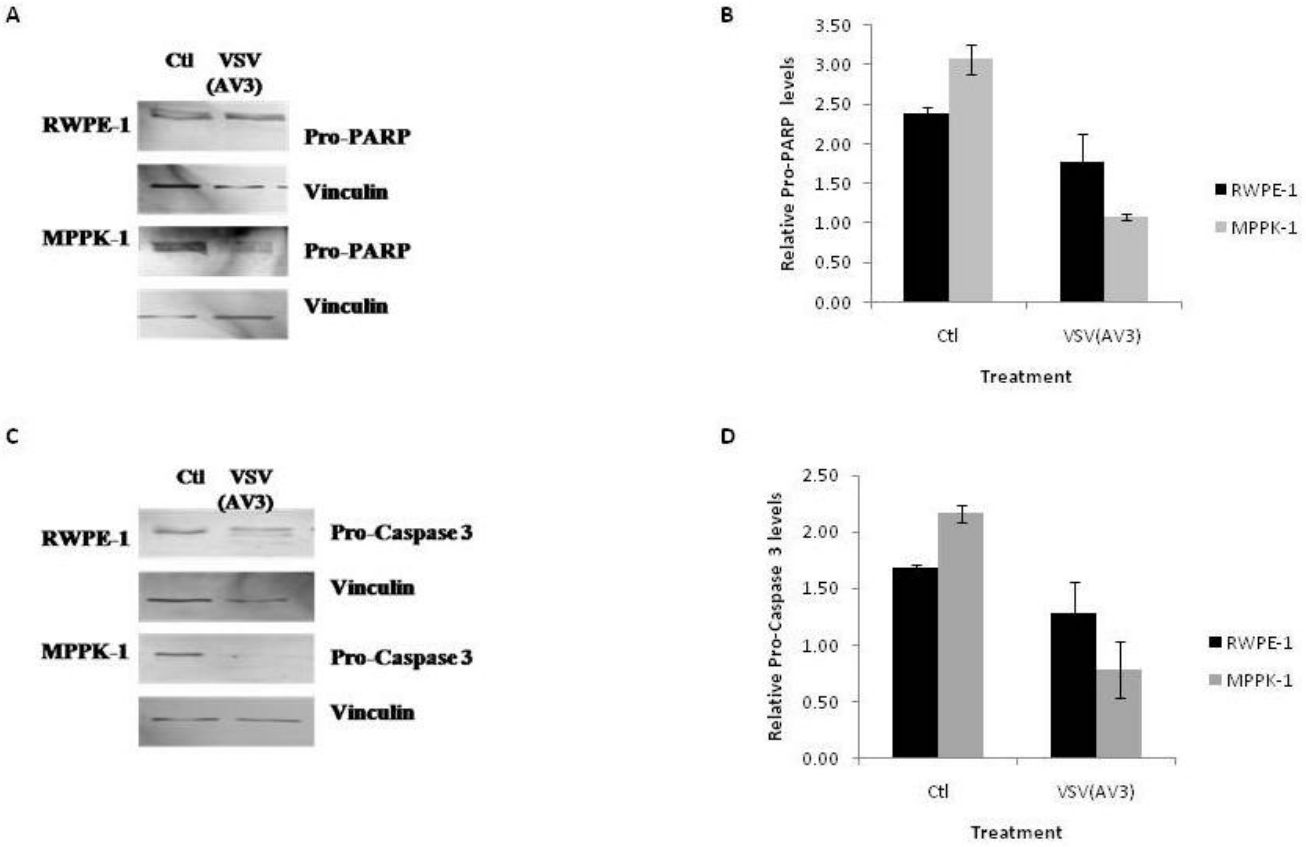

Figure 2.3 MPPK-1 cells undergo apoptosis upon infection with VSV(AV3)

(A) Western blot analysis demonstrating depletion of pro-PARP protein levels upon VSV(AV3) infection (MOI=1.0) demonstrating cell death occurs through apoptosis. (B) Quantification of pro-PARP levels expressed as mean ± SEM, n=2. (C) Western blot analysis demonstrating depletion of pro-Caspase 3 protein levels upon VSV(AV3) infection (MOI=1.0) demonstrating cell death occurs through apoptosis. (D) (B) Quantification of pro-Caspase 3 levels expressed as mean ± SEM, n=2.

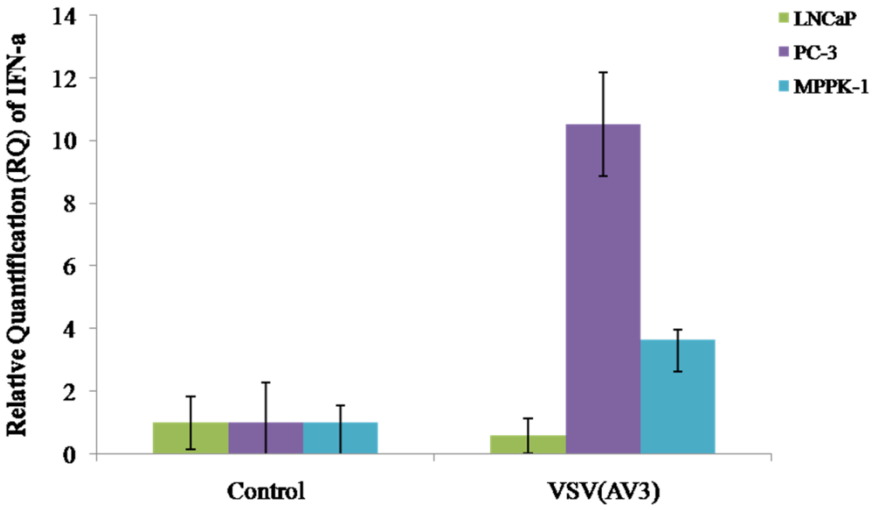

Figure 2.4 Levels of IFN-α mRNA post-VSV(AV3) infection

As shown previously, PC-3 cells are not easily infected by VSV(AV3) due to IFN-α response (225). LNCaP cells have also been previously shown to be susceptible to VSV(AV3) infection due to lack of IFN response. MPPK-1 cells derived from PTEN$^{-/-}$ seem to be partially resistant to VSV(AV3) as they produce low levels of IFN-α.

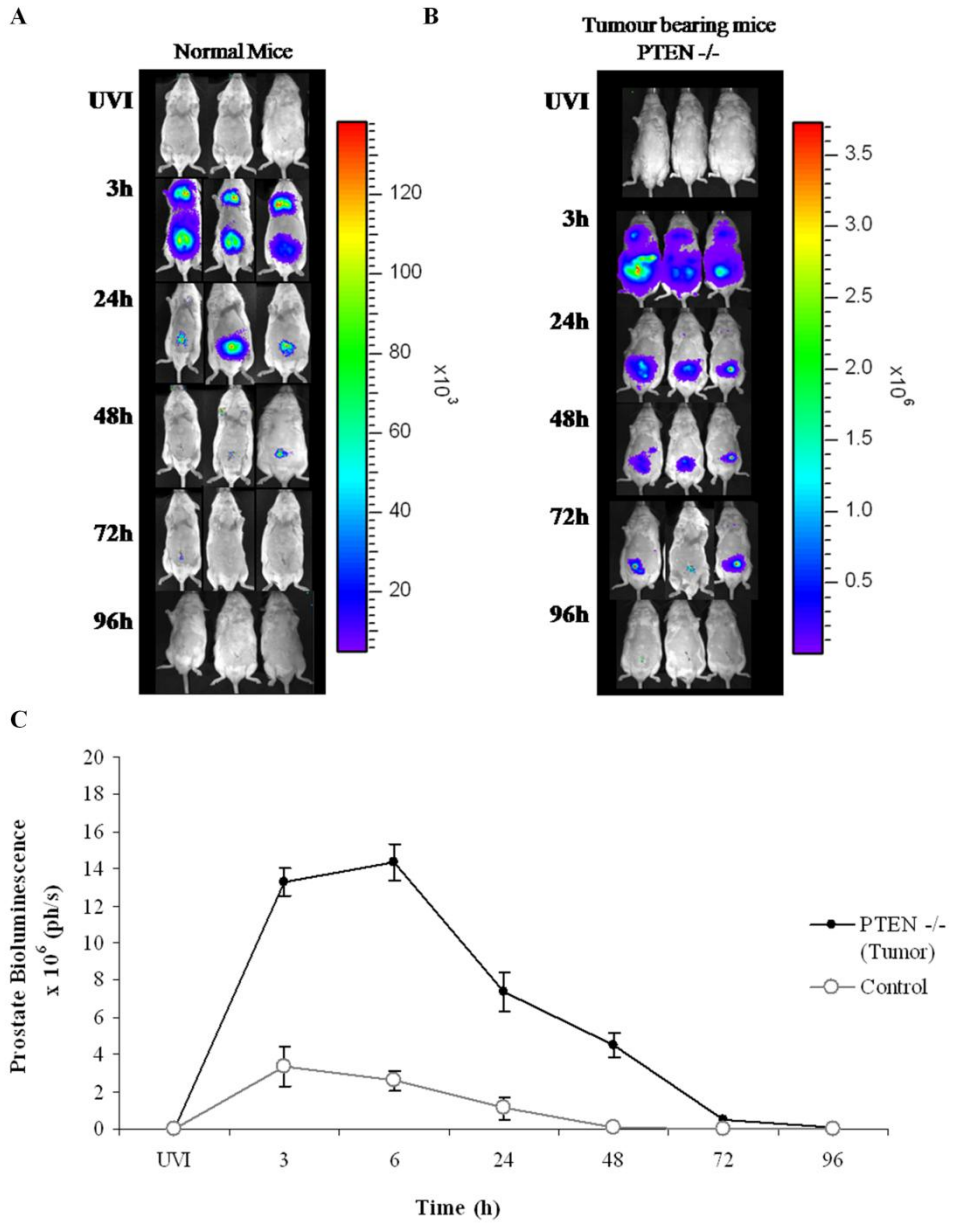

Figure 2.5 ***In Vivo*** **measurement of bioluminescence post-viral injection**

VSV(AV3) ($5x10^8$ pfu/ml) was injected directly into prostates of (A) control and (B) $PTEN^{-/-}$ mice. Viral distribution was tracked by i.p. injections of luciferin (150 mg/kg) over time (3-96 h); UVI was used as control over a 96 h time period. (C) Bioluminescence in the prostate regions of control and $PTEN^{-/-}$ mice presented as mean ± SEM (n = 3).

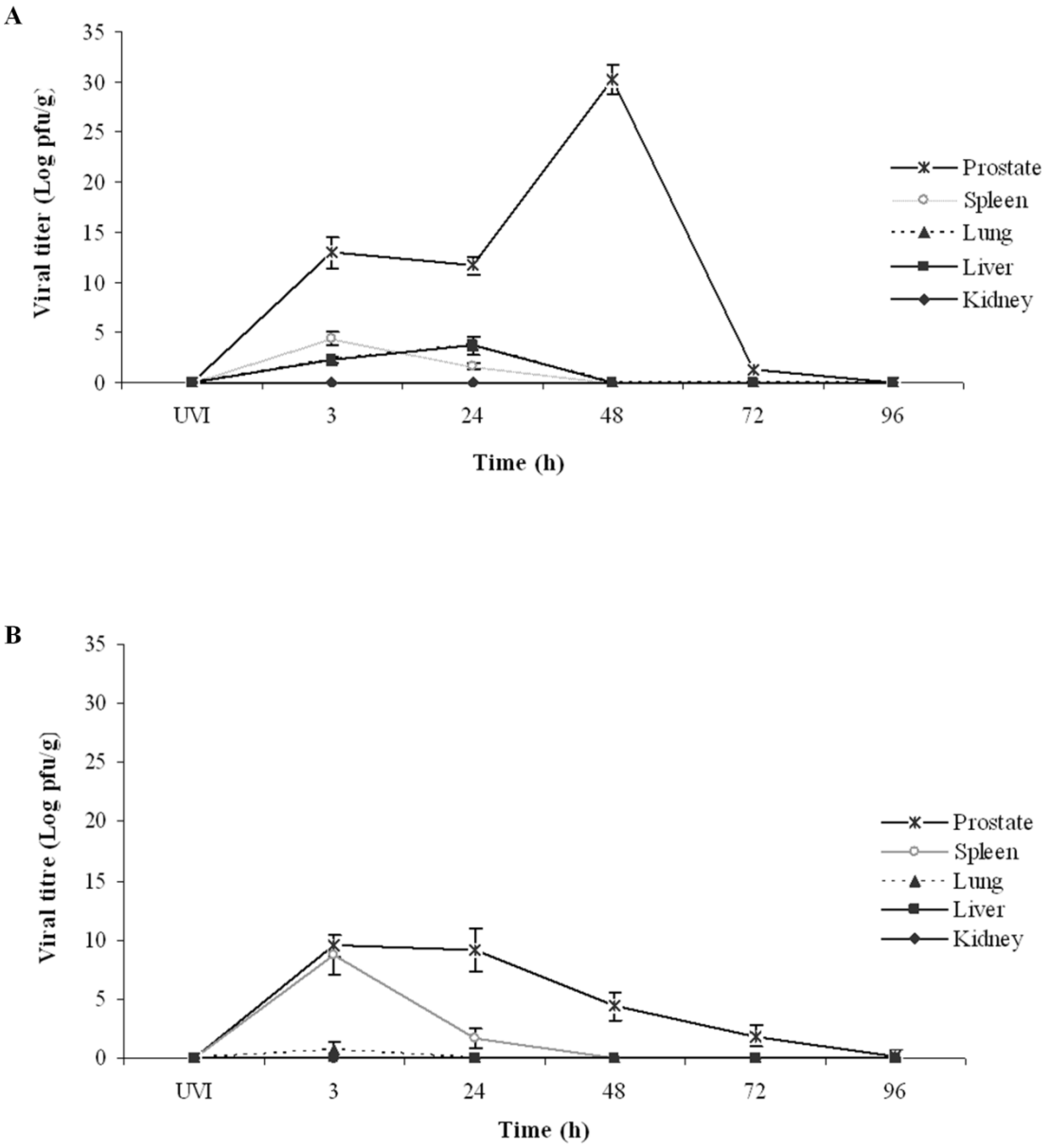

Figure 2.6 Tissue distribution of replication-competent virus

(A) PTEN$^{-/-}$ and (B) control mice were injected with 100 µl of 5x10^{8} pfu/ml of VSV(AV3). Mice were sacrificed at time points of 3, 24, 48, 72 and 96 h after viral inoculation. Organs (prostate, spleen, lung, liver, and kidney) were frozen and virus titres were determined by plaque assay. Results are presented as Log pfu/g ± SEM (n = 3).

		UVI	3h	24h	48h	72h	96h	p-Value
PTEN$^{-/-}$ Tumour	Kidney	1 ± 0.00	0.50 ± 0.02	0.48 ± 0.03	0.48 ± 0.07	0.40 ± 0.13	0.61 ± 0.06	p=0.0007
	Liver	1 ± 0.00	4.49 ± 0.69	1.04 ± 0.58	2.147 ± 0.89	1.119 ± 0.32	1.15 ± 0.45	p= 0.0053
	Lung	1 ± 0.00	2.98 ± 1.25	6.67 ± 0.80	1.60 ± 0.26	0.609 ± 0.21	0.481 ± 0.08	p<0.0001
	Prostate	1 ± 0.00	357.95 ± 141.22	94.16 ± 54.52	2163.45 ± 884.70	5.97 ± 1.82	1.77 ± 0.36	p=0.0075
	Spleen	1 ± 0.00	2.96 ± 0.15	2.65 ± 0.20	2.95 ± 0.94	1.70 ± 0.44	1.01 ± 0.09	p=0.0150
Control	Kidney	1 ± 0.00	0.148 ± 0.13	0.35 ± 0.16	0.53 ± 0.27	0.18 ±0.02	0.19 ± 0.03	p<0.0001
	Liver	1 ± 0.00	0.21 ± 0.11	0.13 ± 0.03	0.18 ± 0.04	0.10 ± 0.03	0.27 ± 0.09	p<0.0001
	Lung	1 ± 0.00	1.68 ± 0.40	1.78 ± 0.69	0.46 ± 0.04	1.51 ± 0.12	0.43 ± 0.25	p=0.0463
	Prostate	1 ± 0.00	4.43 ± 0.35	2.96 ± 1.42	3.63 ± 0.31	1.06 ± 0.40	0.90 ± 0.53	p=0.0080
	Spleen	1 ± 0.00	0.99 ± 0.17	2.52 ± 0.69	3.05 ± 0.51	3.13 ± 0.37	2.31 ± 0.75	p=0.0275

Table 2.1 Viral mRNA levels in prostates of control and PTEN$^{-/-}$

Viral mRNA levels in prostates of control and PTEN$^{-/-}$ were compared post viral infection. IFN-α mRNA level was first normalized to ribosomal RNA level ($\Delta CT = CT_{GFP} - CT_{rRNA}$) and then compared with the negative control group prostates treated with UVI virus ($\Delta\Delta CT = \Delta CT - \Delta CT_{UVI}$). The results were expressed as relative quantification (RQ) = $2^{-\Delta\Delta C} \pm$ SD. (n=3)

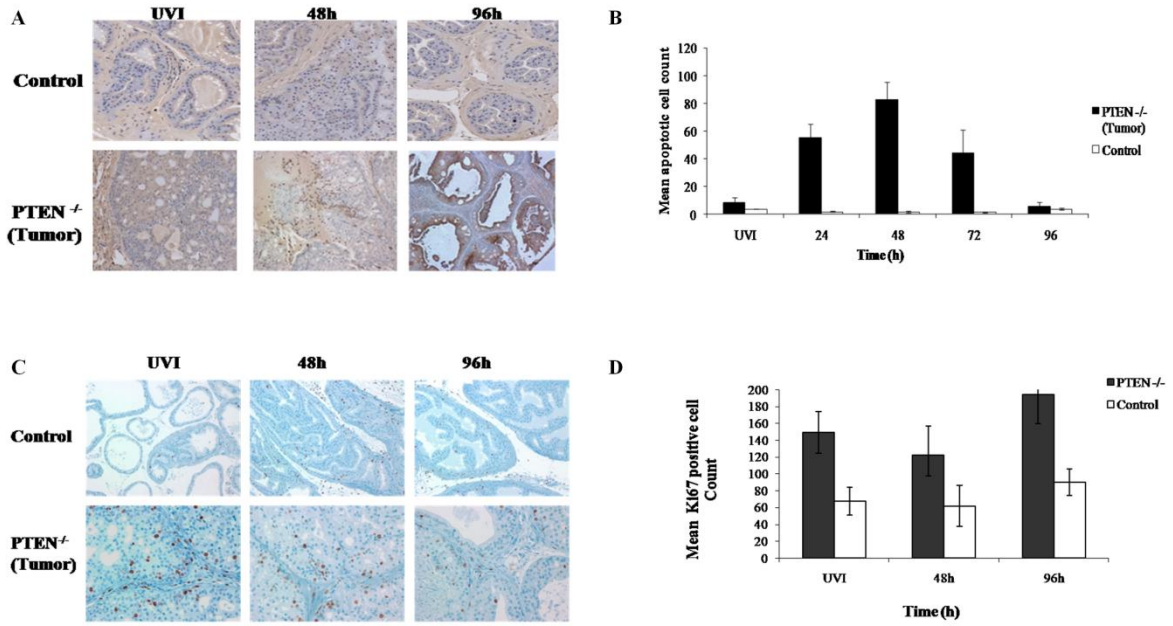

Figure 2.7 Apoptosis in the prostates of PTEN$^{-/-}$ and control mice

Each mouse was injected with 100 µl of 5x10^{8} pfu/ml of VSV(AV3). Mice were euthanized at 24, 48, 72 and 96 h post viral injection. Paraffin-embedded prostates tissues were stained with TUNEL. (A) and Ki67 (C). Representative slides at 40x magnification show presence of apoptotic bodies (stained brown). (B) Apoptotic cells and cells stained with Ki67 (D) were counted in ten fields of view and presented as average number of apoptotic cells ± SD (n = 3).

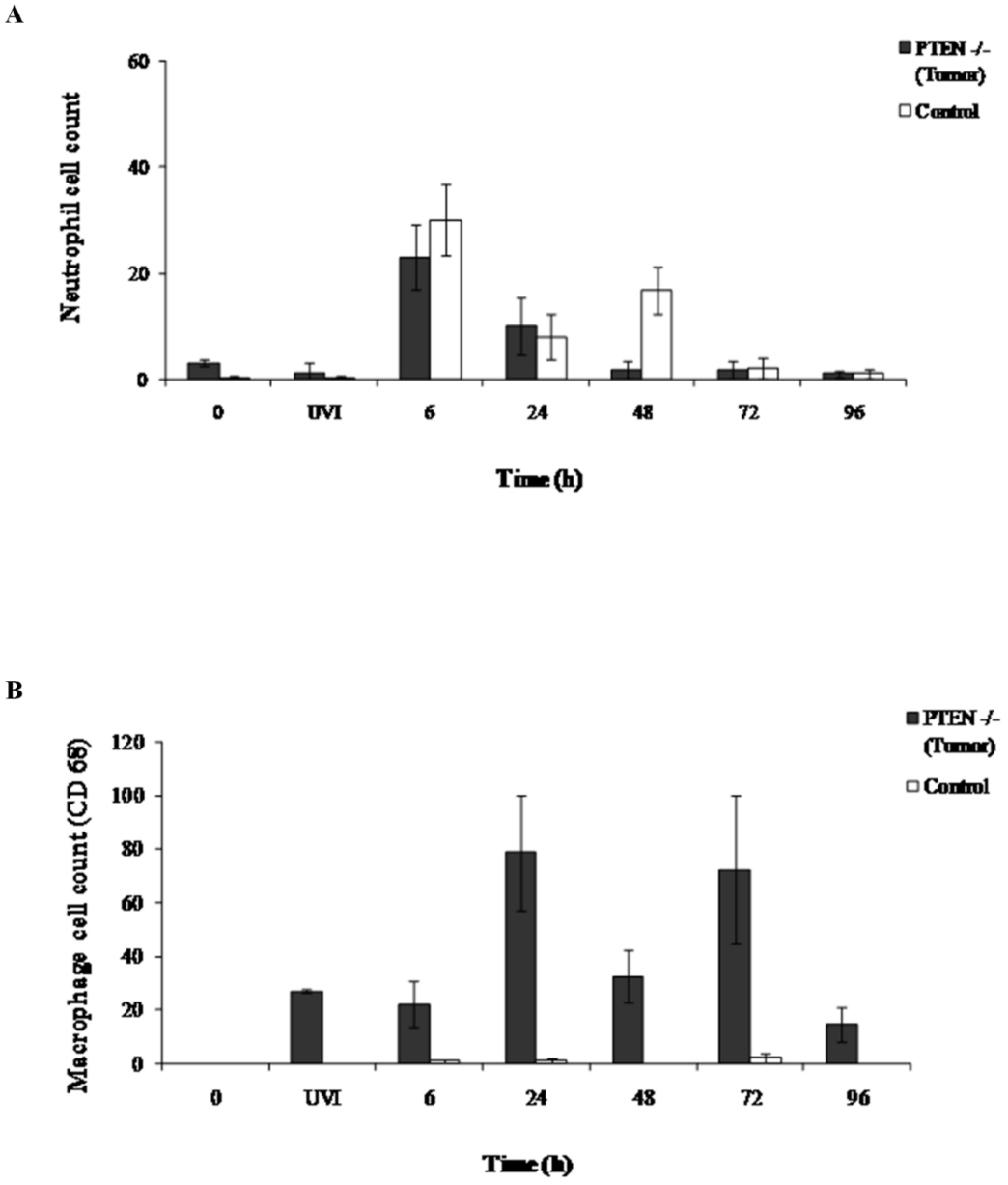

Figure 2.8 Effects of viral infection on immune response parameters

Neutrophils (A) and macrophages (B) were counted and presented as average of total cell count ± SEM (n = 3). There was no significant difference between total neutrophil counts in PTEN$^{-/-}$ compared to control prostates ($p > 0.05$).

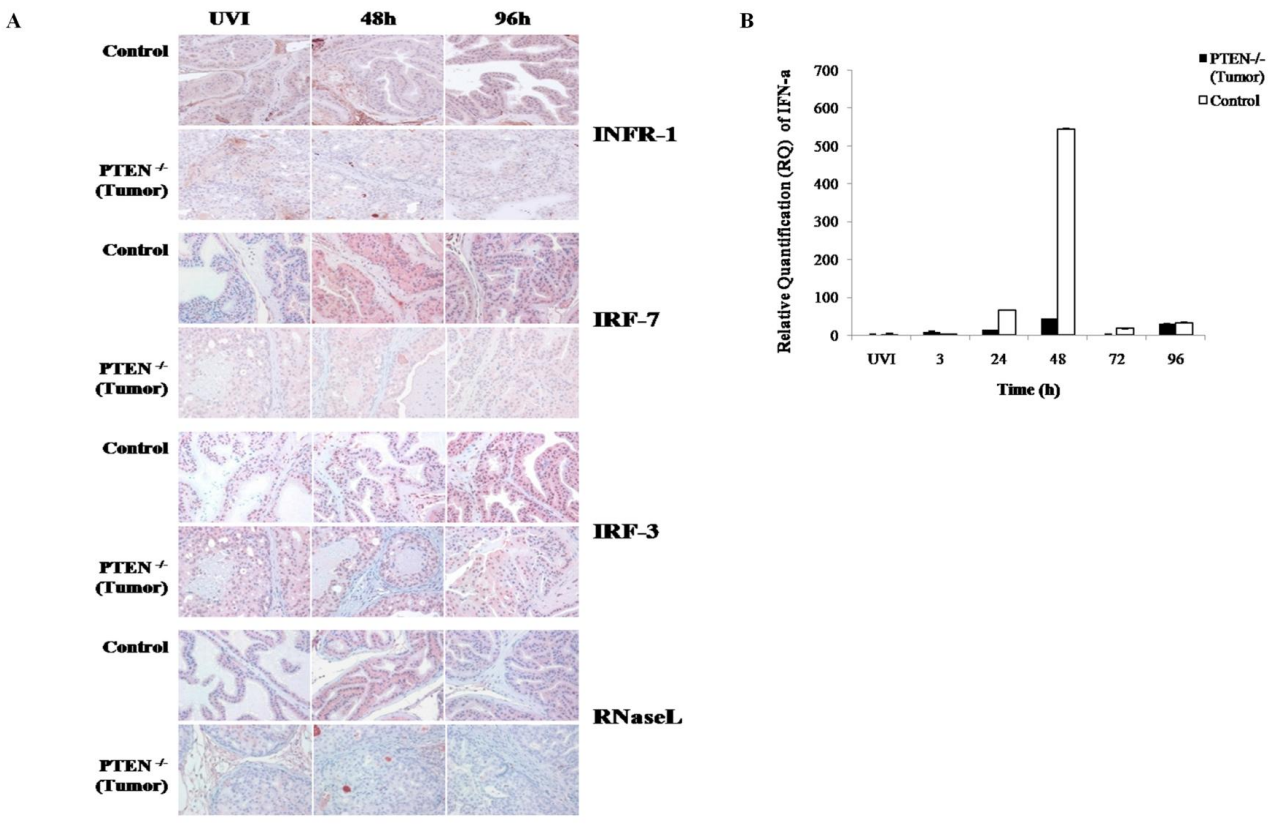

Figure 2.9 Interferon response in PTEN$^{-/-}$ and control prostates

(A) Immunohistochemical staining of IFNR-1 (α/β) receptor, IRF-3, IRF-7 and RNaseL. Paraffin-embedded tissues were stained with IFNR-1α or IRF-7. Representative slides were prepared and visualized at 40x magnification. Results were reviewed by a pathologist and were scored blinded (n = 3).

(B) IFN-α mRNA levels in prostates of control and PTEN$^{-/-}$ were compared post viral infection. IFN-α mRNA level was first normalized to ribosomal RNA level ($\Delta CT = CT_{IFN\text{-}\alpha} - CT_{rRNA}$) and then compared with the negative control group prostates treated with UVI virus ($\Delta\Delta CT = \Delta CT - \Delta CT_{UVI}$). The results were expressed as relative quantification (RQ) = $2^{-\Delta\Delta C}$.

3. Detection of metastatic lesions in the transgenic adenocarcinoma of mouse prostate (TRAMP) model using vesicular stomatitis virus[2]

3.1 Introduction

Metastatic prostate cancer is the second leading cause of cancer related mortality in North American men (25, 26). Currently, the therapeutic options available for treatment of advanced metastatic prostate cancer are limited to androgen-ablation therapy and cytotoxic chemotherapy, both of which are designed to extend the life expectancy of patients, but without curative intent (32, 34, 35, 231). With a median survival of ~18 months, there is a clear need for more efficacious therapies for treatment of advanced disease. In the last decade, oncolytic viruses, either from naturally occurring or genetically engineered virus, have been studied in the context of treatment for several cancers (232-234). Due to its anatomical location, the prostate gland is a good candidate for treatment with oncolytic viruses since direct intra-tumoural injections can be carried out via trans-rectal or trans-urethral routes. Oncolytic viruses typically exploit deficiencies present in the anti-viral defence system of malignant cells, thus selective killing of transformed cancerous cells while sparing normal cells (103-105).

Vesicular Stomatitis Virus (VSV) is a negative strand RNA virus, which has been investigated as an oncolytic agent and shown to replicate in malignant cells which have an incapacitated interferon (IFN) response (231). IFN induced genes are associated with the pathogenesis of prostate cancer such that down-regulation of IFN response genes have been seen in approximately 30% of clinical samples (171, 172). VSV's matrix (M) protein is involved in the cytopathic effects of the virus, which lead to rapid apoptosis. Deletion of methionine at position 51 in the viral M protein, of the VSV(AV3) virus strain, renders the virus even more susceptible to the host anti-viral response, allowing the VSV(AV3) to preferentially infect

[2] A version of Chapter 3 will be submitted for publication. Maryam Moussavi, Tearle, H., Fazli, L.,Bell, J.C., Jia, W., Rennie, P.S. Detection of metastatic lesions in the transgenic adenocarcinoma of mouse prostate (TRAMP) model using Vesicular Stomatitis Virus.

malignant cells with a debilitated IFN response, while ensuring greater protection of normal cells with a competent IFN response (122, 222). Previously, we demonstrated that intra-prostatic injection of VSV(AV3) into prostate-specific PTEN$^{-/-}$ transgenic mice leads to selective infection and oncolysis of malignant prostate cells while sparing normal prostate tissue (Chapter 2). Although the prostate-specific PTEN$^{-/-}$ transgenic mouse model is reliable, typically the incidence of metastatic lesions are low. Thus to study the effects of VSV(AV3) on advanced and invasive prostate cancer the transgenic adenocarcinoma of the mouse prostate (TRAMP) model was used in this study. The main advantages of using the TRAMP model is that it follows disease progression similar to that is seen in the clinic, and it produces reproducible metastatic lesions in a high proportion of the progeny (193), such that by 24 weeks of age, approximately 100% of the mice exhibit poorly differentiated and invasive tumours, with metastasis observed predominantly in the lumbar lymph nodes (235, 236).

The aim of the present study was to determine whether by injecting VSV(AV3) intra-prostatically, the virus could travel to distant metastatic sites and then infect and destroy these metastatic lesions. Our results indicate that VSV(AV3) is capable of finding, infecting, and killing metastatic lesions within the lumbar lymph nodes of the TRAMP mouse model.

3.2 Material and methods

3.2.1 Tissue culture

TRAMP-C2 cells were purchased from the American Type Culture Collection and maintained in DMEM (Invitrogen). Medium was supplemented with 0.005 mg/ml bovine insulin (Sigma), 10nM dehydroisoandrosterone (Sigma), 5% Nu-Serum IV (BD-bioscience) and 5% fetal bovine serum (FBS) (Invitrogen).

3.2.2 Virus propagation

VSV(AV3), a recombinant IFN-inducing mutant of the Indiana serotype, was propagated in Vero cells. VSV(AV3) was constructed to express the GFP-firefly luciferase fusion gene (122). Virons were collected and purified as before (210). Plaque forming units (pfu) were counted and used for calculating infectious titres (122, 209, 210).

3.2.3 Transgenic adenocarcinoma of mouse prostate (TRAMP) model

TRAMP mice hemizygous for the ARR2BP(rat probasin)-SV40Tag transgenes maintained in a pure C57BL/6 background were purchased from Jackson Laboratories. C57BL/6 TRAMP mice were bred in-house with non-transgenic FBV mice (Jackson Laboratories). To confirm TRAMP male mice, genomic DNA was removed from tail clips of F1 male progeny from C57BL/6 TRAMP x FBV cross and tested using PCR with the following primers: (MβCx7F: 5'-GATGTGCTCCAGGCTAAA GTT-3', MβCx7R:5'-AGAAACGGAATGTTGTGGAGT-3', Pb-1F: 5'-CCGGTCGACCGGAAGCTTCCACAAGTGCATTTA-3', and SV40 TagR : 5'-CTCCTTTCAA GACCTAGAAGGTCCA-3'). For this study, all mice used were 25 weeks of age.

3.2.4 *In vivo* studies

A small incision was made in the abdomen of 25 week old TRAMP male mice and 100 µl of VSV(AV3) at 5 x 10^8 pfu/ml was delivered by intra-prostatic injection. For quantification of viral uptake and distribution, animals were injected through the intra-peritoneal (i.p.) route with 150 mg/kg luciferin (Xenogen) at 3, 6, 24, 48, 72 and 96 h post-viral inoculation and imaged with an

IVIS100 Imaging System (Xenogen). Data was analyzed using Living Image 2.50 (Xenogen) software. At least four mice per group were sacrificed at indicated time points. Organs (kidney, liver, lung, prostate and spleen) were removed and either fixed in 10% buffered formalin and paraffin-embedded or snap-frozen in liquid nitrogen. Animal procedures were performed according to the Canadian Council on Animal Care guidelines and approved by local (University of British Columbia) Animal Care Committee.

3.2.5 Titration of VSV from infected tissue

Tissues were removed at the indicated time points, weighed and homogenized in 1ml PBS using a Polytron homogenizer. Serial dilutions were prepared in serum-free media and added to confluent Vero cells for 60 min. Cells were subsequently overlaid with 1% methyl cellulose (Sigma) and plaques were grown for 72 h. Infected Vero cells were then fixed in 4% formaldehyde and stained with crystal violet. Plaques were counted by visual inspection, and titres were calculated as pfu/ml (213, 214).

3.2.6 Immunohistochemical staining

Five micrometer sections were prepared from paraffin-embedded tissues and tissues were extracted from paraffin as described previously (215). TUNEL (Terminal deoxynucleotidyl transferase dUTP nick end labelling) assays were performed according to manifacturer instructions (ROCHE). Tissues were stained with primary antibody to IRF-7 (abcam) and VSV (Dr. John Bell) at 1:75 and 1:500 dilutions, respectively. All sections were reviewed by pathologist and were scored blinded.

3.2.7 Quantitative real-time PCR

Total RNA from mouse tissue was isolated using the Trizol method (Invitrogen). RNA was reverse transcribed and amplified with IFN-α primers (174) on an Applied Biosystems 7900HT Fast Real-time PCR System following the SYBR Green PCR Master Mix protocol. Relative quantification of gene expression was performed using ribosomal RNA as control (237).

3.2.8 *In vitro* cell proliferation assay

Briefly, 1x 10^4 TRAMP-C2 cells were plated into each well of a 96-well plate. Cells were grown for 48 h, stimulated with universal type I IFN (PBL Biomedical Laboratories) for 16 h and then challenged with VSV(AV3) at a multiplicity of infection (MOI) of 0.1 pfu/Cell. MTS[3-(4,5-dimethylthiaol-2-yl)5-(3-carboxymethoxyphenyl)-2-(4-sulphophenyl)-2H-tetrazolium (250 µg/ml) inner salt] (Promega) and 20 µg of PMS (Gibco) solutions were mixed together and added to each well for 2 h. Colorimetric analysis was carried out using an ELISA plate reader at an absorbance of 490 nm (211).

3.2.9 Statistical analysis

Student's t-test was used to assess statistical significance ($p < 0.05$) between groups. To measure statistical differences between mouse stained tissues, the non-parametric Wilcoxon-rank test was used, as there was no assumption of a normal distribution of scores.

3.3 Results

3.3.1 Cytopathic effect of VSV(AV3) on TRAMP-C2 cells

To predetermine whether VSV(AV3) would be capable of infecting TRAMP mice *in vivo*, TRAMP-C2 cells were infected with increasing titres of virus over a 48 h period. The TRAMP-C2 cell line is derived from a heterogeneous prostate of a 32 week old TRAMP mouse (237). Cell viability measured using MTS assays determined that there was a direct relationship between cell death and increasing viral titre. This is evident from the cell viability decreasing by 55% as the viral multiplicity of infection (MOI) increased from 0 to 0.1 Pfu/cell. These results indicate that TRAMP-C2 cells are susceptible to VSV(AV3) infection **(Figure 3.1A)**.

The AV3 strain of VSV is particularly sensitive to IFN. To determine the status of IFN response, TRAMP-C2 cells were pre-incubated with increasing doses of universal type I IFN for 16 h and were then challenged with 0.1 Pfu/cell of VSV(AV3). The results indicate that the IFN response pathway is not fully disrupted in TRAMP-C2 cells. Cell viability increased by 26% in cells that were pre-treated with 10,000 IU/ml of universal type I IFN, suggesting that TRAMP-C2 cells have a partially active IFN response **(Figure 3.1B)**.

3.3.2 Viral distribution after intra-prostatic injection of VSV(AV3) into TRAMP mice

In vivo studies were conducted to compare the VSV(AV3) tissue distribution in tumour-bearing TRAMP mice versus non-transgenic control mice. The prostates of both TRAMP and control mice were injected with 100 µl of $5x10^8$ pfu/ml VSV(AV3). Viral distribution in both cohorts of mice were monitored over a 96 h period by i.p. injection of luciferin and visualised using the Xenogen-IVIS100 system **(Figure 3.2A)**.

Bioluminescence intensity, which is presumed to correlate with viral presence, was shown to be up to 5-fold higher in the prostate region of the TRAMP tumour-bearing mice as compared to control mice **(Figure 3.2B)**. The strongest signal was detected at 24 h post-viral inoculation

with a 4.7-fold increase in bioluminescence detected in TRAMP prostate region compared to control mice. Additionally, as time progressed the bioluminescence was maintained at higher levels in the prostate region of TRAMP tumour-bearing mice, compared to control mice. For example in control mice, the detected signal in the prostate region was decayed by 90% at 48 h with only trace amounts of bioluminescence detected at 72 h post-viral injection. In TRAMP mice, there was only a 32% reduction in bioluminescence detected between 48 h and 72 h post-viral inoculation. At 72 h post-viral inoculation there was 28.1-fold higher bioluminescence detected in prostates of TRAMP compared to control mice. Thus, indicating that VSV(AV3) was maintained at high concentrations over 72 h post-viral infection in tumour-bearing prostates of TRAMP. By 96 h time point there was no detectable bioluminescence observed in the prostate regions of control mice. However, there was a 3-fold increase in bioluminescence seen in prostate regions of TRAMP mice as compared to 72 h, implying an increase in viral presence.

3.3.3 Presence of live virus in organs of TRAMP mice

To evaluate whether the bioluminescent data correlated with presence of live virus, both TRAMP and control mice were sacrificed at 24, 48, 72 and 96 h post-treatment with VSV(AV3), their organs (kidney, liver, lung, lymph, prostate and spleen) harvested, and then snap-frozen. Tissues were homogenized and plaque assays were performed to quantify viral delivery and replication within various tissues **(Figure 3.3)**.

In the TRAMP mice **(Figure 3.3A)**, a substantial amount of live virus (160.0 ± 5.8 Pfu/g) was observed in the prostate tumours 24 h post viral injection. The amount of live viral particles decreased over time, so that by 48 h there was approximately 138.0 ± 1.5 Pfu/g and 48.7 ± 1.8 Pfu/g by 72 h. However, an increase in viral load was observed at 96 h, 520.0 ± 60.8, indicating an increase in viral replication. A similar trend with the amount of live virus is seen in extracted lymph nodes and lung tissues from TRAMP mice. In the lymph nodes, there is approximately 90.0 ± 0.15 Pfu/g seen at 24 h post intra-prostatic injection of VSV(AV3). The amount of live virus increased to 170.0 ± 0.06 Pfu/g by 48 h. However, the amount of extracted replicating

virus significantly decreased by 72 h post viral infection to 10.0 ± 1.4 Pfu/g. Similar to prostate tumours, the amount of replicating virus dramatically increased at 96 h to 80.0 ± 12.1 Pfu/g, suggesting viral replication and amplification in the lymph nodes of TRAMP mice. The lung tissue of the TRAMP mice presented the same trend in presence of virus as seen with the lymph nodes. At 24 h post intra-prostatic injection of VSV(AV3) 73.3 ± 15.3 Pfu/g was seen. This number increased to 123.3 ± 25.2 Pfu/g by 48 h. The amount of virus decreased by 72 h to 12.5 ± 3.5 Pfu/g and once again increased at 96 h to 48.0 ± 83.7 Pfu/g ($p < 0.05$). The amount of live viral particles in the lungs was not statistically ($p > 0.05$) different then the lymph nodes at 24 h, 48 h, 72 h, or 96 h. In the liver, kidney, and spleen there was no significant amount of virus detected at any time indicating that these organs were not readily infected or able to support live virus.

In the control mice (**Figure 3.3B**), VSV(AV3) was present mainly in the prostate (131.0± 37.3 Pfu/g) and spleen (5.3 ± 0.58 Pfu/g) at 24 h post viral injection. This initial viral infection was reduced in the prostates of control mice by 48 h (15.3 ± 4.8 Pfu/g) post intra-prostatic administration of VSV(AV3) and no virus was detected at 72 h post viral infection. In the spleen there was no virus detected after 24 h. Also, there was no virus detected in the lymph, lung, liver, and kidney tissues.

3.3.4 Presence of VSV(AV3) in prostate tissues and metastatic lymph nodes

Detection of VSV(AV3) in both prostate and lymph nodes of TRAMP mice was further determined by immunohistochemistry. Immunohistochemical analysis of the prostates of control mice after VSV(AV3) injection showed an increase in VSV staining initially at 24 h. However, the intensity of VSV immunostaining is lessened over time, specifically at 72 h post VSV(AV3) injection. By comparison, VSV intensity in the prostates of TRAMP mice gradually increased in a time-dependent manner. A closer analysis revealed an increase in intensity of VSV staining by 24 h, which is then lessened at 48 h. However, by the 96 h time point VSV staining intensified to its greatest level; thus indicating an increase in viral presence and infection (**Figure 3.4A)**.

Analysis of lymph nodes, the primary metastatic site in the TRAMP mouse model, revealed a different staining pattern for VSV. In control mice, VSV staining was not observed at any time point, indicating the absence of VSV from the lymph nodes of control mice. However, VSV staining is observed in the lymph nodes of tumour-bearing TRAMP mice. The intensity of VSV staining increased over time with the maximum staining observed at the 48 h time point; signifying the presence of VSV(AV3) in the enlarged and metastatic lymph nodes in the TRAMP mice (**Figure 3.4B**).

3.3.5 VSV(AV3) leads to cell death in TRAMP metastatic lymph nodes

Previously we demonstrated that intra-prostatic infection of VSV(AV3) leads to cancer-specific cell death in prostates of tumour-bearing $PTEN^{-/-}$ mice. To determine whether VSV(AV3) is capable of destroying metastatic malignant cells after it finds and infects them, TUNEL analysis was performed on the enlarged lymph nodes of TRAMP mice and compared to control **(Figure 3.5A and B)**.

Our results indicate that after intra-prostatic injection of VSV(AV3), there was a substantial increase in cell death in the pelvic lymph nodes derived from TRAMP mice compared to lymph nodes derived from control mice. In the TRAMP lymph nodes there was a significant increase in cell death at 24 h post viral injection (75 ± 10 mean apoptotic cells) compared to lymph nodes derived from TRAMP mice, which were treated with UV-inactivated (UVI) virus (22 ± 7 mean apoptotic cells). However, there was no significant ($p > 0.05$) increase in cell death at 48 h in the TRAMP mice (91 ± 7 mean apoptotic cells) compared to either 24 or 72 h (93 ± 10 mean apoptotic cells). Suggesting that the rate of cell death remained constant (**Figure 3.5B**). In control mice, there was no significant increase in cell death in UVI (6 ± 7 mean apoptotic cells) treated mice compared to live VSV(AV3) at 24 h (14 ± 12 mean apoptotic cells) post VSV(AV3) treated mice **(Figure 3.5B)**.

3.3.6 Status of IFN pathway post intra-prostatic injection of VSV(AV3)

Since VSV(AV3) infection leads to activation of a type I IFN response, the status of IFN activity in prostates and metastatic cells of the lumbar lymph nodes of TRAMP mice was assessed. Prostate tissue and lymph nodes were extracted from control and TRAMP mice treated with VSV(AV3) over a 72 h time period. Tissues were stained with interferon response factor (IRF)-7, since activation of IRF-7 has been shown to be indicative of IFN type 1 activity. Immunohistochemical staining of prostate tissues from control mice demonstrated an extensive increase in the intensity of IRF-7 staining post VSV(AV3) injection, signifying activation of type I IFN response (**Figure 3.6A)**. However, in the prostates of TRAMP mice after treatment with VSV(AV3), no IRF-7 staining was seen; indicating that the type I IFN pathway was not activated. Levels of IFN-α mRNA present in prostates tissues of VSV(AV3)-infected TRAMP and control mice were determined and compared by quantitative real-time PCR analysis. Our results demonstrated that there was approximately a 500-fold increase in IFN-α mRNA levels by 48 h post intra-prostatic injection of VSV(AV3) in the control prostates. By comparison, in TRAMP prostates there is only ~31-fold increase in IFN-α mRNA levels by 48 h post VSV(AV3) treatment, indicating a much lower IFN response **(Figure 3.6B)**.

Immunohistochemical staining of lymph nodes derived from control mice demonstrate a slight increase in IRF-7 staining intensity by 24 h post-VSV(AV3) injection **(Figure 3.7A)**. This finding is supported by ~24-fold elevation of IFN-α mRNA levels seen in control lymph nodes 24 h post intra-prostatic injection with VSV(AV3) **(Figure 3.7B)**. However, there was a major increase in IRF-7 intensity at 48 h post VSV(AV3) administration in enlarged metastatic lymph nodes derived from TRAMP mice. Similarly, there is approximately 219-fold increase in IFN-α mRNA levels by 48 h in TRAMP derived lymph nodes. These data demonstrate that intra-prostatic administration of VSV(AV3) has triggered a substantial IFN response in the lymph node lesions derived from TRAMP mice.

3.4 Discussion

Post-androgen ablation therapy and progression of prostate cancer to castration resistant prostate cancer (CRPC), chemotherapeutic agents, such as docetaxel, are the main line of therapy used today. It has been shown that treatment of prostate cancer through chemotherapy by in large has palliative benefits. However, this line of treatment is not curative (231). Recently, oncolytic viruses have been studied as a possible treatment modality for prostate cancer (109, 110, 151). Oncolytic viruses are biological arsenals designed to kill cancer cells while sparing normal healthy cells. These viruses, influence the host cell through activation of gene products that enables cellular invasion, inhibition of apoptotic pathways, and ultimately evasion of cells intrinsic to the host immune response. Coincidentally, viruses use many of the same biological pathways that are deregulated during the process of tumour progression (238). For example, studies have shown that ~75% of tumour cells have a defective IFN response (172, 221, 222). VSV is an oncolytic virus that exploits defective IFN pathways for infection and destruction of cancer cells.

Previously, we demonstrated in the transgenic prostates of $PTEN^{-/-}$ model, that VSV(AV3) is capable of selectively targeting and killing IFN-defective prostate cancer cells *in vivo* (Chapter 2) (239). In the current study, we explored the possibility of using VSV(AV3) for targeted killing of metastatic prostate cancer. To study metastatic prostate cancer, we used the well established TRAMP transgenic mouse (193).

In order to demonstrate that VSV(AV3) can infect TRAMP mice *in vivo*, TRAMP-C2 cells, derived from TRAMP prostates, were infected with increasing VSV(AV3) viral titres. It was evident from MTS analysis that there was an inverse correlation between increasing viral titer and cell survival **(Figure 3.1A)**; indicating that the prostate cancer cells from TRAMP mice are susceptible to VSV(AV3) infection. Since VSV(AV3) exploits a defective cellular IFN antiviral pathway, TRAMP-C2 cells were pre-treated with increasing doses of universal type I IFN prior to treatment with VSV(AV3) to determine status of IFN response. Interestingly, it was determined

that an increasing dose of IFN rescued the TRAMP-C2 cells from cell death induced by VSV(AV3). This finding suggests that the IFN response is not fully dysfunctional in TRAMP-C2 cells **(Figure 3.1B)**.

It has previously been shown that some prostate tumours are more resistant to VSV infection. It was concluded that the presence of IFN bioactivity reduced the oncolytic activity of VSV in these tumours (225). In a more recent study, it was reported that advanced metastatic PC-3 prostate cancer cell line cell lines required a higher dose of VSV compared to LNCaP prostate cancer cells for infection (225, 240). Accordingly, it is reasonable that TRAMP-C2 cells may also require higher doses of VSV infection. Similarly, production and escape of VSV progeny from the surface of the initially infected cell may be delayed as has been seen in PC-3 cells (240). Alternatively, it is possible that TRAMP-C2 cells are unable to produce IFN due to faulty IFN production pathways. However, they are capable of using IFN to launch secondary IFN pathways to protect themselves from further viral infection.

Bioluminescence data derived from *in vivo* intra-prostatic administration of VSV(AV3), demonstrated higher levels of virus presence in the prostate region of tumour-bearing TRAMP mice in comparison to control mice **(Figure 3.2)**. These data are corroborated by immunohistochemical staining for VSV of the prostates of both control and TRAMP mice, which demonstrated a higher intensity of VSV staining in the TRAMP tumour-bearing prostates compared to controls **(Figure 3.4A)**. Additionally, plaque analyses determined a significant increase in viral titer at 24 h post VSV(AV3) administration in the prostates of TRAMP mice **(Figure 3.3)**. The above results are in agreement with our earlier experiments in $PTEN^{-/-}$ tumour-bearing transgenic mice, which also demonstrated higher bioluminescence and viral amplification in tumour-bearing prostates compared to controls (Chapter 2) (239).

A similar trend in the amount of live virus was seen in extracted lymph node and lung tissues from TRAMP mice **(Figure 3.3A)**. Both of these tissues have previously been implicated as key locations for growth of metastatic lesions in the TRAMP model (178). In fact, in the

enlarged lymph nodes extracted from TRAMP mice there was evidence of viral presence as indicated by a dramatic increase in the intensity of VSV stained lymph nodes compared to control tissue **(Figure 3.4B)**. These findings are corroborated by earlier reports of VSV's ability to find distant metastatic lesions in metastatic brain carcinomas (241).

TUNEL analyses on lymph nodes taken from both control and TRAMP mice post-VSV(AV3) infection, demonstrated a significant increase in apoptotic cell count in tumour-bearing mice **(Figure 3.5)**. It was evident from analyses of lymph nodes from TRAMP mice that the majority of metastatic tumours in VSV(AV3) infected animals were undergoing a considerably higher cell death rate compared to metastatic lymph node tumours in animals that had been treated with UV-inactivated virus. This suggests that VSV(AV3) can target and kill metastatic prostate cancer cells found in lymph nodes of TRAMP mice. The above data are in agreement with previous findings in other metastatic disease models, such as gliomoa, breast, and colon carcinomas (241-243).

VSV infection of normal cells leads to activation of the type I IFN (IFN-α/β) pathway. We previously demonstrated that VSV(AV3) is able to infect cancer cells mainly due to a defective IFN response (239). Therefore, the status of the IFN response pathway was investigated in both prostate and lymph nodes derived from TRAMP mice and compared to that of control mice. Interferon response factor -7 (IRF-7) plays a key role the transcription of IFN-α/β, whose role is to alert neighbouring cells through activation of their innate immune response and elevation of their anti-viral status (229). Immunohistochemical analysis of prostate tumours of TRAMP mice demonstrated that IRF-7 is not produced post-VSV infection. However, in control prostates, there was an increase in IRF-7 intensity upon viral infection. Furthermore, by 48 h after infection there is an increase in IFN-α mRNA levels in prostates of control mice relative to TRAMP mice **(Figure 3.6)**.

There was a very large increase in IRF-7 levels observed in the metastatic lymph nodes derived from TRAMP mice. These data were substantiated by an equally large increase in IFN-α mRNA levels in the TRAMP derived metastatic lymph nodes **(Figure 3.7)**. Since lymph nodes are largely comprised of lymphocytes (235), the amplification of VSV in TRAMP lymph nodes could potentially lead to hyper-activation of an IFN response in the resident non-cancerous lymphocytes. In control lymph nodes, there was no remarkable change in either IRF-7 or IFN-α mRNA levels. This was likely due to the relative absence of virus in the control lymph nodes **(Figure 3.4)**.

In conclusion, we have demonstrated that VSV(AV3) is capable of finding and killing metastatic prostate cancer lesions in TRAMP mice. However, activation of IFN response in metastatic lesions may potentially hinder VSV(AV3)s activity. One way to overcome this limitation may be through insertion of other cancer specific targeting genes (discussed within Chapter 4) into the viral genome of VSV(AV3) as a way to target cancer cells through IFN independent manner. Alternatively, combination of VSV(AV3) with other current therapies such as chemotherapy or radiation therapy could enhance VSV(AV3)-directed killing despite of an intact IFN response in metastatic lesions.

3.5 Figures

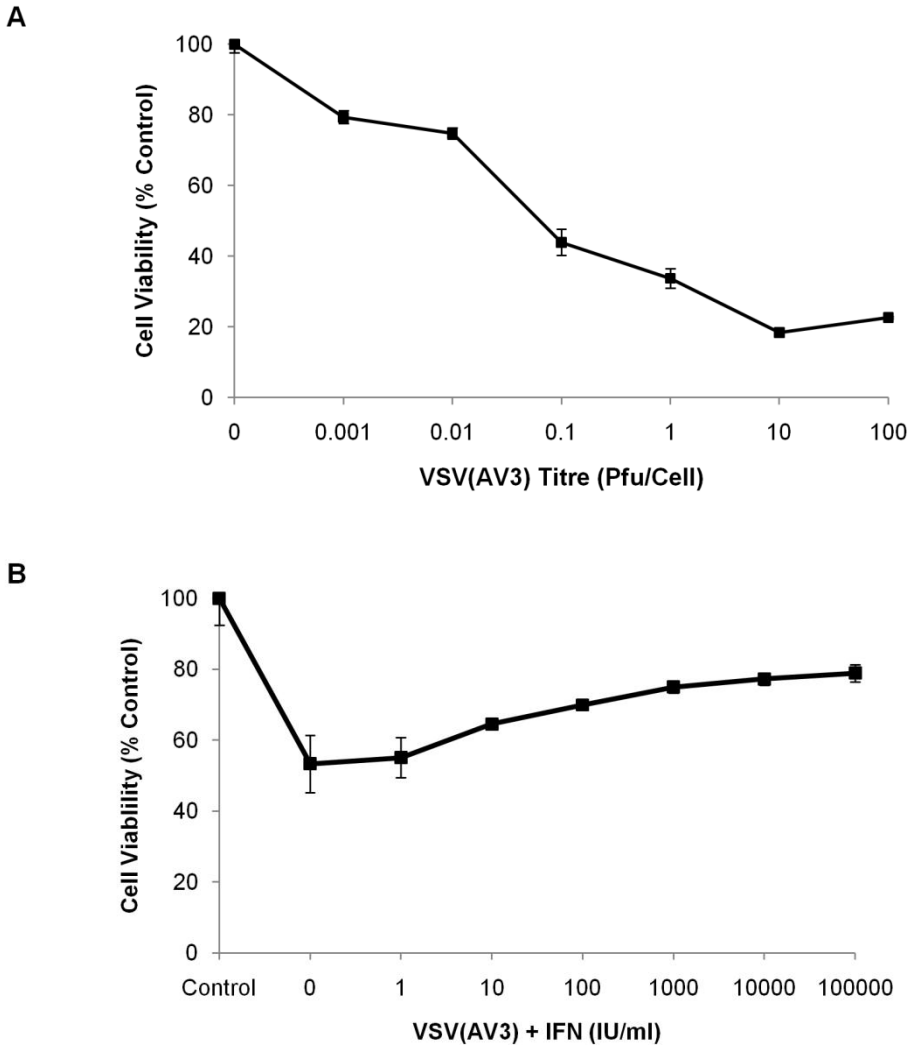

Figure 3.1 Cytoxicity of VSV(AV3) and the IFN response in TRAMPC-2 cells

A) TRAMP-C2 cells were infected with VSV(AV3) at viral titres ranging from 0-100 Pfu/cell. MTS assay was preformed 48 h post viral infection.

B) TRAMP-C2 cells were pre-incubated with increasing concentrations of IFN (0-100,000 IU/ml) for 16 h and then challenged with VSV(AV3) at MOI 0.1 for 48 h. Control represents untreated cells. Each graph is representative of three independent experiments with minimum four replicates each.

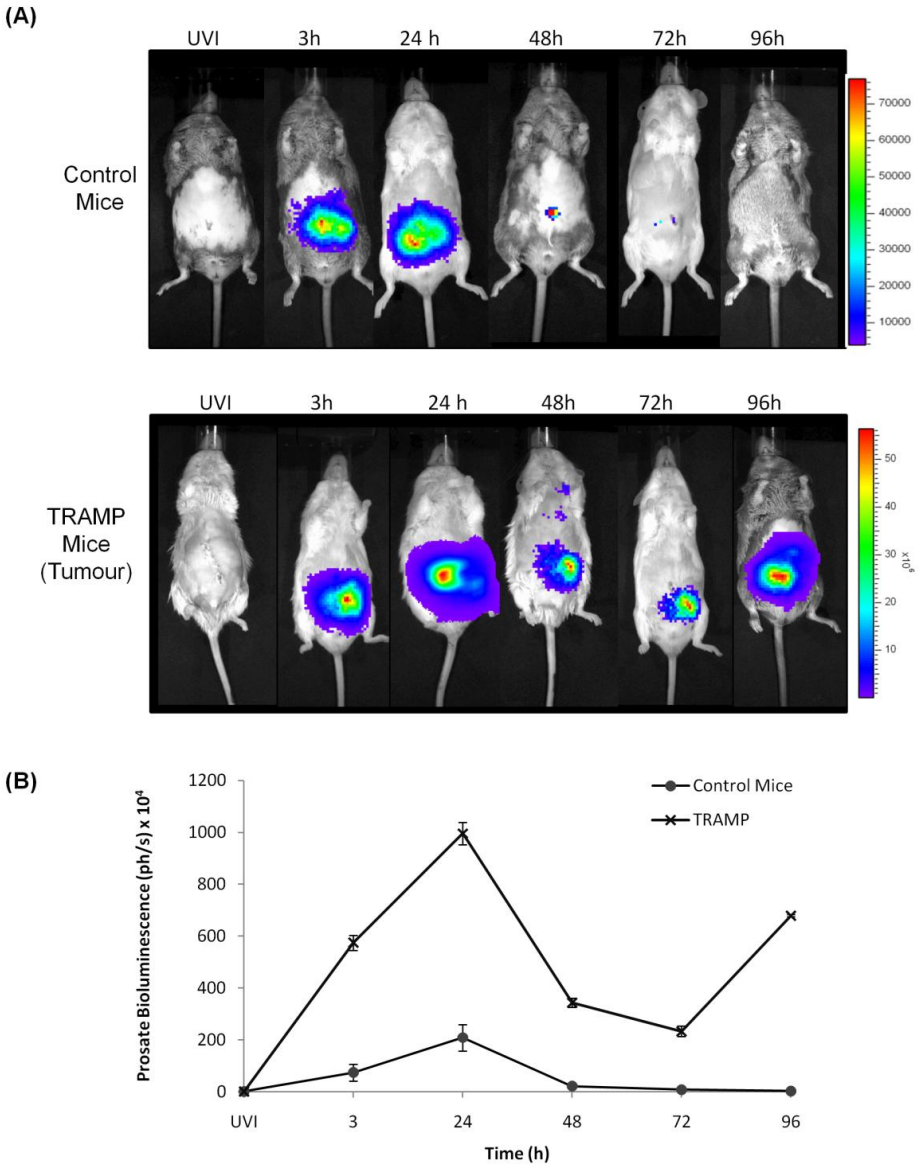

Figure 3.2 ***In vivo*** **bioluminescence measurement after intra-prostatic injection of VSV(AV3)**

TRAMP and control mice were intra-prostatically injected with 100 µl of $5x10^8$ pfu/ml of VSV(AV3). A) Visual representation of viral distribution, tracked by i.p. injections of luciferin over 3-96 h time period. UVI (UV-inactivated virus) was used as control. B) Bioluminescence in the prostate regions of control and TRAMP mice were averaged and are presented as mean ± SEM (n=3).

(A)

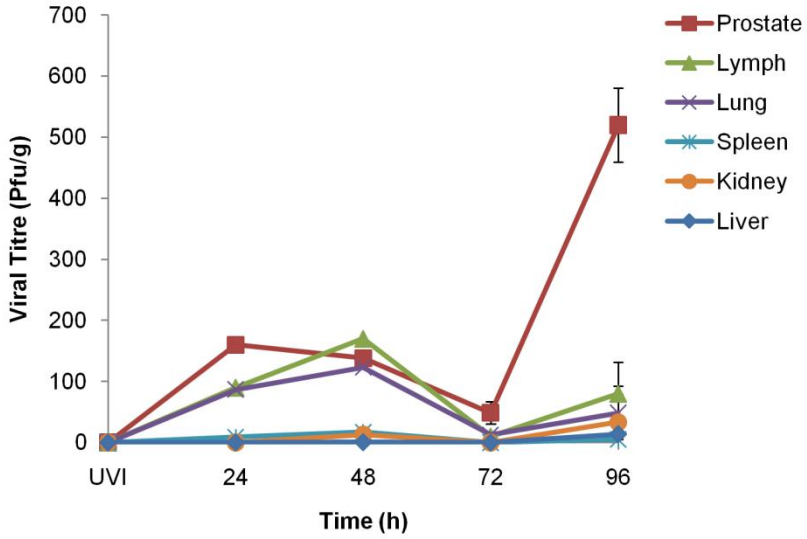

(B)

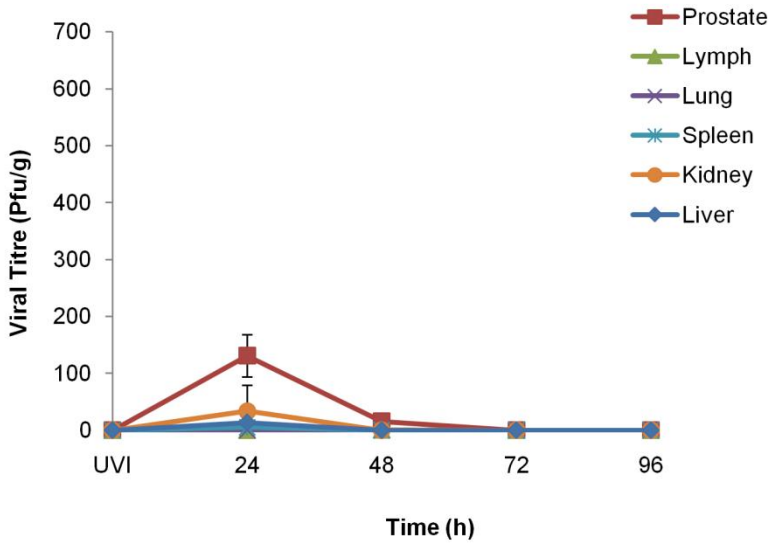

Figure 3.3 Tissue distribution of replication-competent virus

A) TRAMP and B) control mice were injected with 100 µl of $5x10^8$ pfu/ml of VSV(AV3). Mice were sacrificed at 24, 48, 72 and 96 h post-viral injection. Prostate, lymph nodes, lung, spleen kidney, and liver tissues were harvested at each time point. Organs were snap frozen, and then plaque analysis was preformed. Results are presented at Pfu/g ± SEM (n=3).

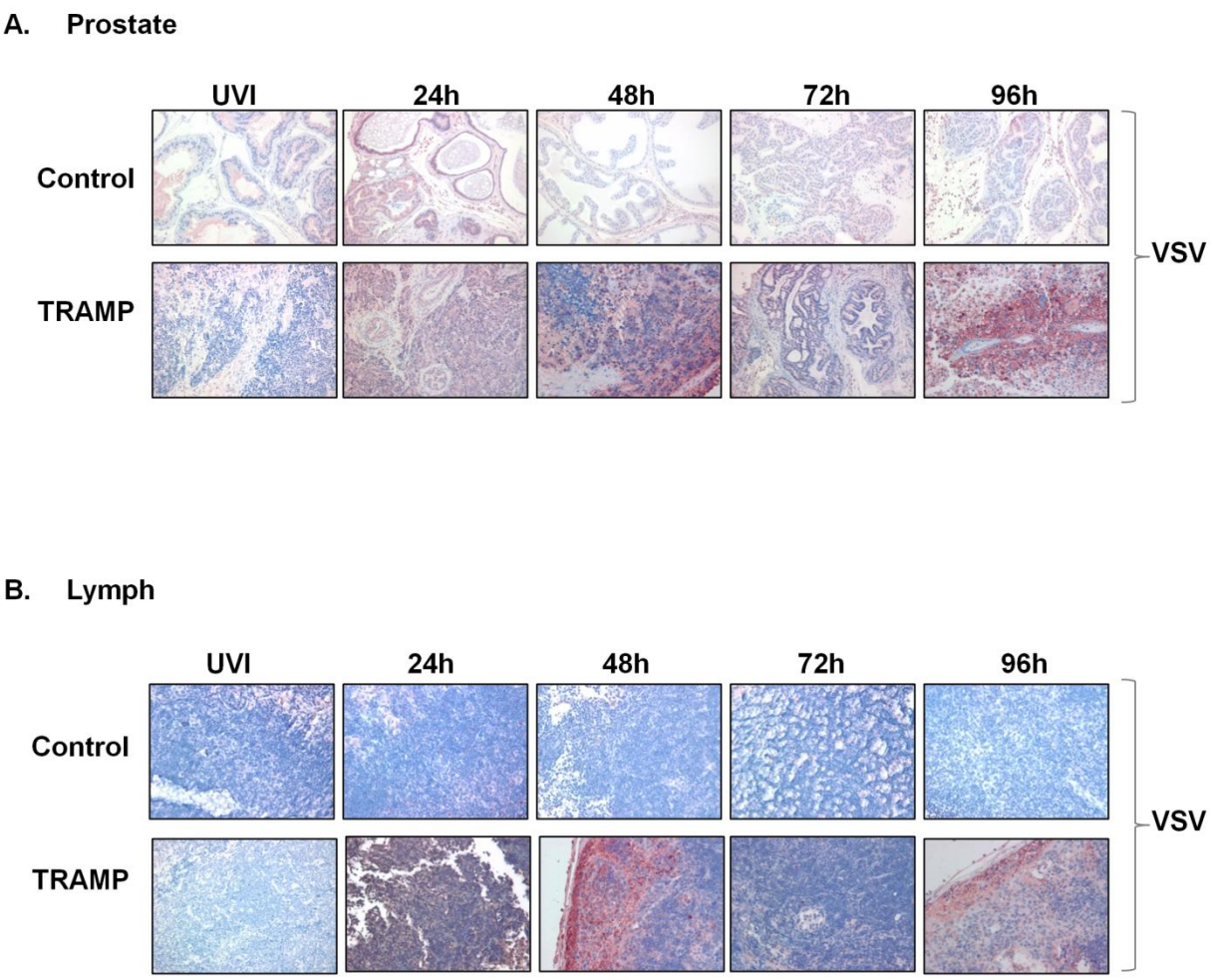

Figure 3.4 Immunohistochemical analysis detecting presence of VSV(AV3)

Presence of VSV was established by immunohistochemical staining of A) prostate and B) lymph nodes derived from TRAMP and control mice with anti-VSV antibody. Representative slides were prepared and visualized at 40x magnification. Results were reviewed by a pathologist and scored blinded (n=3).

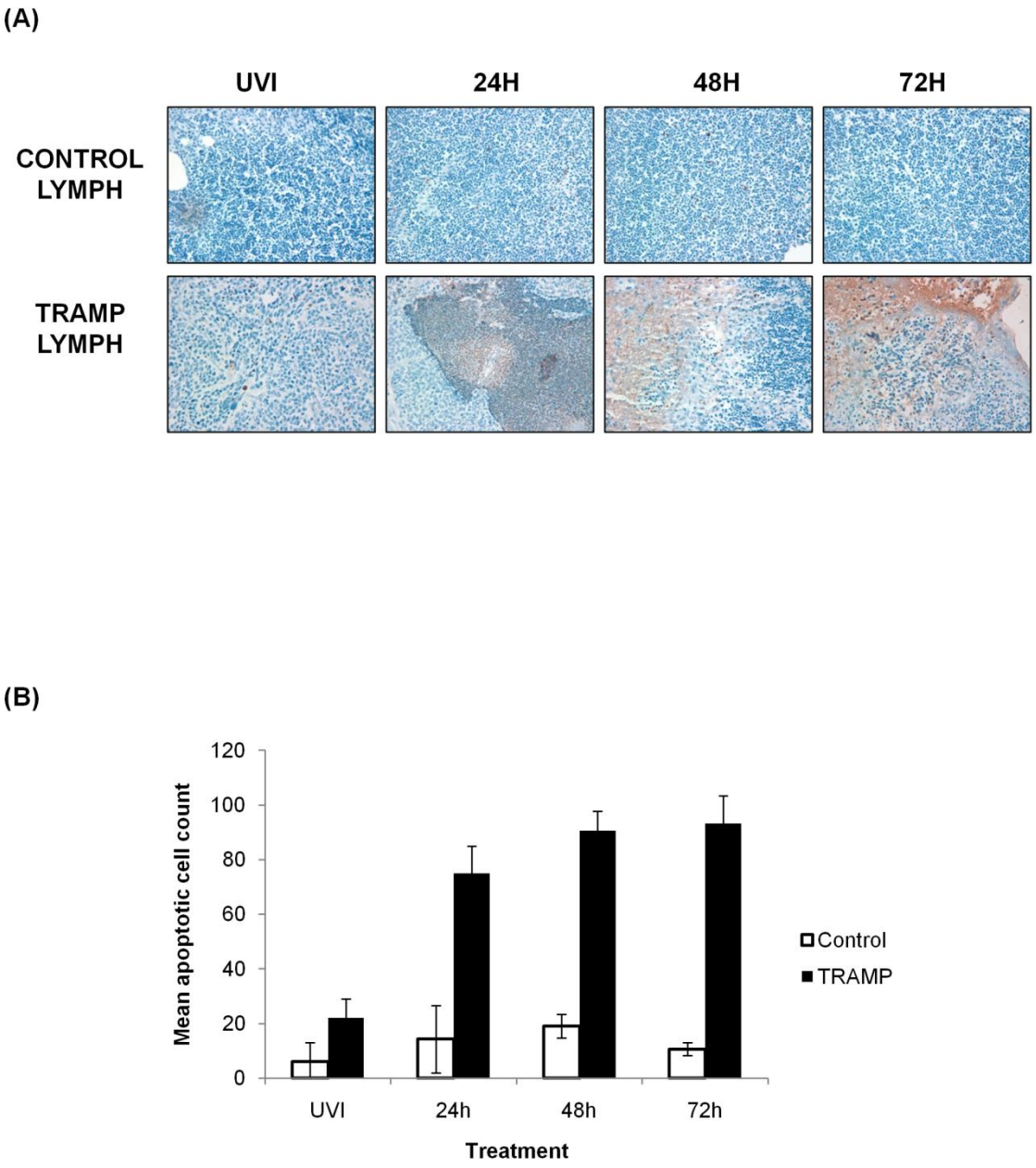

Figure 3.5 TUNEL analysis of cell death in the lymph nodes of tumour-bearing TRAMP and control mice

A) Paraffin-embedded lymph node tissues of TRAMP and control mice were stained with TUNEL, and visualized at 40x magnification.

B) Apoptotic cells were counted in 10 fields of view and presented as mean apoptotic cells ± SD.

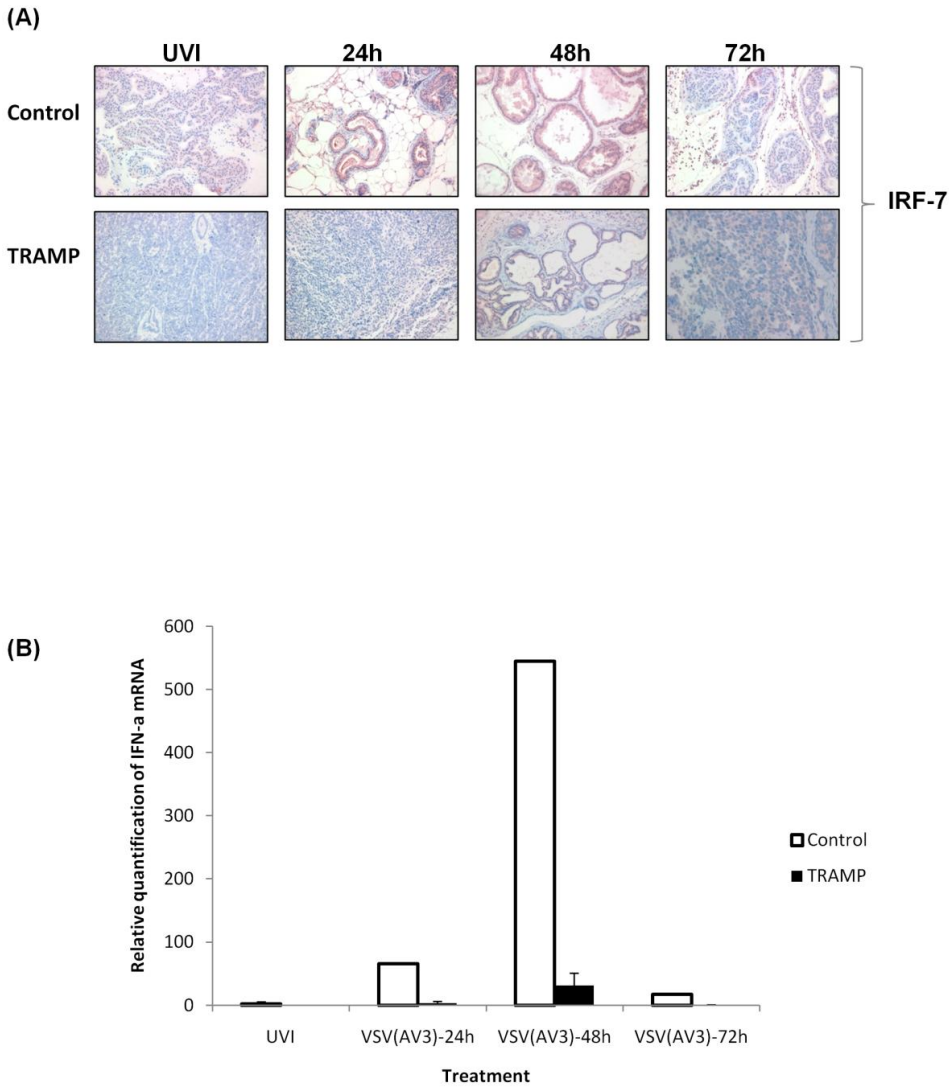

Figure 3.6 Analysis of IRF-7 and IFN-α expression in prostates of control and TRAMP mice

A) Paraffin-embedded prostate tissues were stained with IRF-7. Representative slides were prepared and visualized at 40x magnification. Results were reviewed by a pathologist and scored blinded (n=3).

B) IFN-α mRNA levels in prostate of control and TRAMP mice are compared after VSV(AV3) injection. UVI is UV-inactivated control virus. IFN-α mRNA levels were first normalized to rRNA level ($\Delta C_T = C_{T\ IFN\text{-}\alpha} - C_{T\ UVI}$). The results were expressed as mean relative quantification = $2^{-\Delta\Delta CT}$ ± SEM.

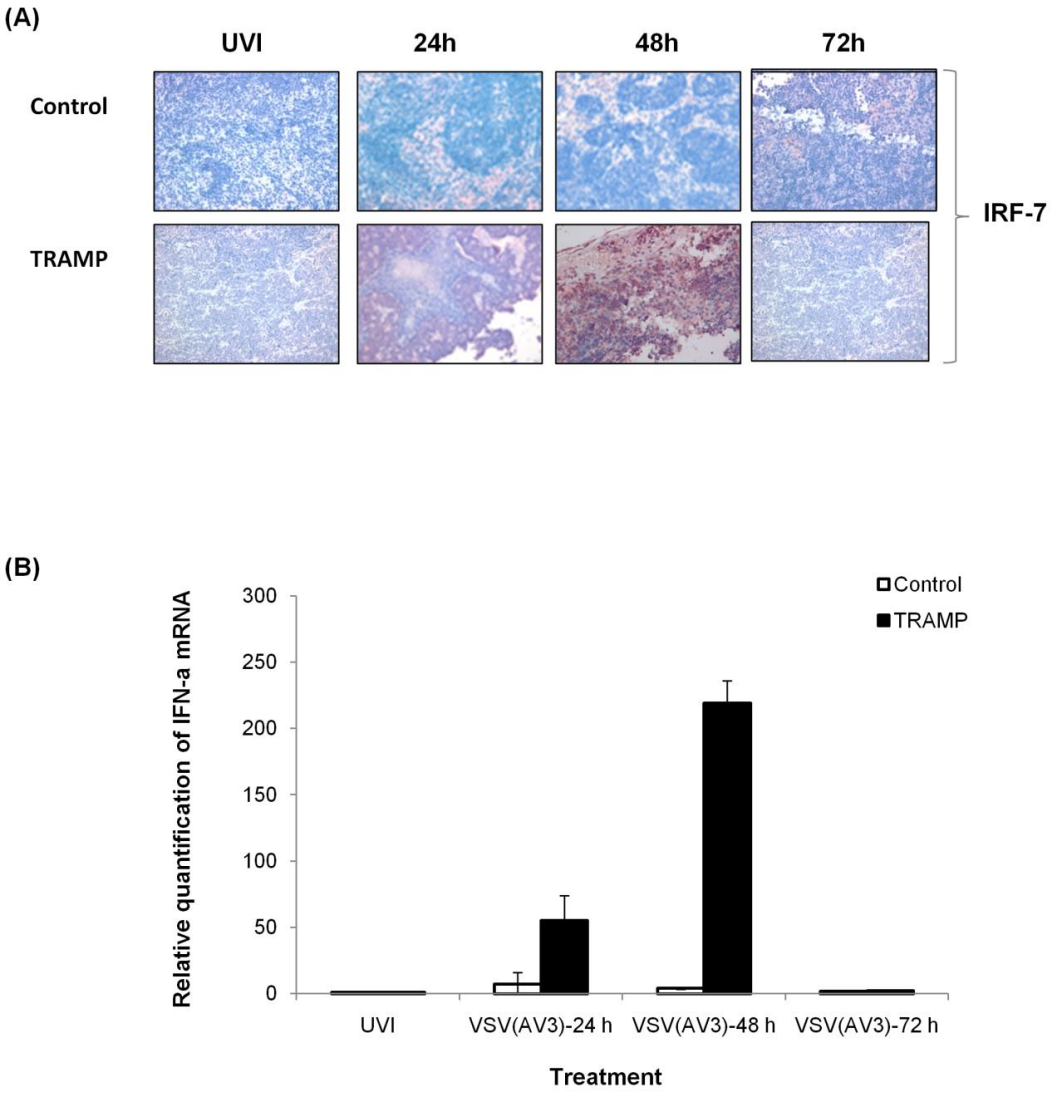

Figure 3.7 Analysis of IRF-7 and IFN-α expression in lymph nodes of control and TRAMP mice

A) Paraffin-embedded lymph nodes were stained with IRF-7. Representative slides were prepared and visualized at 40x magnification. Results were reviewed a pathologist and scored blinded (n=3).

B) IFN-α mRNA levels in lymph nodes of control and TRAMP mice are compared after VSV(AV3) injection. UVI is UV-inactivated control virus. IFN-α mRNA levels were first normalized to rRNA level ($\Delta C_T = C_{T\ IFN\text{-}\alpha} - C_{T\ UVI}$). The results were expressed as relative quantification = $2^{-\Delta\Delta CT}$.

4. Viral targeting of prostate cancer in human prostatic cells and prostate-specific PTEN$^{-/-}$ transgenic mice using fibroblast growth factor and ornithine decarboxylase 5'UTRs[3]

4.1 Introduction

Prostate cancer remains the second leading cause of cancer related mortality in North American men (25). Patients with localized disease are often treated by surgery or radiation therapy, though the majority of prostate cancer related mortality is due to advanced and metastatic disease (32-35).

Viral-based gene therapies, such as oncolytic viral therapy, have the potential to become a viable alternative to common treatments. Previous results from our laboratory demonstrated that the oncolytic virus, Vesicular Stomatitis Virus (VSV), was capable of increasing cell death in locally advanced prostate cancer *in vivo* (239). In addition, there is clinical evidence that viruses can be used to safely control treatment-resistant prostate cancer (244). Viruses such as VSV often demonstrate a preference to infect and replicate in tumour cells due to the presence of a faulty interferon response (160, 239). These studies demonstrate the potential use of viruses as an option for targeted therapy. However, not all cancer cells have a defective interferon response. Accordingly, it would be advantageous to create recombinant viruses which preferentially restrict their gene expression and replication to malignant cells.

To enhance tumour specificity of viruses, eukaryotic translation initiation factor 4E (eIF4E), was chosen as a potential selection criteria since it is characteristically over-expressed in tumours (33, 148). Previous studies have illustrated an increase in the intrinsic levels eIF4E in a variety of malignancies, including prostate cancer (33). Elevations in eIF4E lead to increases in

[3] A version of Chapter 4 has been submitted for publication and is currently under review. Moussavi M, Moshgabadi N, Fazli L, Lebland E, Jia W, Rennie PS. Viral targeting of prostate cancer in human prostatic cells and prostate-specific PTEN$^{-/-}$ transgenic mice using fibroblast growth factor and ornithine decarboxylase 5'UTRs.

cell proliferation, suppression of apoptosis and other characteristics associated with neoplastic transformation. EIF4E has been implicated in the control of translation of a few select proteins involved in developmental processes such as growth factors, proto-oncogenes, and transcription factors (245). Typically, the 5' untranslated region (UTR) of these mRNAs contains excessive secondary structures which are normally discriminated against by the translational machinery; therefore, higher levels of eIF4E/eIF4F complex are required to unwind their 5'UTRs for efficient translation (147). Similarly a genetically engineered virus whose replication mechanisms are under the control of eIF4E should be expressed more selectively in tumour cells with higher levels of eIF4E protein. To this end the goal of this study was to select a 5'UTR that displays the greatest tumour specific discrimination when incorporated into the backbone of a lentivirus. Three different 5'UTRs were selected, including one derived from fibroblast growth factor- 2 (FGF-2) (33, 148) and two derived from Ornithine Decarboxylase (ODC) (246). The 5'UTRs from FGF-2 and ODC have previously been shown to contain extensive, stable secondary structures and it has previously been reported that their translation is tightly controlled (148, 246, 247).

We found that two out of the three 5'UTR tested *in vitro* showed excellent potential for tumour specific targeting based on eIF4E levels and the extent of enhanced green fluorescent protein (GFP) expression. Infection of prostate tumours in the $PTEN^{-/-}$ transgenic mouse model confirmed this finding.

4.2 Material and methods

4.2.1 Cell culture

BPH-1 and PNT1B non-neoplastic human epithelial prostate cells, and LNCaP, C4-2, DU145 and PC-3 human prostate cancer cells were purchased from the American Type Culture Collection. PNT1B cells were maintained in DMEM (Invitrogen). All other cell lines (LNCaP, C4-2, DU145, PC-3 and MPPK-1) were maintained in RPMI (Invitrogen). MPPK-1 cells were previously described (239). All cells were supplemented with 10% fetal bovine serum (FBS) (Invitrogen) and 100 units/ml penicillin/streptomycin.

4.2.2 Plasmid construction

The lentiviral vector, FUGW, which contains an ubiquitin promoter upstream of the enhanced green fluorescent protein (GFP) expression gene (197), was a gift from David Baltimore (California Institute for Technology). FUGW was used as the backbone for lentiviral vector construction in this study. 5'UTR from FGF-2 (533 bp) was obtained as previously described and cloned into the BamHI site of FUGW, downstream of the ubiquitin promoter and upstream of GFP (33). The PCR product from the full-length 5'UTR derived from ODC (ODC_{274}) (274 bp) and the loop portion of the 5'UTR of ODC (ODC_{149}) (149 bp) were purified and digested from PCDNA3 vector and inserted at the BamHI site of FUGW.

4.2.3 Viral propagation and titration

ProFection Mammalian Transfection System (Promega) was used according to the manufacturer's instructions for lentiviral propagation. Briefly, 1.5×10^6 293T cells on 10 cm plate were co-transfected with 10 µg of transducing vector (FUGW, FU-UTR-GW), 10 µg of packaging vector pR8.91 and 5 µg of Vesicular Stomatitis containing (VSV-G) envelope glycoprotein vector in unconditioned DMEM for 12-16h. After this time period, the medium on the cells were replaced with 5% FBS containing DMEM. The supernatant was collected at 24 h, 48 h and 72 h and was then centrifuged at 3750 g for 5 min at 4 ˚C in a bench top centrifuge

(Beckman, Fullton, CA). The clear supernatant containing lentiviruses was then passed through a 0.45 µm filter to remove cellular debris and was further concentrated by ultra-centrifugation (123,000 g for 90 min using Beckman ultracentrifuge with rotor S28). To quantify the viruses, concentrated lentiviruses were serially diluted and used to infect 333,333 of 293T cells. At 72 h post infection, cells were trypsinized and analyzed by flow cytometry. A transducing unit per ml of viruses was calculated as percent GFP positive cells (after infection with 1 ml of virus) multiplied by the number of cells plated for infection.

4.2.4 Cell transfection

Approximately 3 x 10^5 prostate cell lines were grown in 6-well plates until they were ~80% confluent. Lipofectamine™ 2000 (Invitrogen) was used for gene transfection according to the manufacturer's instructions. Briefly, 5 µg/µl of lentiviral plasmid and 20 nM siRNA (sense: GGA CGA UGG CUAA UUA CAU; anti sense: AUG UAA UUA GCC AUC GUCC) against eIF4E was diluted with OPTIMEN® (Invitrogen) medium for 20 min at room temperature. Simultaneously Lipofectamine™ 2000 was mixed with OPTIMEM® medium. After 20 min incubation at room temperature, Lipofectamine™ 2000 was mixed with plasmid and siRNA against eIF4E and added to the cells. After 8 h incubation the medium was replaced with fresh medium. Experiments were terminated 48 h post transfection.

4.2.5 Western blot analysis

Cell lysates, prepared in a lysis buffer (50 mM Tris HCI, pH 7.5,150 mM NaCl, 1% NP40 and 5 mM EDTA) in the presence of a protease and phosphatase inhibitor cocktail (Sigma, St Louis, MO),containing equivalent amounts of protein (60 µg), were resolved using 10% SDS–PAGE and transferred on to a nitrocellulose membrane using Bio-RAD transblot apparatus at 350 mA for 90 min. The nitrocellulose membrane (Gibco) was then blocked with Odyssey blocking buffer for 45 min and stained with primary antibodies to eIF4E (BD Transduction) and GFP (Roche) at a dilution of 1:1000. Antigen-bound primary antibodies were detected by IRDye

800CW goat anti-mouse or goat anti-rabbit IgG and scanned on an Odyssey scanner (LI-COR Biosciences, Lincoln, NE).

4.2.6 Prostate-specific PTEN$^{-/-}$ mouse tumour model

The ARR$_2$probasin-Cre transgenic line, a gift from Dr. P. Roy-Burman (University of Southern California) (188), was crossed in-house with PTEN $^{flox/flox}$ mice from Dr. Tak Mak (University of Toronto) (212) to create prostate-specific PTEN knockout mice (PTEN$^{-/-}$). To confirm PTEN deletion, genomic DNA was removed from tail clips of F2 offspring. The PTEN$^{-/-}$ mice display a high grade carcinoma between 12-15 weeks (189). For this study, all mice used were 15 weeks of age. For viral delivery, mice were anesthetized with isoflurane and subsequently injected with 1.5 mg/kg Metacam as analgesia pre-surgery. A small incision was made in the abdomen of PTEN$^{-/-}$ male mice and 100 µl of lentiviruses at 10^9 pfu/ml was delivered by intra-prostate injection. At least three mice per group were sacrificed three days post viral delivery. Prostate organs were extracted and either fixed as frozen organs in OCT solution or snap-frozen in liquid nitrogen. Animal procedures were performed according to the Canadian Council on Animal Care guidelines and approved by the local (University of British Columbia) Animal Care Committee.

4.2.7 Immunofluorescence staining of tissues

Four micrometer cryosections at -20 ºC were cut and mounted on a slide. Each section was fixed in 4% formaldehyde at room temperature for 10 min. Sections were washed with PBS and incubated with 0.1% Triton in PBS for five minutes. Slides were washed again and placed in a pre-warmed steamer within Citrate Buffer (4.5 mL of 0.1M Citric Acid; 20.5 mL of 0.1M sodium citrate; fill up to 250 ml with dH2O; pH 5.6) in a Coplan Jar for 30 minutes. After cooling to room temperature, slides were washed again in PBS and then incubated for 10 min in 3% H_2O_2. Excess H_2O_2 was washed away with PBS and Mouse on Mouse (Vector) was used according to the manufacturer's instructions. Dilutions of 1: 20 of

anti-eIF4E (BD Transduction) or 1:250 of anti-GFP (abcam) were used as the primary antibody. Either 1:200 Texax Red anti-mouse secondary or 1:200 FITC anti-Rabbit secondary antibody was applied to slides for 30 min. Slides were covered with a drop (10 µl) of mounting media (Vectorshield) containing DAPI prior to being covered by a cover-slip.

4.2.8 Immunohistochemical staining

Five micrometer sections were prepared from paraffin-embedded tissues and the tissues were extracted from paraffin as described previously (215, 239). Tissues were stained with 1:25anti-eIF4E, 1:200 anti-4EBP1, 1:50 anti-phospho-4EBP1, 1:50 anti-phosphor-4G and 1:50 anti-PTEN antibodies. All antibodies were purchased from Cell Signaling. All sections were reviewed by pathologist and scored blinded.

4.2.9 Statistical analysis

GraphPad InStat 3 was used for all statistical analyses. To measure statistical differences between mice stained tissues, the non-parametric Wilcoxon-rank test was used, as there was no assumption of a normal distribution of scores.

4.3 Results

4.3.1 Levels of eIF4E are elevated in prostate cancer cell lines

Various prostate cell lines were checked for their status of eIF4E protein levels. When levels of eIF4E from prostate cancer cells such as LNCaP, C4-2, PC-3 and DU145 were compared to non-cancer derived cell lines (BPH-1 and PNT1B) there was consistently a significant increase of approximately 1.5- to 2-fold in eIF4E protein expression ($p < 0.05$) in the human prostate cancer lines (**Figure 4.1**). Similarly, levels of eIF4E in $PTEN^{-/-}$ derived prostate cancer cells, MPPK-1, were approximately 1.5-fold higher than those of BPH-1 and PNT1B non-cancer derived cells. Our data confirm previous findings that eIF4E is consistently higher in prostate cancer cell lines relative to non-malignant cells (131).

4.3.2 Lentiviral constructs containing ODC and FGF-2 5'UTRs were most sensitive to eIF4E protein levels *in vitro*

Three different 5'UTR, known for their stable secondary structures, were inserted downstream of an ubiquitin promoter and upstream of a green fluorescence protein marker gene (GFP) in the FUGW plasmid. Two of the UTR's, ODC_{274} (274 bp) and ODC_{149} (149 bp), were derived from ornithine decarboxylase. The ODC_{149} contained the loop portion of the ODC 5'UTR while the ODC_{274} is the full-length 5'UTR of ODC (246). The other 5'UTR tested was derived from FGF-2 (33, 147). A schematic representation of lentiviral plasmid constructs are presented in **Figure 4.2**.

In order to determine which construct is the most dependent on eIF4E levels for expression of GFP protein *in vitro*, both non-neoplastic and neoplastic prostate cell lines were transfected with FUGW, FU-ODC_{149}-GW, FU-ODC_{274}-GW, or FU-FGF2-GW plasmid with or without 20 nM siRNA against eIF4E. BPH-1 and PNT1B cells, which are non-malignant prostate cell lines, displayed low levels of eIF4E (**Figure 4.1**). These cell lines were transfected with each construct (**Figure 4.2**) and GFP protein levels were compared 48 h post transfection. Levels of GFP

protein expression between the various constructs containing different types of 5'UTRs were compared and normalized to FUGW control plasmid using Western blot analysis. GFP protein expression in FU-FGF2-GW transfected BPH-1 cells was determined to be the lowest, with a 91% decrease when compared to the GFP levels from FUGW plasmid transfection in the same cell line (**Figure 4.3A**). Similarly, in PNT1B cells, the level of GFP expression was decreased ~ 83% in FU-FGF2-GW transfected cell lines, followed by FU-ODC_{274}-GW GFP levels which were reduced by 34% (**Figure 4.3B**).

Next we determined the effect of each 5'UTR on GFP expression in prostate cancer cell lines LNCaP, C4-2, PC-3 and DU145 given that they displayed higher levels of eIF4E (**Figure 4.1**). Each cell line was either transfected with plasmid alone (**Figure 4.2**) or co-transfected with 20 nM of an eIF4E siRNA antisense, which effectively decreased levels of eIF4E *in* vitro (**Figure 4.4**). When LNCaP cells were co-transfected with 20 nM of eIF4E siRNA plus FU-ODC_{274}-GW, GFP protein levels were significantly reduced by ~94% ($p < 0.05$) when compared to FU-ODC_{274}-GW alone. However there was no significant difference ($p > 0.05$) in GFP expression for either FU-FGF2-GW or FU-ODC_{149}-GW in the presence or after knockdown of eIF4E (**Figure 4.5A**). In C4-2 cell lines, the levels of GFP expression after siRNA silencing of eIF4E were most drastically reduced by 91% in cells transfected with FU-ODC_{274}-GW (**Figure 4.5B**). This was followed by a 65% decrease in GFP expression in FU-FGF2-GW transfected C4-2 cells. In DU145 cells, GFP levels were decreased by almost 87% when co-transfected with FU-FGF2-GW together with eIF4E siRNA, followed by an approximately 49% decrease in GFP protein expression when transfected with FU-ODC_{274}-GW alone compared to when co-transfected with siRNA (**Figure 4.5C**).

Similar results were seen in PC-3 cell lines. There was approximately a 90% decrease in GFP expression in cells co-transfected with both FU-FGF2-GW and eIF4E siRNA, followed by a 45% reduction in GFP levels in PC-3 cells transfected with FU-ODC_{149}-GW and siRNA. However, there was no significant difference in GFP expression in PC-3 cells that were

expressing either FU- ODC_{274}-GW with eIF4E knockdown (**Figure 4.5D**). Overall, FU- ODC_{274}-GW and FU-FGF2-GW were the most sensitive to eIF4E protein levels. FU-ODC_{149}-GW expression did not correlate with presence or absence of eIF4E in the majority of the cell lines tested.

4.3.3 Levels of eIF4E are elevated in prostate tissues derived from tumour-bearing transgenic $PTEN^{-/-}$ mouse prostates

Since eIF4E is a downstream protein in the PTEN/Akt/mTOR signalling pathway, it is expected that there would be elevated expression of eIF4E in the absence of PTEN (248). Immunohistochemical analysis of prostates from 15 week old $PTEN^{-/-}$ transgenic mice and control mice were compared in a blinded study and scored by a pathologist (**Figure 4.6**). The data confirmed that deletion of PTEN in prostates led to an increase in eIF4E levels when compared to control prostates (**Figure 4.6A**). Additionally, we studied the level of other components of the eIF4E translational machinery. We observed an increase in the phosphorylated levels of eIF4E binding protein (4E-BP1) in $PTEN^{-/-}$ prostates compared to control prostates (**Figure 4.6B**). Typically when 4E-BP1 is bound to eIF4E it renders eIF4E inactive in the cytoplasm. Upon phosphorylation of 4E-BP1, it dissociates from eIF4E, allowing eIF4E to be phosphorylated and leading to an overall increase in translation (135). We found that the level of expression of the phosphorylated form of eIF4G (4G) is also higher in the prostates of $PTEN^{-/-}$ transgenic mice compared to controls (**Figure 4.6B**). 4G, which is also bound to eIF4E, is activated upon phosphorylation of eIF4E in such a way that it is now able to interact with the 40S ribosomal subunit and initiate translation (134, 135). Together, these findings confirm that there is an increase in the activity of eIF4E and a concomitant increase in the translational machinery in $PTEN^{-/-}$ prostates.

4.3.4 Protein expression driven by lentiviruses containing FU-FGF2-GW is much greater in PTEN$^{-/-}$ prostates than in PTEN$^{+/+}$ controls

To determine which 5'UTR is best expressed *in vivo*, lentiviruses were packaged with FUGW, FU- ODC_{274}-GW and FU-FGF2-GW plasmids. After titration, viruses were injected (10^9 pfu/100µl) into PTEN$^{-/-}$ and control prostates. Three days after intra-prostatic viral injection, the prostates were removed and stained with anti-eIF4E (red), anti-GFP (green) and DAPI (blue). FUGW-lentivirus was used as a control virus and its expression was monitored through GFP immunofluorescence staining (**Figure 4.7**). Protein expression of FUGW lentivirus did not stringently depend on cellular eIF4E protein levels. The level of GFP protein expression was further confirmed through Western blot analyses (**Figure 4.8**). Although there was approximately a 2-fold increase in eIF4E protein level in PTEN$^{-/-}$ prostates compared to control mouse prostates (data not shown), there was no significant difference in viral protein expression as determined by GFP levels ($p < 0.05$) in FUGW infected mice.

FU- ODC_{274}-GW-lentivirus was also injected into prostates of both PTEN$^{-/-}$ and control mice (**Figure 4.8**). Western blot analysis from three independent replicates demonstrated that there is no significant ($p > 0.05$) increase in GFP expression in FU- ODC_{274}-GW treated PTEN$^{-/-}$ mice compared to control. Conversely, PTEN$^{-/-}$ mice treated with FU-FGF2-GW showed an almost 2-fold increase in viral protein expression, ($p < 0.05$), as determined by GFP protein level, compared to control (**Figure 4.8**), indicating that, after infection with FU-FGF2-GW, lentivirus viral protein expression is more sensitive to eIF4E levels when compared to FU- ODC_{274}-GW.

4.4 Discussion

Currently, there are few treatment options available for prostate cancer patients with locally advanced or metastatic disease who have failed androgen ablation therapies (249). While docetaxel may extend survival for a few months, the patients are subjected to toxicity of normal tissue and may suffer from several adverse side effects (35). By comparison, targeted virotherapy has the potential to selectively kill cancer cells while sparing normal cells (244, 250).

In this regard, our laboratory has previously demonstrated that eIF4E is a good discriminatory factor between normal and cancer cells since eIF4E levels are substantially elevated in the latter (33, 131, 197). EIF4E is the rate limiting subunit of the eIF4F complex, which is comprised of eIF4E, the cap binding protein; eIF4A, an ATPase and RNA helicase; and eIF4G, a scaffolding protein. EIF4E is critical for initiating the process of translation by binding to the 5' cap 7-methylguanosine (m7G) present on all nuclear transcribed mRNAs (251), and together with the eIF4F complex, unwinds the excess secondary structures within the 5'UTR to facilitate the loading of the 40S ribosomal subunit to the mRNA (135, 252). In normal cells with low levels of eIF4E, mRNAs with long G/C rich 5'UTRs, such as growth factors and other oncogenic proteins, are translated less efficiently (253). However, in cancer cells, which generally have intrinsically higher eIF4E levels, these complex secondary 5'UTR structures are more readily translated (33).

In the present study we constructed three different lentiviruses containing different types and lengths of 5'UTRs derived from FGF-2 or ODC. These 5'UTR regions were chosen because of their high G/C rich secondary structures, which require elevated eIF4E for translation. Comparison of eIF4E levels in prostate cancer cell lines to those in non-malignant prostate cells (**Figure 4.1**) revealed that eIF4E levels were higher in cancer cell lines, in agreement with what has been previously shown (131). To establish that our lentiviral plasmids containing complex 5'UTRs are translated at a lower rate in non-malignant cells, lentiviral transfer plasmids (FUGW, FU-ODC_{149}-GW, FU-ODC_{274}-GW and FU-FGF2-GW) were transfected into non-malignant

prostate cells. Expression of each plasmid was estimated through GFP protein expression and normalized to control FUGW plasmid. We found (**Figure 4.3**) that in lentiviral expression plasmids containing complex secondary 5'UTR structures, upstream of protein coding sequences (GFP) the transcripts were expressed at lower levels as compared to control (FUGW). To ensure that this lower expression of complex 5'UTR-containing expression plasmids correlated with eIF4E levels, prostate cancer cell lines were co-transfected with the plasmids together with siRNA against eIF4E. As expected, in the presence of siRNA, eIF4E levels were markedly reduced in all cell lines (**Figure 4.4**). To determine which 5'UTR was more sensitive to eIF4E levels, the expression of GFP protein in prostate cancer cells transfected with lentiviral plasmids expressing transcripts with different 5'UTRs was measured in the presence or absence of the eIF4E siRNA. Our results indicated that FU-ODC_{149}-GW expression was not strictly dependent on eIF4E levels in the majority of the cell lines. However, FU-FGF2-GW expression was reduced substantially in conjunction with decreased eIF4E in the majority of cell lines tested (**Figure 4.5**). FU- ODC_{274}-GW expression was also significantly decreased in cells which were co-transfected with siRNA against eIF4E. Expression levels of FU-ODC_{274}-GW plasmid in LNCaP cells upon eIF4E knockdown with siRNA showed the greatest reduction. Hence two of the three lentivirus (FU-ODC_{274}-GW and FU-FGF2-GW), containing complex secondary 5'UTR structures, were selected for further testing *in vivo*.

Prostate specific $PTEN^{-/-}$ mice are transgenic model that develop prostate cancer with disease progression which mimics that seen in patients. Several studies have demonstrated that deletion and/or mutation of the PTEN gene leads to up-regulation of the AKT/mTOR pathway, which can lead to increased eIF4E expression (248, 254-256). To confirm this increase in translation machinery activity in our transgenic prostate-specific $PTEN^{-/-}$ mouse model, protein levels of eIF4E, along with other components of translational machinery (such as phosphorylated 4G (p4G) and phosphorylated 4E-BP (p-4EBP), were evaluated and compared

between $PTEN^{-/-}$ and control mice (**Figure 4.6**). Our results confirmed that eIF4E along with other p-4G and p-4EBP were up-regulated in prostates of $PTEN^{-/-}$ mice.

To test the efficacy and specificity of expression of each of the modified 5'UTR containing plasmids, FU-ODC_{274}-GW, FU-FGF2-GWand FUGW (control) lentiviruses were engineered and injected directly into $PTEN^{-/-}$ and control prostates. Three days later, GFP levels were evaluated by immunefluorescence and Western blot analyses. Although both FU-ODC_{274}-GW and FU-FGF2-GW were expressed predominantly in the prostates of tumour-bearing mice (**Figure 4.7**), the FU-FGF2-GW lentivirus showed a more selective preference for $PTEN^{-/-}$ prostates compared to the FU-ODC_{274}-GW virus (**Figure 4.8**). Thus GFP reporter gene expression from a virus containing a 5'UTR derived from FGF-2 proved to be more discriminatory for tumours with high levels of eIF4E.

In conclusion, we have determined that by using a 5'UTR derived from FGF-2 in genetically engineered viruses, it is possible to select tumours with high levels of eIF4E. This finding is in keeping with recent studies which have suggested that direct targeting of the translational machinery, specifically eIF4E, is required for efficient targeted therapies of androgen-independent prostate cancers (32, 257, 258). Hence, the careful testing and selection of 5'UTRs such as that derived from FGF-2 may enable the construction of a virus suitable for gene therapy in that its therapeutic proteins are selectively expressed only in tumours and not in normal tissues.

4.5 Figures

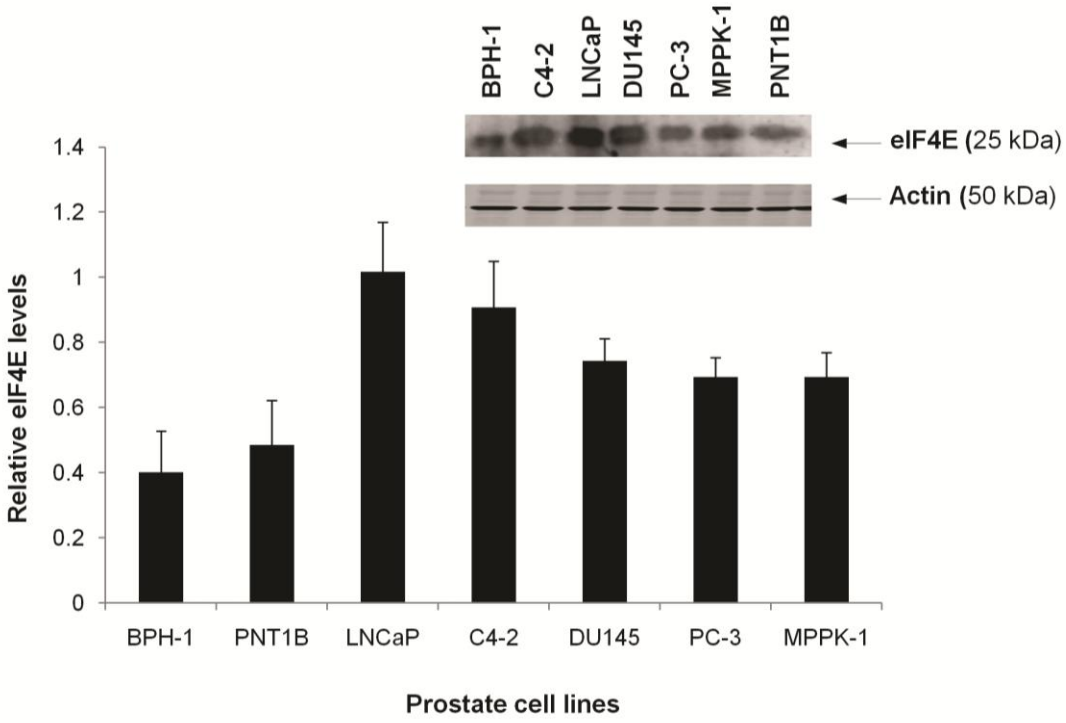

Figure 4.1 Relative expression of eIF4E in control and malignant prostate cancer cells

Relative expression of eIF4E protein in non-cancerous control (BPH-1 and PNT1B) and malignant (C4-2, LNCaP, DU145, PC-3, and MPPK-1) cell lines. Whole cell protein extracts from the cell lines indicated were resolved on SDS-PAGE and compared by Western blotting for eIF4E. Density ratios of eIF4E levels were normalized to β-actin. Results are from at least three independent experiments and expressed as means ± SEM.

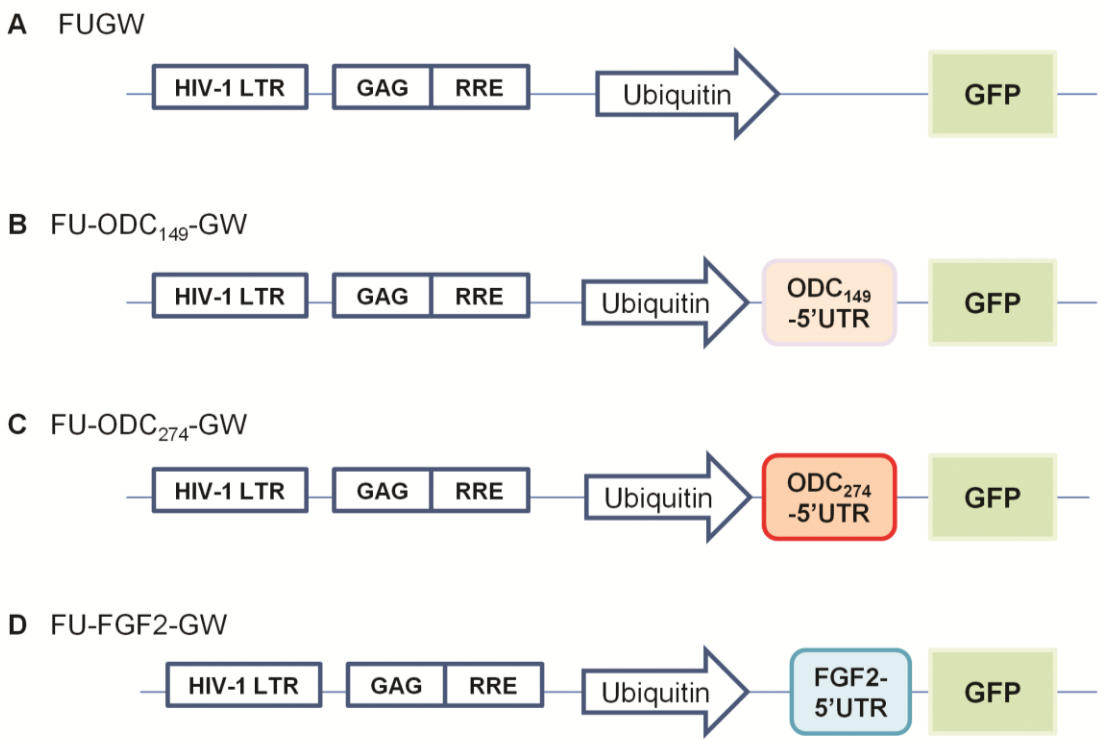

Figure 4.2 The four lentiviral transfer vectors used in this study

(A) The control vector FUGW, contains ubiquitin promoter upstream of a GFP expression gene.

(B) Lentiviral transfer vector containing the loop portion of ODC's 5'UTR mRNA, (FU-ODC_{149}-GW).

(C) Lentiviral transfer vector containing the complete 5'UTR from ODC mRNA, (FU-ODC_{274}-GW).

(D) Lentiviral transfer vector containing the 5'UTR from FGF-2 growth factor, (FU-FGF2-GW).

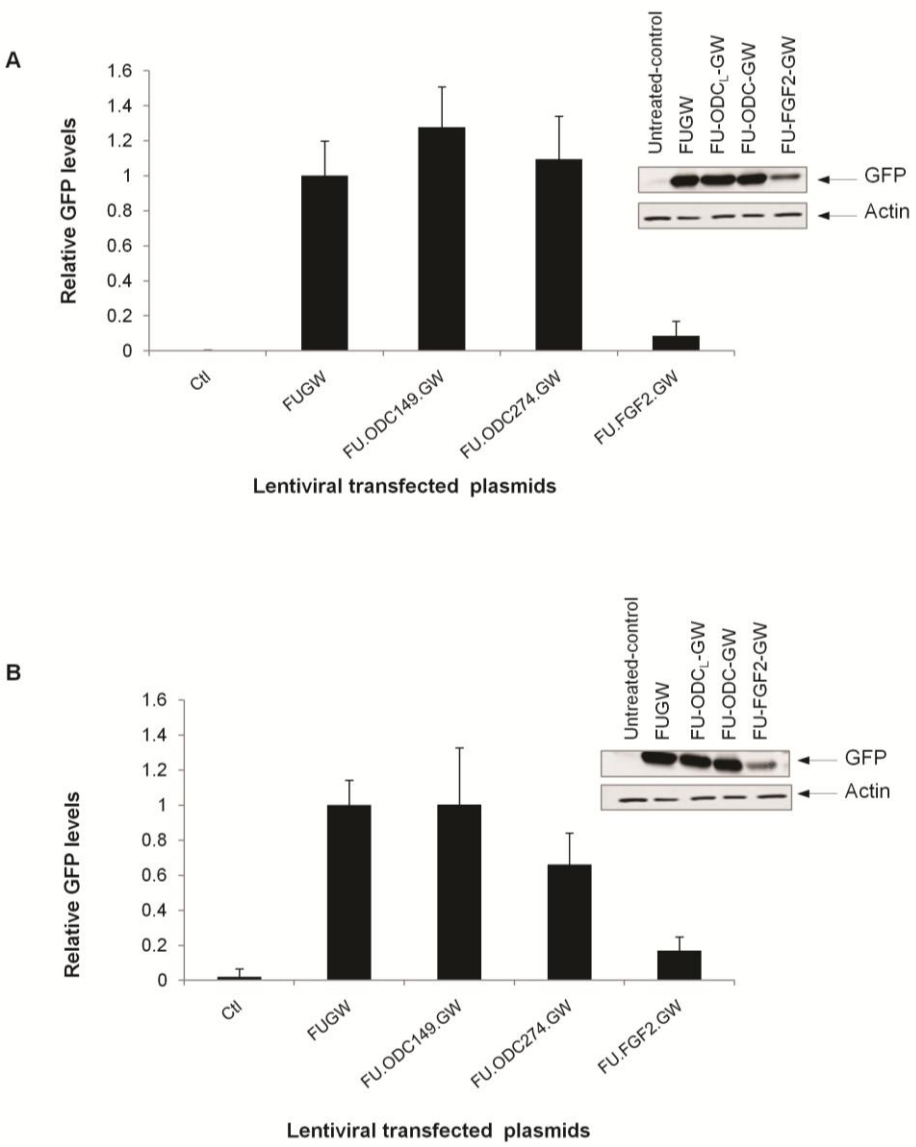

Figure 4.3 Expression of lentiviral plasmids containing 5'UTRs in control prostate cells

Measurement of GFP expression after transfection of non-malignant prostate cells with different lentiviral plasmids (FUGW, FU-ODC$_{149}$-GW, FU-ODC$_{274}$-GW, and FU-FGF2-GW). (A) BPH-1 and (B) PNTIB cells were transfected with lentiviral plasmids containing different 5'UTRs. GFP levels were measured and ratios of GFP levels normalized to β-actin and FUGW control plasmid were graphed (n=3; as means ± SEM).

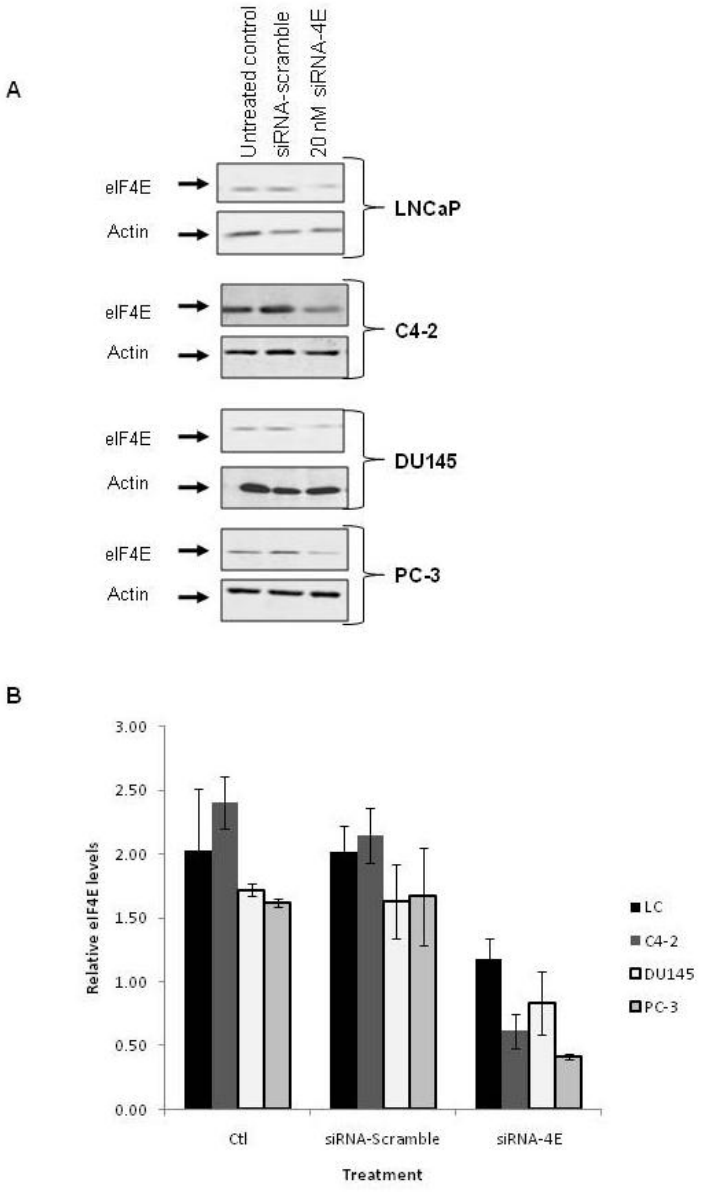

Figure 4.4 siRNA knock-down of eIF4E in prostate cancer cells

Human prostate cancer cell lines (LNCaP, C4-2, DU145 and PC-3) were transfected with 20 nM of siRNA against eIF4E. (A) Western blot analysis demonstrated that eIF4E protein level is reduced in each cell line transfected with siRNA compared to non-transfected control and siRNA-scrambled. (B) Density ratios of eIF4E levels were normalized to β-actin. Results are from at least four independent experiments and expressed as means ± SD.

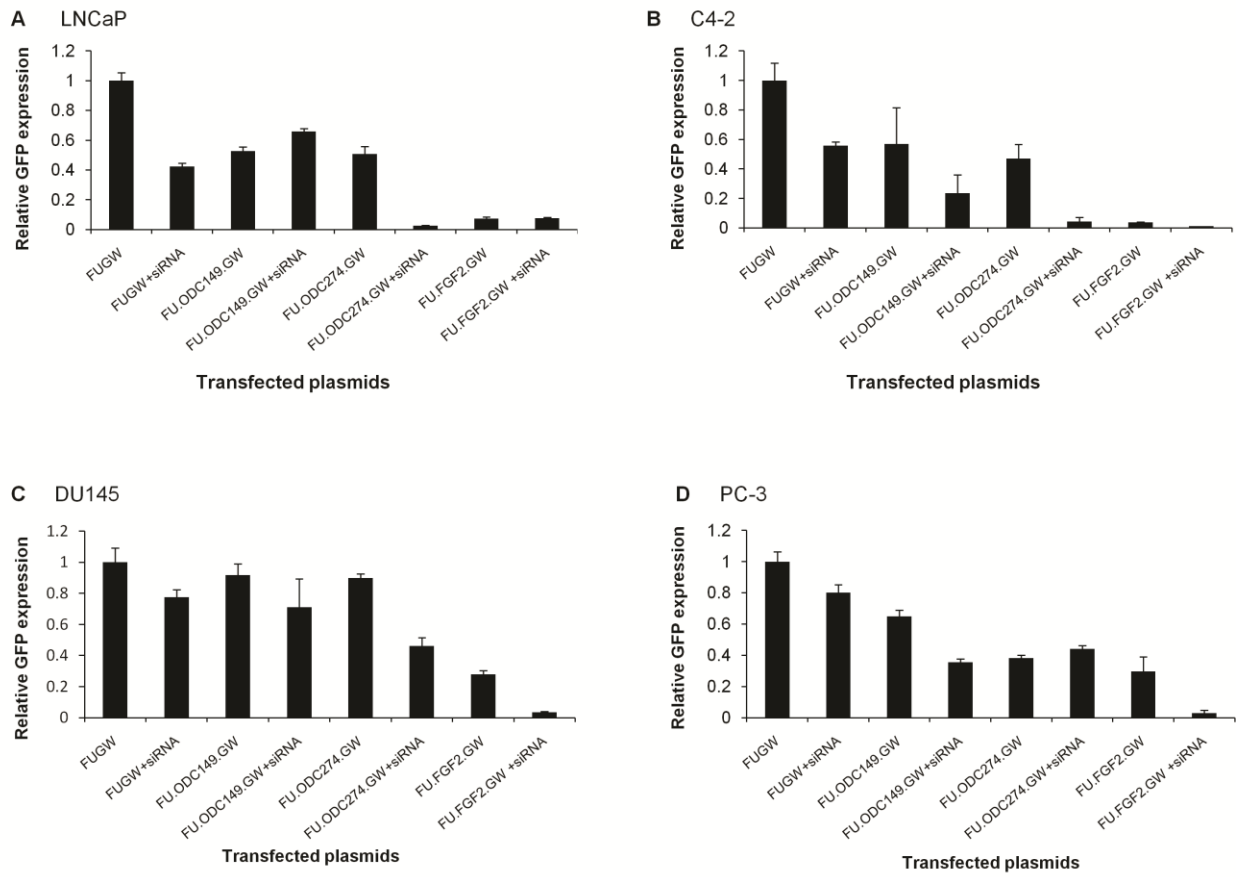

Figure 4.5 Expression of lentiviral plasmids containing 5'UTRs in prostate cancer cells

To determine which 5'UTR is most dependent on eIF4E expression, prostate cancer cell lines were co-transfected with the lentivirus transfer plasmids both alone and in the presence of 20 nM of siRNA against eIF4E. GFP protein levels in (A) LNCaP, (B) C4-2, (C) DU145 and (D) PC-3 prostate cancer cells co-transfected with 20 nM of si4E and lentiviral vectors were measured. Density ratios of GFP protein levels were normalized to β-actin and FUGW control plasmid in transfected cells. Results are from at least three independent experiments and expressed as means ± SEM.

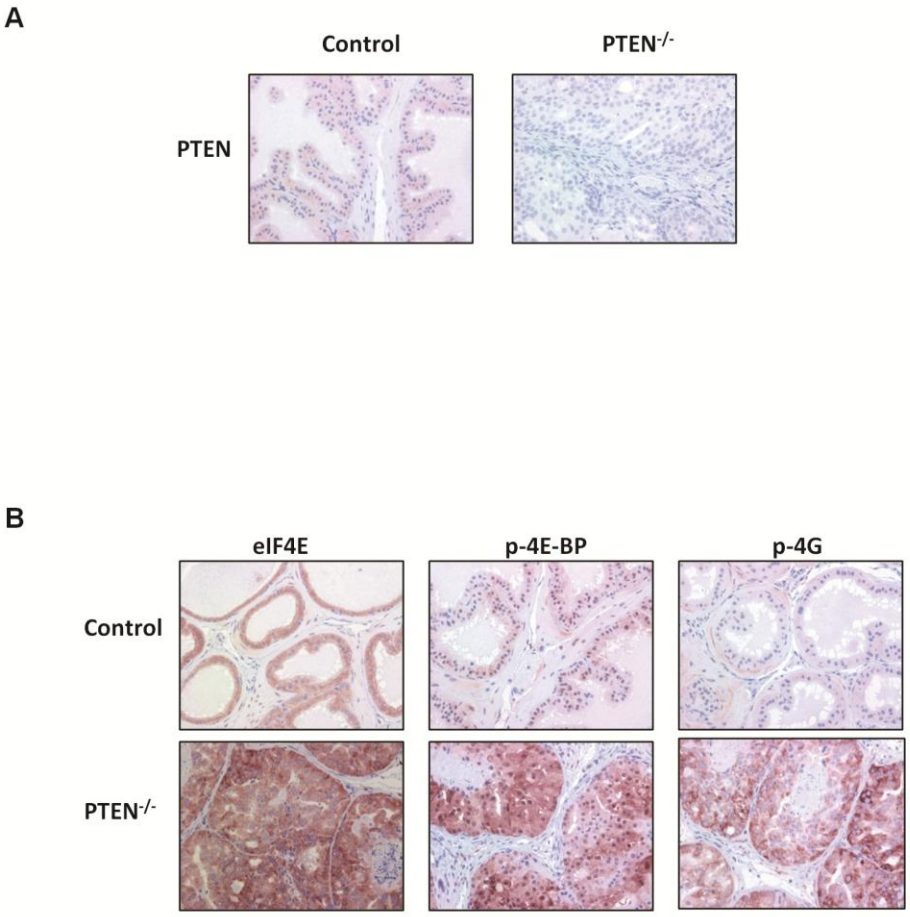

Figure 4.6 Levels of eIF4E family of translational initiation factors were analyzed in prostate tissues derived from PTEN$^{-/-}$ and control mice

(A) Paraffin-embedded tissues were stained with PTEN antibody to demonstrate PTEN knockout in tumour-bearing PTEN$^{-/-}$ mice.

(B) Paraffin-embedded tissues were stained with anti-eIF4E, anti-eIF4E Binding Protein 1 (4E-BP1), anti-phospho-4E-BP1 and anti-phospho-4G antibodies. Representative slides were prepared and visualized at 20x magnification. Results were scored by a pathologist (n = 3).

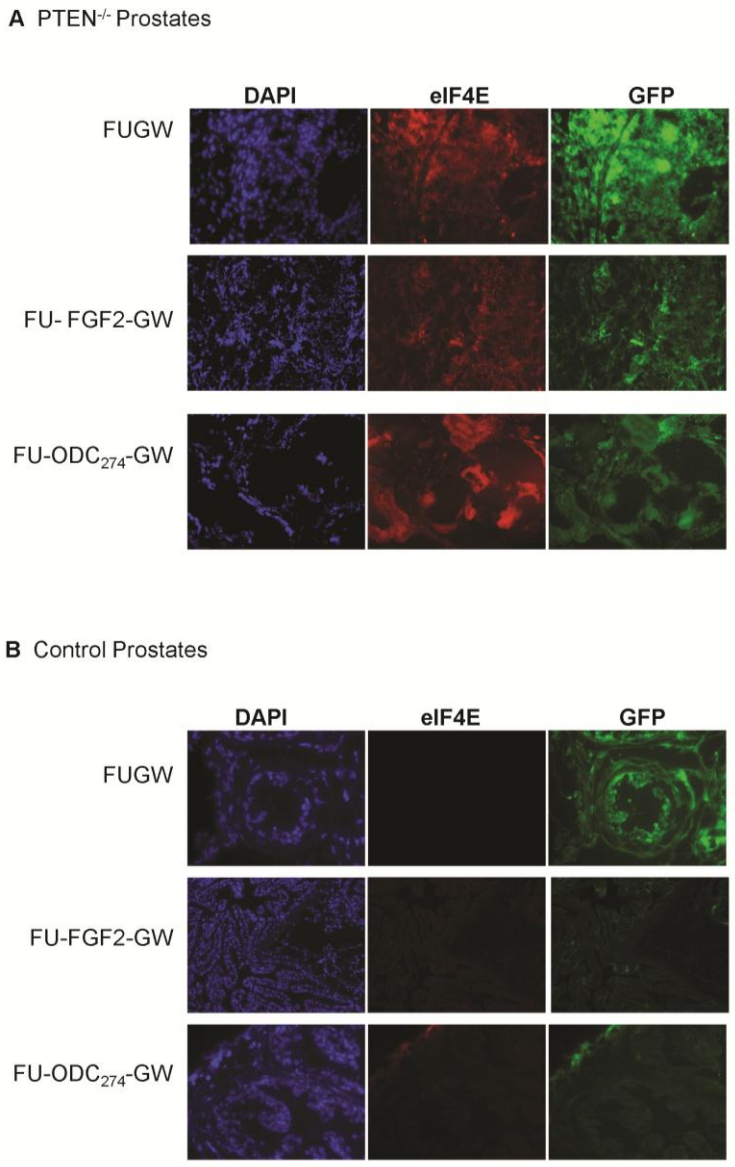

Figure 4.7 Representative immunofluorescence staining of prostate tissues from PTEN$^{-/-}$

(A) and control (B) mouse prostate tissue. Tissues were stained for eIF4E and GFP proteins 72 h post intra-prostatic lentiviral injection with FUGW, FU-ODC$_{274}$-GW or FU-FGF2-GW virus. The nuclei of the prostate cells have been stained with DAPI. Data is representative of three independent experiments at 40x magnification.

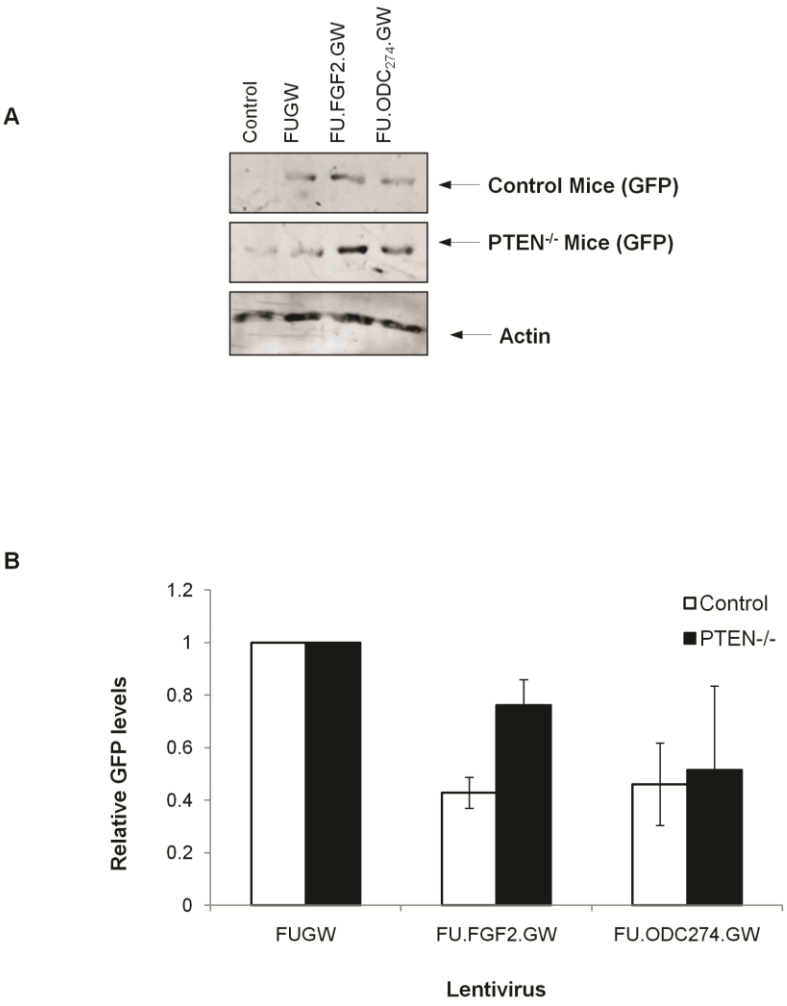

Figure 4.8 GFP protein levels in prostates of PTEN$^{-/-}$ and control mice after intra-prostatic injection of lentivirus containing 5' UTRs

GFP protein levels in PTEN$^{-/-}$ and control prostates infected with 100 µl of 10^9 pfu/ml of lentivirus containing FUGW, FU-ODC$_{274}$-GW, or FU-FGF2-GW. In each group, control mice were intra-prostatically injected with 100 µl PBS, labelled as control. (A) GFP and β-actin expression was determined by Western blot analysis. (B) Density ratio of GFP levels were normalized to both β-actin and control virus containing FUGW27

transfer plasmid. Results are from three independent experiments and expressed as means ± SEM.

5. General summary, conclusions and future directions

5.1 Summary and discussion

Prostate cancer is the second leading cause of cancer-related mortality in North American men. The Canadian cancer society predicts that 1 in 7 men will develop prostate cancer in his lifetime (26). Androgen ablation therapy remains the gold standard treatment for advanced prostate cancer (73, 74). Initially, approximately 70-80% of patients that receive androgen ablation therapy respond to this line of treatment; however, the majority of patients progress to castration-resistant prostate cancer (CRPC) within 12 to 18 months (129). Even though new lines of chemotherapy agents, such as doecetaxel, improve the quality of life in CRPC patients, they remain palliative in nature and not curative (129). Therefore, the development of a non-conventional approach to the treatment of prostate cancer is needed.

A unique approach to combat prostate cancer is through the use of viruses. Oncolytic viruses are biological arsenals packaged as replication-competent viruses, which may provide a non-surgical treatment approach for prostate cancer. Recently, the anti-tumour capabilities of oncolytic viruses, such as adenovirus and reovirus, have been clinically tested in prostate cancer patients. These trials have demonstrated that prostate cancer is a good candidate for oncolytic viral therapy, as viral delivery is relatively easy due to the anatomical location of the prostate gland. However, viral efficacy remains limited. To date, the majority of pre-clinical testing of various oncolytic viral treatments are in xenograft mouse models. These models, though convenient in the laboratory setting, do not imitate organ-confined disease progression as seen in humans. Additionally, xenograft models are typically immune-compromised animals; therefore, the immune response to viral therapy is not taken into account. Hence, it is important to conduct pre-clinical testing of oncolytic viruses in various transgenic, organ-confined, and immune-competent animals.

This thesis, for the first time, explores the oncolytic ability of a modified Vesicular Stomatitis Virus (VSV(AV3)) in pre-clinical transgenic prostate cancer models. Thus, the main hypothesis investigated in this study proposes that the oncolytic VSV(AV3) can efficiently and selectively kill prostate adenocarcinoma cells over normal cells in mouse models that mimic human prostate cancer development. Both VSV and VSV(AV3) have been previously discussed in section 1.5.1. Briefly, VSV is a non-pathogenic, negative, single-stranded RNA virus that is sensitive to the antiviral action of type I interferons (IFNs). The VSV(AV3) strain contains a deletion mutation of methionine at position 51 of the viral M-protein, thus making the virus even more susceptible to the host IFN response. Additionally, an insertion of GFP-luciferase fusion gene between G and L in the VSV(AV3)'s genome allows us to track the virus *in vitro* and *in vivo*.

The rationale for using VSV(AV3) is based on the results of previous studies demonstrating that ~30% of prostate cancers have a defective innate immune IFN response (171, 172). In this study, the effect of intra-prostatic injections of VSV(AV3) have been explored in organ-confined and metastatic prostate cancer disease using prostate-specific $PTEN^{-/-}$ (Chapter 2) and TRAMP (Chapter 3) mice, respectively (**Figure 5.1**). Additionally, an alternate targeting strategy based on the elevation of eIF4E protein in prostate cancer has been employed to enhance future oncolytic viral targeted killing of prostate cancer (Chapter 4).

5.1.1 *In vitro* analysis of cytotoxicity and IFN response in prostate cancer cell lines

It is generally accepted that the goal of viral therapy is to target and kill cancer cells while sparing normal cells (218, 219). Hence, pre-clinical *in vitro* and *in vivo* testing of oncolytic viruses are key steps to ensure the potential efficacy and safety of each viral therapy prior to clinical application. Initially, VSV(AV3)'s cytotoxicity was evaluated in prostate cancer cells and compared to normal prostate epithelial cells (Chapter 2). It was determined that both human (LNCaP) and mouse (MPPK-1 and TRAMP-C2) prostate cancer cells were highly susceptible to

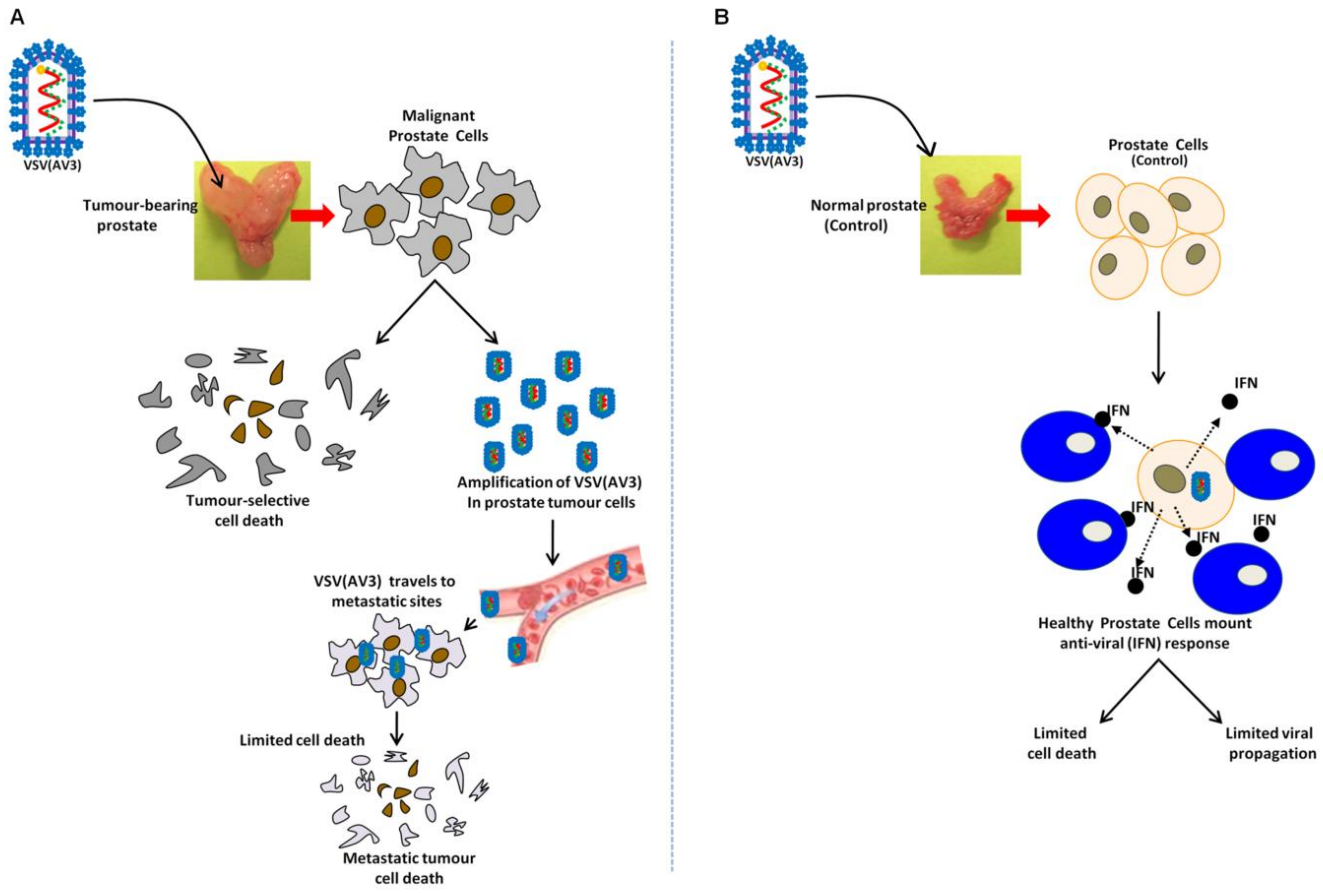

Figure 5.1 Summary of VSV(AV3)s effect on pre-clinical models of prostate cancer

(A) Intra-prostatic injection of VSV(AV3) into tumour-bearing prostates leads to cell death and increase in viral load. VSV(AV3) was then able to travel to distant metastatic sites to infect and kill malignant cells.

(B) Intra-prostatic injection of VSV(AV3) into control prostates lead to activation of anti-viral response. Infected prostate cells produced interferon (IFN) and signalled their neighbouring cells to limit viral propagation and viral-induced cell death.

VSV(AV3) infection, as determined through cell-survival (MTS) analysis (Chapter 2 and 3). Conversely, normal prostate epithelial cells, such as RWPE-1, did not display the same vulnerability to VSV(AV3) infection. This was later determined to be due to an intact IFN response present in control prostate cells (Chapter 2). However, not all prostate cancer cells are equally susceptible to VSV(AV3) infection. A previous study has demonstrated that PC-3 prostate cancer cells are more resistant to VSV infection (Chapter 2), thus, suggesting that prostate cancer cells vary in the extent of defects in their antiviral immune response, namely IFN pathways (225). Similarly, we demonstrate that although TRAMP-C2 cells are susceptible to VSV(AV3) infection, pre-incubation of these cells with IFN partially rescues them from VSV(AV3)-induced cell death (Chapter 2 and 3). This partial IFN response can be advantageous in the clinic and may be used as a safety mechanism for viral clearance from the body through the administration of IFN.

5.1.2 *In vivo* demonstration of VSV(AV3) spread, amplification, and infection

Intra-prostatic administration of VSV(AV3) into two transgenic mouse models was conducted to observe the potency of VSV(AV3) on prostate disease at the organ-confined (prostate specific PTEN$^{-/-}$) and metastatic (TRAMP) stages (Chapter 2 and 3). Viral spread and load were monitored through bioluminescence and plaque analysis. It was determined that virus spread begins as early as 3-6 h post viral administration and lasts for longer periods with higher bioluminescence (photon/second) in tumour-bearing animals compared to the control. In both PTEN$^{-/-}$ and TRAMP mice, there were evidence of viral amplification in the prostate tumours, suggesting that intra-prostatic injections of VSV(AV3) lead to increase in viral load at the tumour site which in theory, is then able to travel and find distant metastatic lesions. This ability of VSV(AV3) to travel and seek metastatic lesions is evident in the TRAMP mice, where there was evidence of viral presence in distant metastatic lesions (lymph nodes and lungs). These data were substantiated through plaque analysis and immunohistochemical staining for VSV in the enlarged pelvic lymph nodes (Chapter 3). These data corroborate earlier findings demonstrating

VSV's ability to find and infect distant metastatic lesions of gliomas, colon cancer, and breast cancer (241, 242, 259).

Initially, post-VSV(AV3) administration, live viral particles were found in the spleens of control, PTEN$^{-/-}$, and TRAMP mice. The spleen is an important lymphoid organ in which a complex interplay occurs between innate and adaptive immunity (260). Previous studies have demonstrated that splenic macrophages act to harness VSV infection and, in their absence, VSV is able to disseminate ubiquitously even in the presence of a high type I IFN response (260). Therefore, the presence of VSV in the spleen of infected mice, regardless of tumour status, may be indicative of the attempt by the host anti-viral immunity to clear VSV from the body.

5.1.3 VSV(AV3) induced tumour-selective toxicity *in vivo*

As previously mentioned, the aim of viral-therapy is to selectively kill malignant tissue while sparing normal tissue (218, 219). Thus, to determine whether VSV(AV3) treatment led to targeted cell death, TUNEL staining was employed. Prostate tissues from PTEN$^{-/-}$ and control mice were extracted at daily intervals between 24-96 h post viral injection (Chapter 2). TUNEL analysis determined a higher level of apoptotic cell death in the prostate tumours treated with VSV(AV3) compared to tumours treated with UV-inactivated virus. Also, a substantially higher amount of cell death was observed in the tumours of PTEN$^{-/-}$ mice compared to control. Cell proliferation was also monitored post-VSV(AV3) infection, and it was determined that VSV(AV3) did not manipulate or halt cell proliferation (Chapter 2). These data are analogous with previous work demonstrating VSVs' ability to induce apoptosis in malignant prostate cancer cell lines and xenograft models (225).

Theoretically, a key advantage of using oncolytic virus as a treatment option is its ability to multiply in tumour cells, thus increasing viral load that has a better chance of seeking and infecting distant metastatic sites. Previous studies, in breast cancer and brain gliomas, have shown viral targeting of metastatic cancer after the intravenous injection of VSV into nude and

Balb/c mice (241, 242). Additionally, VSVs' ability to enhance tumour cell death has been previously shown in gliomas. Here, for the first time, we demonstrate that after intra-prostatic injection of VSV(AV3), the virus travels to known metastatic lesions, such as lymph nodes of TRAMP mice, causing infection and cell death (Chapter 3). TUNEL analysis of enlarged lymph nodes in TRAMP mice shows a significant increase in cell death compared to UV-inactivated treated metastatic lymph nodes. Additionally, similar to that seen in the prostate, there is a significant increase in apoptotic cell death seen in metastatic lymph nodes when compared to normal lymph nodes extracted from non-tumour-bearing mice (Chapter 3). The immune evasion ability of VSV(AV3) in malignant tissues was further evaluated in the two prostate specific $PTEN^{-/-}$ and TRAMP transgenic models.

5.1.4 VSV(AV3) and the innate anti-viral immune response

Some of the advantages of using transgenic mice for pre-clinical testing include the fact that the cancer arises *in situ* in the target tissues with the appropriate microenvironment, and the mice have an intact immune system (178, 188, 189). Previous studies have shown that VSV infection of subcutaneous tumours in Balb/c mice caused apoptotic cell death through the loss of blood flow to the interior of the tumour (209). It was determined that the absence of vascular perfusion seen in the infected tumours was induced by the recruitment of neutrophils. Neutrophils are phagocytic cells that originate from white blood cells (WBC) and are part of the innate immunity (226). They typically act as first responders to infection. In order to see if neutrophils were involved in increased apoptotic cell death seen in VSV(AV3)-treated tumours, the prostates of $PTEN^{-/-}$ and control mice were stained for the presence of neutrophils (Chapter 2). Although, there was initial neutrophil infiltration in prostates of both control and tumour-bearing mice, there is no evidence of an association between neutrophils and induction of apoptotic cell death in the VSV(AV3)-treated $PTEN^{-/-}$prostate tumours. However, macrophages, which are another type of phagocytic innate immune response cells, were found in abundance in prostate tumours compared to control tissue. It is noteworthy that the increase in macrophage

infiltration of tumours is predominantly seen post-apoptotic episodes (i.e. maximum apoptosis observed at 48 h post-treatment, followed by an increase in macrophages seen at 72 h post-viral injection). The increase in macrophages could be necessary for clearance of apoptotic cells and the inhibition of viral replication through phagocytic clearance of the virus from the infected tissue (227, 228).

VSV infection of normal cells leads to the production of type I IFN (IFN-α/β), an innate host anti-viral response (discussed in section 1.5.2). The status of IFN pathway components has been evaluated in infected prostate tumours (Chapter 2 and 3) and metastatic lymph nodes (Chapter 3). The IFN pathway components IRF-3 and IRF-7, which play key roles in the transcription of IFN-α/β, were shown to be dysfunctional in tumour-bearing prostates of both PTEN$^{-/-}$ (Chapter 2) and TRAMP (Chapter 3) mice, thus enabling viral infection. The lack of IRF-7 activity is corroborated with low levels of IFN-α mRNA in the prostate tumours of PTEN$^{-/-}$ and TRAMP mice post-viral infection. However, there is clear evidence of IFN activity in the metastatic lymph nodes derived from TRAMP mice. In general, lymph nodes are largely comprised of lymphocytes (235). Thus, the presence of VSV in metastatic lymph nodes of TRAMP mice could induce hyper-activation of IFN response in the resident lymphocytes.

This observation of IFN activity, along with previous reports that a portion of prostate cancers have an intact IFN immune response, can potentially hinder VSV(AV3) effectiveness in the clinic (171, 172). Therefore, alternate targeting strategies need to be employed to enhance VSV(AV3) efficacy.

5.1.5 Using eIF4E over-expression as an alternate targeting strategy

Over-expression of eukaryotic translation initiation factor 4E (eIF4E) and its link to carcinogenesis have been well documented (139, 144-146). In prostate cancer, eIF4E over-expression has been seen in tissue micro-arrays derived from prostate cancer patients (33). For this reason, eIF4E was chosen as a potential selection criterion to enhance tumour specificity of

viruses (discussed in detail in sections 1.4.1.4.1 to 1.4.1.4.4) (33, 148). Briefly, eIF4E plays an important role in the translation of select proteins involved in developmental processes such as growth factors, proto-oncogenes, and transcription factors (245). Usually, the 5'UTR of these mRNAs contains highly complex secondary structures that require higher levels of eIF4E/eIF4F complex to unwind their 5'UTRs for efficient translation (147). Thus, a genetically engineered virus whose replication mechanisms are under the control of eIF4E should be expressed more selectively in tumour cells with higher levels of eIF4E protein (148).

There are various choices of 5'UTRs that could potentially be suitable for targeting prostate cancer. The 5'UTRs from FGF-2 and ODC, for example, have previously been shown to contain extensive stable secondary structures (148, 246, 247). In this study, three different lentiviruses containing different types and lengths of 5'UTRs derived from FGF-2 or ODC ranging from low (ODC_{149}) , medium (ODC_{274}) and high (FGF-2) size and complexity, were constructed and tested to determine the best 5'UTR for targeting prostate cancer (Chapter 4). Each 5'UTR was inserted downstream of ubiquitin promoter and upstream of enhanced fluorescent green reporter protein (GFP) in a lentiviral transfer plasmid. The dependence of each 5'UTR on eIF4E levels was tested through transfection of each lentiviral plasmid into non-malignant control (PNT1B and BPH-1) and malignant (LNCaP, C4-2, DU145, and PC-3) prostate cells. The expression of the GFP reporter gene in each plasmid was estimated by measuring GFP protein levels. In non-malignant cells, plasmids containing complex secondary 5'UTR structures within the GFP transcripts, displayed lower plasmid expression (GFP) as compared to control. Transfection of malignant cells with lentiviral plasmids containing different complexity of 5'UTR in the presence or absence of siRNA against eIF4E indicated that the expression of 5'UTRs derived from full-length ODC (ODC_{274}) and FGF-2 were the most dependent on eIF4E levels. The two selected 5'UTRs (FGF-2 and ODC_{274}) were then tested in prostate-specific $PTEN^{-/-}$ mice *in vivo.*

Previous studies have demonstrated that deletion and/or mutation of the PTEN gene leads to an up-regulation of the AKT/mTOR pathway, which can lead to increased eIF4E expression (248). To evaluate the status of eIF4E levels *in vivo,* prostate tissues from $PTEN^{-/-}$ and control mice were compared. Our results confirmed that eIF4E, along with other components of translational machinery, were up-regulated in prostates of $PTEN^{-/-}$ mice. Next, the specificity of expression of GFP transcripts downstream of the modified 5'UTR (FGF-2 and ODC_{274}) were tested *in vivo*. Lentivirus containing either 5'UTRs (FGF-2 and ODC_{274}) were intra-prostatically injected into $PTEN^{-/-}$ and control mice. As expected, lentiviruses containing 5'UTRs (ODC_{274} and FGF2) were expressed predominantly in the prostates of tumour-bearing $PTEN^{-/-}$ mice as compared prostates of control mice. The FGF-2 derived 5'UTR containing lentivirus, showed a greater cancer specificity compared to the ODC_{274} derived 5'UTR virus. Thus, virus containing FGF-2 derived 5'UTR proved to be more discriminatory toward tumours with high levels of eIF4E (Chapter 4). This data enables future targeting of prostate cancer with oncolytic viral therapy using FGF-2 5'UTR.

5.2 Overall thesis conclusions and future directions

The main objective of this thesis has been to test the efficacy of a previously unused oncolytic virus, VSV(AV3), in targeting and destroying malignant prostate cancer cells in various transgenic models of prostate cancer. More specifically, our initial aim was to determine whether VSV(AV3) was able to infect and destroy prostate tumours of $PTEN^{-/-}$ mice. To test this aim, VSV(AV3) was intra-prostatically injected into $PTEN^{-/-}$ transgenic mice. Intra-prostatic injection of VSV(AV3) led to the targeted infection and killing of prostate cancer cells *in vivo* (Chapter 2). It was concluded that the presence of a defective IFN response in the tumour-bearing prostates of $PTEN^{-/-}$ mice was responsible for VSV(AV3)'s ability to cause prostate cancer selective infection and cell death. Although previous reports in xenograft tumours alluded to tumour death being a by-product of neutrophil infiltration (209), here, we found that neutrophil infiltration was not associated with cell death and tumour-specific cell death in VSV-treated prostate

tumours due to viral oncolysis. These results suggest that the control of locally advanced human prostate cancer may be achievable through intra-prostatic injections and the amplification of a safe oncolytic virus such as VSV(AV3).

The second aim of this thesis was to explore whether VSV(AV3) would be able to find and infect distant metastatic lesions. This objective was tested by the injection of VSV(AV3) into the prostates of TRAMP mice (Chapter 3). Immunohistochemical staining and plaque analysis of enlarged lymph nodes from the TRAMP mice revealed that the VSV(AV3) was able to travel and infect these metastatic lesions. Additionally, we demonstrated that the virus was capable of causing apoptotic cell death. These results suggest that VSV(AV3) can be used for targeting metastatic lesions. However, in the TRAMP mice, there is evidence of IFN anti-viral response, which is probably caused by the normal lymphocyte present in the lymph nodes. Although the activation of type I IFNs did not eliminate VSV(AV3)'s ability to kill metastatic cells, it is possible that it may hinder further viral amplification, spread, and oncolysis. Therefore, the future long term effects of IFN activation on VSV(AV3)'s ability to eliminate these metastatic cells in the lymph nodes should be further studied.

The third aim was to construct new viral vectors containing complex 5'UTR sequences as an alternate targeting strategy of prostate tumours based on elevated eIF4E levels. Three different lentiviral plasmids, containing different length 5'UTRs derived from either FGF-2 or ODC, were constructed. Initially, the dependence of each 5'UTR on eIF4E expression was tested *in vitro*. The expression of each 5'UTR containing lentiviral plasmid was evaluated and compared between malignant cells with high eIF4E to malignant cells treated with siRNA against eIF4E. Results of *in vitro* analysis, demonstrated that FGF-2 and full-length ODC (ODC_{274}) 5'UTRs were the most sensitive to eIF4E levels. Thus, lentivirus containing either FGF-2 or full-length ODC (ODC_{274}) 5'UTRs were propagated and intra-prostatically injected into $PTEN^{-/-}$ and control mice. Ultimately, 5'UTR derived from FGF-2 was determined to be more cancer-specific *in vivo* and thus superior to 5'UTR derived from ODC (ODC_{274}). These

experiments were conducted so as to incorporate translational targeting into VSV(AV3) as a means to enhance the cancer-specific targeting of malignant cells that have an intact IFN anti-viral response.

In addition to the third aim devised in this thesis, using VSV(AV3) in combination with other chemical, radiological, and/or biological therapies may enhance tumour killing. Currently, there are numerous studies conducted in other (non-prostate) tumour models testing effects of oncolytic viral therapy in combination with existing standard treatments. One study has revealed enhancement of VSV(AV3) efficacy in colon carcinoma xenografts that are typically resistant to VSV(AV3) infection through pre-treatment of the tumours with another oncolytic agent, Vaccinia Virus (VV). Such combination treatments can potentially increase viral efficacy and thus, accelerate acceptance of these therapies into the clinic.

5.3 Thesis significance

Over the past two decades, significant progress has been made in the field of oncolytic viral therapy (113, 122, 261). More recently, an increase of interest in using oncolytic viruses as a therapeutic option for the treatment of prostate cancer has become a reality, and several promising advances have been reported (109, 110, 129, 130). Thus far, extensive clinical reports on the application of adenovirus and reovirus have been accounted (129, 149, 151, 244). Current data demonstrate the safety of the application of viral therapy; however, the efficacy of these treatments remains low. To overcome this deficiency, new pre-clinical research on other potential therapeutic oncolytic viruses is required.

The results presented in this research project demonstrate the oncolytic effects of VSV(AV3) in pre-clinical prostate cancer animal models. Intra-prostatic injections of VSV(AV3) was shown to selectively infect prostate tumour cells. Infection of prostate tumour cells led to amplification in viral load and eventually, cancer-specific cell death. This increase in viral load created the potential for VSV(AV3) to travel unimpeded to distant metastatic sites, where it was able to infect and kill metastatic cells. In addition, initial steps to enhance anti-tumour efficacy

and specificity of VSV(AV3) have been made through exploitation of increased expression of eIF4E-dependent 5'UTRs in prostate cancer cells. Ultimately, this research provides a pre-clinical demonstration of anti-tumour ability of a previously unused oncolytic virus VSV(AV3). A combination of VSV(AV3), with current prostate cancer therapies, will be the subject of future studies, which may provide a possible curative option for the treatment of prostate cancer. Especially since oncolytic viruses have unique cytotoxic mechanisms that are distinct from typical drug induced mechanisms. Indicating that oncolytic VSV(AV3) may be used for treatment of patients with advanced metastatic prostate cancer, which have displayed resistance to current chemotherapeutic options.

References

1. Kumar VL, Majumder PK. Prostate gland: structure, functions and regulation. Int Urol Nephrol 1995;27:231-43.

2. Amirghofran Z, Monabati A, Khezri A, Malek-Hosseini Z. Apoptosis in transitional cell carcinoma of bladder and its relation to proliferation and expression of p53 and bcl-2. Pathol Oncol Res 2004;10:154-8.

3. Chen Y, Sawyers CL, Scher HI. Targeting the androgen receptor pathway in prostate cancer. Curr Opin Pharmacol 2008;8:440-8.

4. Cunha GR, Tuohimaa P, Visakorpi T. Steroids and prostate cancer. J Steroid Biochem Mol Biol 2004;92:219-20.

5. McNeal JE. The zonal anatomy of the prostate. Prostate 1981;2:35-49.

6. Cohen RJ, Shannon BA, Phillips M, Moorin RE, Wheeler TM, Garrett KL. Central zone carcinoma of the prostate gland: a distinct tumor type with poor prognostic features. J Urol 2008;179:1762-7; discussion 7.

7. Long RM, Morrissey C, Fitzpatrick JM, Watson RW. Prostate epithelial cell differentiation and its relevance to the understanding of prostate cancer therapies. Clin Sci (Lond) 2005;108:1-11.

8. Niu YN, Xia SJ. Stroma-epithelium crosstalk in prostate cancer. Asian J Androl 2009;11:28-35.

9. Huss WJ, Gray DR, Werdin ES, Funkhouser WK, Jr., Smith GJ. Evidence of pluripotent human prostate stem cells in a human prostate primary xenograft model. Prostate 2004;60:77-90.

10. Bonkhoff H, Stein U, Remberger K. The proliferative function of basal cells in the normal and hyperplastic human prostate. Prostate 1994;24:114-8.

11. Evangelou AI, Winter SF, Huss WJ, Bok RA, Greenberg NM. Steroid hormones, polypeptide growth factors, hormone refractory prostate cancer, and the neuroendocrine phenotype. J Cell Biochem 2004;91:671-83.

12. Sherwood ER, Theyer G, Steiner G, Berg LA, Kozlowski JM, Lee C. Differential expression of specific cytokeratin polypeptides in the basal and luminal epithelia of the human prostate. Prostate 1991;18:303-14.

13. di Sant'Agnese PA. Neuroendocrine cells of the prostate and neuroendocrine differentiation in prostatic carcinoma: a review of morphologic aspects. Urology 1998;51:121-4.

14. Marcu M, Radu E, Sajin M. Neuroendocrine transdifferentiation of prostate carcinoma cells and its prognostic significance. Rom J Morphol Embryol;51:7-12.

15. Abrahamsson PA. Neuroendocrine cells in tumour growth of the prostate. Endocr Relat Cancer 1999;6:503-19.

16. di Sant'Agnese PA, De Mesy Jensen KL. Endocrine-paracrine cells of the prostate and prostatic urethra: an ultrastructural study. Hum Pathol 1984;15:1034-41.

17. Hermann M, Untergasser G, Rumpold H, Berger P. Aging of the male reproductive system. Exp Gerontol 2000;35:1267-79.

18. Sampson N, Untergasser G, Plas E, Berger P. The ageing male reproductive tract. J Pathol 2007;211:206-18.

19. Peeling WB, Pike A, Harper ME, Pierrepoint CG, Griffiths K. Testosterone metabolism in vivo by human prostatic tissue. Biochem J 1970;120:443-5.

20. Welen K, Damber JE. Prostate diseases - role of sex steroids and their inhibitors. Best Pract Res Clin Endocrinol Metab;25:355-67.

21. Canales BK, Zapzalka DM, Ercole CJ, et al. Prevalence and effect of varicoceles in an elderly population. Urology 2005;66:627-31.

22. Levinger U, Gornish M, Gat Y, Bachar GN. Is varicocele prevalence increasing with age? Andrologia 2007;39:77-80.

23. Gat Y, Gornish M, Heiblum M, Joshua S. Reversal of benign prostate hyperplasia by selective occlusion of impaired venous drainage in the male reproductive system: novel mechanism, new treatment. Andrologia 2008;40:273-81.

24. Frieben RW, Lin HC, Hinh PP, Berardinelli F, Canfield SE, Wang R. The impact of minimally invasive surgeries for the treatment of symptomatic benign prostatic hyperplasia on male sexual function: a systematic review. Asian J Androl;12:500-8.

25. Jemal A, Siegel R, Ward E, et al. Cancer statistics, 2008. CA Cancer J Clin 2008;58:71-96.

26. Society CC. [cited; Available from: http://www.cancer.ca/Canada-wide/About%20cancer/Cancer%20statistics/Stats%20at%20a%20glance/Prostate%20cancer.aspx?sc_lang=en

27. Mazhar D, Waxman J. Early chemotherapy in prostate cancer. Nat Clin Pract Urol 2008;5:486-93.

28. Shen MM, Abate-Shen C. Molecular genetics of prostate cancer: new prospects for old challenges. Genes Dev;24:1967-2000.

29. Abate-Shen C, Shen MM. Molecular genetics of prostate cancer. Genes Dev 2000;14:2410-34.

30. Bostwick DG. Prostatic intraepithelial neoplasia (PIN). Urology 1989;34:16-22.

31. Bostwick DG. The pathology of early prostate cancer. CA Cancer J Clin 1989;39:376-93.

32. Andrieu C, Taieb D, Baylot V, et al. Heat shock protein 27 confers resistance to androgen ablation and chemotherapy in prostate cancer cells through eIF4E. Oncogene;29:1883-96.

33. Yu D, Scott C, Jia WW, et al. Targeting and killing of prostate cancer cells using lentiviral constructs containing a sequence recognized by translation factor eIF4E and a prostate-specific promoter. Cancer Gene Ther 2006;13:32-43.

34. Fusi A, Procopio G, Della Torre S, et al. Treatment options in hormone-refractory metastatic prostate carcinoma. Tumori 2004;90:535-46.

35. Petrylak DP. Future directions in the treatment of androgen-independent prostate cancer. Urology 2005;65:8-12.

36. Ford ME, Wahlquist AE, Ridgeway C, et al. Evaluating an intervention to increase cancer knowledge in racially diverse communities in South Carolina. Patient Educ Couns.

37. Giri VN, Ruth K, Hughes L, et al. Racial differences in prediction of time to prostate cancer diagnosis in a prospective screening cohort of high-risk men: effect of TMPRSS2 Met160Val. BJU Int.

38. Steinberg GD, Carter BS, Beaty TH, Childs B, Walsh PC. Family history and the risk of prostate cancer. Prostate 1990;17:337-47.

39. Spitz MR, Currier RD, Fueger JJ, Babaian RJ, Newell GR. Familial patterns of prostate cancer: a case-control analysis. J Urol 1991;146:1305-7.

40. Casey G, Neville PJ, Plummer SJ, et al. RNASEL Arg462Gln variant is implicated in up to 13% of prostate cancer cases. Nat Genet 2002;32:581-3.

41. Carpten J, Nupponen N, Isaacs S, et al. Germline mutations in the ribonuclease L gene in families showing linkage with HPC1. Nat Genet 2002;30:181-4.

42. Gallagher RP, Fleshner N. Prostate cancer: 3. Individual risk factors. CMAJ 1998;159:807-13.

43. Perner S, Demichelis F, Beroukhim R, et al. TMPRSS2:ERG fusion-associated deletions provide insight into the heterogeneity of prostate cancer. Cancer Res 2006;66:8337-41.

44. Demichelis F, Fall K, Perner S, et al. TMPRSS2:ERG gene fusion associated with lethal prostate cancer in a watchful waiting cohort. Oncogene 2007;26:4596-9.

45. Perner S, Rubin MA. A variant TMPRSS2 isoform and ERG fusion product in prostate cancer with implications for molecular diagnosis. Mod Pathol 2008;21:1056; author reply -7.

46. Sarker D, Reid AH, Yap TA, de Bono JS. Targeting the PI3K/AKT pathway for the treatment of prostate cancer. Clin Cancer Res 2009;15:4799-805.

47. Yoshimoto M, Cutz JC, Nuin PA, et al. Interphase FISH analysis of PTEN in histologic sections shows genomic deletions in 68% of primary prostate cancer and 23% of high-grade prostatic intra-epithelial neoplasias. Cancer Genet Cytogenet 2006;169:128-37.

48. Schlomm T, Iwers L, Kirstein P, et al. Clinical significance of p53 alterations in surgically treated prostate cancers. Mod Pathol 2008;21:1371-8.

49. Kolonel LN. Major new grant in cancer epidemiology. Hawaii Med J 2001;60:74.

50. Kolonel LN, Hankin JH, Whittemore AS, et al. Vegetables, fruits, legumes and prostate cancer: a multiethnic case-control study. Cancer Epidemiol Biomarkers Prev 2000;9:795-804.

51. Parker SL, Tong T, Bolden S, Wingo PA. Cancer statistics, 1997. CA Cancer J Clin 1997;47:5-27.

52. Kasperzyk JL, Fall K, Mucci LA, et al. One-carbon metabolism-related nutrients and prostate cancer survival. Am J Clin Nutr 2009;90:561-9.

53. Ledesma MC, Jung-Hynes B, Schmit TL, Kumar R, Mukhtar H, Ahmad N. Selenium and Vitamin E for Prostate Cancer: Post-SELECT Status. Mol Med.

54. Peters U, Leitzmann MF, Chatterjee N, et al. Serum lycopene, other carotenoids, and prostate cancer risk: a nested case-control study in the prostate, lung, colorectal, and ovarian cancer screening trial. Cancer Epidemiol Biomarkers Prev 2007;16:962-8.

55. Hsu A, Bruno RS, Lohr CV, et al. Dietary soy and tea mitigate chronic inflammation and prostate cancer via NFkappaB pathway in the Noble rat model. J Nutr Biochem.

56. Gardner CD, Chatterjee LM, Franke AA. Effects of isoflavone supplements vs. soy foods on blood concentrations of genistein and daidzein in adults. J Nutr Biochem 2009;20:227-34.

57. Gardner CD, Oelrich B, Liu JP, Feldman D, Franke AA, Brooks JD. Prostatic soy isoflavone concentrations exceed serum levels after dietary supplementation. Prostate 2009;69:719-26.

58. Wang LI, Giovannucci EL, Hunter D, Neuberg D, Su L, Christiani DC. Dietary intake of Cruciferous vegetables, Glutathione S-transferase (GST) polymorphisms and lung cancer risk in a Caucasian population. Cancer Causes Control 2004;15:977-85.

59. Chan JM, Oh WK, Xie W, et al. Plasma selenium, manganese superoxide dismutase, and intermediate- or high-risk prostate cancer. J Clin Oncol 2009;27:3577-83.

60. Lippman SM, Klein EA, Goodman PJ, et al. Effect of selenium and vitamin E on risk of prostate cancer and other cancers: the Selenium and Vitamin E Cancer Prevention Trial (SELECT). JAMA 2009;301:39-51.

61. Harris R, Lohr KN. Screening for prostate cancer: an update of the evidence for the U.S. Preventive Services Task Force. Ann Intern Med 2002;137:917-29.

62. Yousef GM, Diamandis EP. The new human tissue kallikrein gene family: structure, function, and association to disease. Endocr Rev 2001;22:184-204.

63. Miller JI, Ahmann FR, Drach GW, Emerson SS, Bottaccini MR. The clinical usefulness of serum prostate specific antigen after hormonal therapy of metastatic prostate cancer. J Urol 1992;147:956-61.

64. Tornblom M, Eriksson H, Franzen S, et al. Lead time associated with screening for prostate cancer. Int J Cancer 2004;108:122-9.

65. Draisma G, Boer R, Otto SJ, et al. Lead times and overdetection due to prostate-specific antigen screening: estimates from the European Randomized Study of Screening for Prostate Cancer. J Natl Cancer Inst 2003;95:868-78.

66. Gleason DF, Mellinger GT. Prediction of prognosis for prostatic adenocarcinoma by combined histological grading and clinical staging. J Urol 1974;111:58-64.

67. Bostwick DG. Staging prostate cancer--1997: current methods and limitations. Eur Urol 1997;32 Suppl 3:2-14.

68. Lamb DJ, Weigel NL, Marcelli M. Androgen receptors and their biology. Vitam Horm 2001;62:199-230.

69. Yeh S, Tsai MY, Xu Q, et al. Generation and characterization of androgen receptor knockout (ARKO) mice: an in vivo model for the study of androgen functions in selective tissues. Proc Natl Acad Sci U S A 2002;99:13498-503.

70. McPhaul MJ. Androgen receptor mutations and androgen insensitivity. Mol Cell Endocrinol 2002;198:61-7.

71. Feldman BJ, Feldman D. The development of androgen-independent prostate cancer. Nat Rev Cancer 2001;1:34-45.

72. Huggins C, Hodges CV. Studies on prostatic cancer. I. The effect of castration, of estrogen and of androgen injection on serum phosphatases in metastatic carcinoma of the prostate. 1941. J Urol 2002;167:948-51; discussion 52.

73. Huggins C, Hodges CV. Studies on prostatic cancer: I. The effect of castration, of estrogen and of androgen injection on serum phosphatases in metastatic carcinoma of the prostate. 1941. J Urol 2002;168:9-12.

74. Huggins C, Hodges CV. Studies on prostatic cancer. I. The effect of castration, of estrogen and androgen injection on serum phosphatases in metastatic carcinoma of the prostate. CA Cancer J Clin 1972;22:232-40.

75. Singh J, Trabulsi EJ, Gomella LG. Is there an optimal management for localized prostate cancer? Clin Interv Aging;5:187-97.

76. Davis JW, Kim J, Ward JF, et al. Radical prostatectomy findings in patients predicted to have low-volume/low-grade prostate cancer diagnosed by extended-core biopsies: an analysis of volume and zonal distribution of tumour foci. BJU Int;105:1386-91.

77. Trabulsi EJ, Valicenti RK, Hanlon AL, et al. A multi-institutional matched-control analysis of adjuvant and salvage postoperative radiation therapy for pT3-4N0 prostate cancer. Urology 2008;72:1298-302; discussion 302-4.

78. Thompson IM, Tangen CM, Paradelo J, et al. Adjuvant radiotherapy for pathological T3N0M0 prostate cancer significantly reduces risk of metastases and improves survival: long-term followup of a randomized clinical trial. J Urol 2009;181:956-62.

79. Roach M, 3rd. Dose escalated external beam radiotherapy versus neoadjuvant androgen deprivation therapy and conventional dose external beam radiotherapy for clinically localized prostate cancer: do we need both? Strahlenther Onkol 2007;183 Spec No 2:26-8.

80. Pilepich MV, Winter K, John MJ, et al. Phase III radiation therapy oncology group (RTOG) trial 86-10 of androgen deprivation adjuvant to definitive radiotherapy in locally advanced carcinoma of the prostate. Int J Radiat Oncol Biol Phys 2001;50:1243-52.

81. Perez CA, Hanks GE, Leibel SA, Zietman AL, Fuks Z, Lee WR. Localized carcinoma of the prostate (stages T1B, T1C, T2, and T3). Review of management with external beam radiation therapy. Cancer 1993;72:3156-73.

82. Gage AA. History of cryosurgery. Semin Surg Oncol 1998;14:99-109.

83. Bahn DK, Lee F, Badalament R, Kumar A, Greski J, Chernick M. Targeted cryoablation of the prostate: 7-year outcomes in the primary treatment of prostate cancer. Urology 2002;60:3-11.

84. Oefelein MG, Agarwal PK, Resnick MI. Survival of patients with hormone refractory prostate cancer in the prostate specific antigen era. J Urol 2004;171:1525-8.

85. Fleshner N. Defining high-risk prostate cancer: current status. Can J Urol 2005;12 Suppl 1:14-7; discussion 94-6.

86. Goldenberg SL, Gleave ME, Taylor D, Bruchovsky N. Clinical Experience with Intermittent Androgen Suppression in Prostate Cancer: Minimum of 3 Years' Follow-Up. Mol Urol 1999;3:287-92.

87. Gleave M, Goldenberg SL, Bruchovsky N, Rennie P. Intermittent androgen suppression for prostate cancer: rationale and clinical experience. Prostate Cancer Prostatic Dis 1998;1:289-96.

88. Slovin SF. Neuroendocrine differentiation in prostate cancer: a sheep in wolf's clothing? Nat Clin Pract Urol 2006;3:138-44.

89. Scher HI, Buchanan G, Gerald W, Butler LM, Tilley WD. Targeting the androgen receptor: improving outcomes for castration-resistant prostate cancer. Endocr Relat Cancer 2004;11:459-76.

90. Scher HI, Beer TM, Higano CS, et al. Antitumour activity of MDV3100 in castration-resistant prostate cancer: a phase 1-2 study. Lancet;375:1437-46.

91. Attard G, Richards J, de Bono JS. New strategies in metastatic prostate cancer: targeting the androgen receptor signaling pathway. Clin Cancer Res;17:1649-57.

92. O'Donnell A, Judson I, Dowsett M, et al. Hormonal impact of the 17alpha-hydroxylase/C(17,20)-lyase inhibitor abiraterone acetate (CB7630) in patients with prostate cancer. Br J Cancer 2004;90:2317-25.

93. Hieronymus H, Lamb J, Ross KN, et al. Gene expression signature-based chemical genomic prediction identifies a novel class of HSP90 pathway modulators. Cancer Cell 2006;10:321-30.

94. Welsbie DS, Xu J, Chen Y, et al. Histone deacetylases are required for androgen receptor function in hormone-sensitive and castrate-resistant prostate cancer. Cancer Res 2009;69:958-66.

95. Nagata Y, Lan KH, Zhou X, et al. PTEN activation contributes to tumor inhibition by trastuzumab, and loss of PTEN predicts trastuzumab resistance in patients. Cancer Cell 2004;6:117-27.

96. Ziada A, Barqawi A, Glode LM, et al. The use of trastuzumab in the treatment of hormone refractory prostate cancer; phase II trial. Prostate 2004;60:332-7.

97. Drake CG. Prostate cancer as a model for tumour immunotherapy. Nat Rev Immunol;10:580-93.

98. Small EJ, Schellhammer PF, Higano CS, et al. Placebo-controlled phase III trial of immunologic therapy with sipuleucel-T (APC8015) in patients with metastatic, asymptomatic hormone refractory prostate cancer. J Clin Oncol 2006;24:3089-94.

99. Kantoff PW, Higano CS, Shore ND, et al. Sipuleucel-T immunotherapy for castration-resistant prostate cancer. N Engl J Med;363:411-22.

100. Kantoff PW, Schuetz TJ, Blumenstein BA, et al. Overall survival analysis of a phase II randomized controlled trial of a Poxviral-based PSA-targeted immunotherapy in metastatic castration-resistant prostate cancer. J Clin Oncol;28:1099-105.

101. Kaufman HL, Wang W, Manola J, et al. Phase II randomized study of vaccine treatment of advanced prostate cancer (E7897): a trial of the Eastern Cooperative Oncology Group. J Clin Oncol 2004;22:2122-32.

102. Grover KE, Green KL, Pettit JW, Monteith LL, Garza MJ, Venta A. Problem solving moderates the effects of life event stress and chronic stress on suicidal behaviors in adolescence. J Clin Psychol 2009;65:1281-90.

103. Alajez NM, Mocanu JD, Shi W, et al. Efficacy of systemically administered mutant vesicular stomatitis virus (VSVDelta51) combined with radiation for nasopharyngeal carcinoma. Clin Cancer Res 2008;14:4891-7.

104. Ribacka C, Hemminki A. Virotherapy as an approach against cancer stem cells. Curr Gene Ther 2008;8:88-96.

105. Zhang W, Cai R, Luo J, et al. The oncolytic adenovirus targeting to TERT and RB pathway induced specific and potent anti-tumor efficacy in vitro and in vivo for hepatocellular carcinoma. Cancer Biol Ther 2007;6:1726-32.

106. Wojton J, Kaur B. Impact of tumor microenvironment on oncolytic viral therapy. Cytokine Growth Factor Rev;21:127-34.

107. Bischoff JR, Kirn DH, Williams A, et al. An adenovirus mutant that replicates selectively in p53-deficient human tumor cells. Science 1996;274:373-6.

108. Vogelstein B, Kinzler KW. Cancer genes and the pathways they control. Nat Med 2004;10:789-99.

109. Freytag SO, Khil M, Stricker H, et al. Phase I study of replication-competent adenovirus-mediated double suicide gene therapy for the treatment of locally recurrent prostate cancer. Cancer Res 2002;62:4968-76.

110. Freytag SO, Stricker H, Pegg J, et al. Phase I study of replication-competent adenovirus-mediated double-suicide gene therapy in combination with conventional-dose three-dimensional conformal radiation therapy for the treatment of newly diagnosed, intermediate- to high-risk prostate cancer. Cancer Res 2003;63:7497-506.

111. Garber K. China approves world's first oncolytic virus therapy for cancer treatment. J Natl Cancer Inst 2006;98:298-300.

112. Crompton AM, Kirn DH. From ONYX-015 to armed vaccinia viruses: the education and evolution of oncolytic virus development. Curr Cancer Drug Targets 2007;7:133-9.

113. Mineta T, Rabkin SD, Yazaki T, Hunter WD, Martuza RL. Attenuated multi-mutated herpes simplex virus-1 for the treatment of malignant gliomas. Nat Med 1995;1:938-43.

114. Chou J, Roizman B. The gamma 1(34.5) gene of herpes simplex virus 1 precludes neuroblastoma cells from triggering total shutoff of protein synthesis characteristic of programed cell death in neuronal cells. Proc Natl Acad Sci U S A 1992;89:3266-70.

115. Cinatl J, Jr., Michaelis M, Driever PH, et al. Multimutated herpes simplex virus g207 is a potent inhibitor of angiogenesis. Neoplasia 2004;6:725-35.

116. Aghi M, Visted T, Depinho RA, Chiocca EA. Oncolytic herpes virus with defective ICP6 specifically replicates in quiescent cells with homozygous genetic mutations in p16. Oncogene 2008;27:4249-54.

117. Sundaresan P, Hunter WD, Martuza RL, Rabkin SD. Attenuated, replication-competent herpes simplex virus type 1 mutant G207: safety evaluation in mice. J Virol 2000;74:3832-41.

118. Varghese S, Rabkin SD. Oncolytic herpes simplex virus vectors for cancer virotherapy. Cancer Gene Ther 2002;9:967-78.

119. Toda M, Martuza RL, Kojima H, Rabkin SD. In situ cancer vaccination: an IL-12 defective vector/replication-competent herpes simplex virus combination induces local and systemic antitumor activity. J Immunol 1998;160:4457-64.

120. Markert JM, Medlock MD, Rabkin SD, et al. Conditionally replicating herpes simplex virus mutant, G207 for the treatment of malignant glioma: results of a phase I trial. Gene Ther 2000;7:867-74.

121. Markert JM, Liechty PG, Wang W, et al. Phase Ib trial of mutant herpes simplex virus G207 inoculated pre-and post-tumor resection for recurrent GBM. Mol Ther 2009;17:199-207.

122. Stojdl DF, Lichty BD, tenOever BR, et al. VSV strains with defects in their ability to shutdown innate immunity are potent systemic anti-cancer agents. Cancer Cell 2003;4:263-75.

123. Wickham TJ. Ligand-directed targeting of genes to the site of disease. Nat Med 2003;9:135-9.

124. Menotti L, Cerretani A, Campadelli-Fiume G. A herpes simplex virus recombinant that exhibits a single-chain antibody to HER2/neu enters cells through the mammary tumor receptor, independently of the gD receptors. J Virol 2006;80:5531-9.

125. Zhang KX, Moussavi M, Kim C, et al. Lentiviruses with trastuzumab bound to their envelopes can target and kill prostate cancer cells. Cancer Gene Ther 2009;16:820-31.

126. Kuhnel F, Schulte B, Wirth T, et al. Protein transduction domains fused to virus receptors improve cellular virus uptake and enhance oncolysis by tumor-specific replicating vectors. J Virol 2004;78:13743-54.

127. Rodriguez R, Schuur ER, Lim HY, Henderson GA, Simons JW, Henderson DR. Prostate attenuated replication competent adenovirus (ARCA) CN706: a selective cytotoxic for prostate-specific antigen-positive prostate cancer cells. Cancer Res 1997;57:2559-63.

128. DeWeese TL, van der Poel H, Li S, et al. A phase I trial of CV706, a replication-competent, PSA selective oncolytic adenovirus, for the treatment of locally recurrent prostate cancer following radiation therapy. Cancer Res 2001;61:7464-72.

129. Fukuhara H, Homma Y, Todo T. Oncolytic virus therapy for prostate cancer. Int J Urol;17:20-30.

130. Small EJ, Carducci MA, Burke JM, et al. A phase I trial of intravenous CG7870, a replication-selective, prostate-specific antigen-targeted oncolytic adenovirus, for the treatment of hormone-refractory, metastatic prostate cancer. Mol Ther 2006;14:107-17.

131. Lee CY, Bu LX, DeBenedetti A, Williams BJ, Rennie PS, Jia WW. Transcriptional and translational dual-regulated oncolytic herpes simplex virus type 1 for targeting prostate tumors. Mol Ther;18:929-35.

132. Rychlik W, Domier LL, Gardner PR, Hellmann GM, Rhoads RE. Amino acid sequence of the mRNA cap-binding protein from human tissues. Proc Natl Acad Sci U S A 1987;84:945-9.

133. Gingras AC, Gygi SP, Raught B, et al. Regulation of 4E-BP1 phosphorylation: a novel two-step mechanism. Genes Dev 1999;13:1422-37.

134. Gingras AC, Raught B, Sonenberg N. Regulation of translation initiation by FRAP/mTOR. Genes Dev 2001;15:807-26.

135. Pestova TV, Kolupaeva VG, Lomakin IB, et al. Molecular mechanisms of translation initiation in eukaryotes. Proc Natl Acad Sci U S A 2001;98:7029-36.

136. Pause A, Belsham GJ, Gingras AC, et al. Insulin-dependent stimulation of protein synthesis by phosphorylation of a regulator of 5'-cap function. Nature 1994;371:762-7.

137. Poulin F, Gingras AC, Olsen H, Chevalier S, Sonenberg N. 4E-BP3, a new member of the eukaryotic initiation factor 4E-binding protein family. J Biol Chem 1998;273:14002-7.

138. Graff JR, Konicek BW, Lynch RL, et al. eIF4E activation is commonly elevated in advanced human prostate cancers and significantly related to reduced patient survival. Cancer Res 2009;69:3866-73.

139. Mamane Y, Petroulakis E, Rong L, Yoshida K, Ler LW, Sonenberg N. eIF4E--from translation to transformation. Oncogene 2004;23:3172-9.

140. Chu EC, Tarnawski AS. PTEN regulatory functions in tumor suppression and cell biology. Med Sci Monit 2004;10:RA235-41.

141. Inoki K, Zhu T, Guan KL. TSC2 mediates cellular energy response to control cell growth and survival. Cell 2003;115:577-90.

142. Proud CG. Role of mTOR signalling in the control of translation initiation and elongation by nutrients. Curr Top Microbiol Immunol 2004;279:215-44.

143. Hiremath LS, Webb NR, Rhoads RE. Immunological detection of the messenger RNA cap-binding protein. J Biol Chem 1985;260:7843-9.

144. De Benedetti A, Harris AL. eIF4E expression in tumors: its possible role in progression of malignancies. Int J Biochem Cell Biol 1999;31:59-72.

145. Kerekatte V, Smiley K, Hu B, Smith A, Gelder F, De Benedetti A. The proto-oncogene/translation factor eIF4E: a survey of its expression in breast carcinomas. Int J Cancer 1995;64:27-31.

146. Rosenwald IB, Chen JJ, Wang S, Savas L, London IM, Pullman J. Upregulation of protein synthesis initiation factor eIF-4E is an early event during colon carcinogenesis. Oncogene 1999;18:2507-17.

147. DeFatta RJ, Chervenak RP, De Benedetti A. A cancer gene therapy approach through translational control of a suicide gene. Cancer Gene Ther 2002;9:505-12.

148. DeFatta RJ, Li Y, De Benedetti A. Selective killing of cancer cells based on translational control of a suicide gene. Cancer Gene Ther 2002;9:573-8.

149. Thirukkumaran CM, Nodwell MJ, Hirasawa K, et al. Oncolytic viral therapy for prostate cancer: efficacy of reovirus as a biological therapeutic. Cancer Res 2010;70:2435-44.

150. Lu Y. Viral based gene therapy for prostate cancer. Curr Gene Ther 2001;1:183-200.

151. Freytag SO, Movsas B, Aref I, et al. Phase I trial of replication-competent adenovirus-mediated suicide gene therapy combined with IMRT for prostate cancer. Mol Ther 2007;15:1016-23.

152. Vidal L, Pandha HS, Yap TA, et al. A phase I study of intravenous oncolytic reovirus type 3 Dearing in patients with advanced cancer. Clin Cancer Res 2008;14:7127-37.

153. Rose JKaMAW. Rhabdoviridae: the virus and their replication Field's Virology Lippincott Williams & Wilkins, Philadelphia, 4th edition 2001;1:1221-44.

154. Cooper D, Wright KJ, Calderon PC, et al. Attenuation of recombinant vesicular stomatitis virus-human immunodeficiency virus type 1 vaccine vectors by gene translocations and g gene truncation reduces neurovirulence and enhances immunogenicity in mice. J Virol 2008;82:207-19.

155. Barber GN. VSV-tumor selective replication and protein translation. Oncogene 2005;24:7710-9.

156. Fields BN, Hawkins K. Human infection with the virus of vesicular stomatitis during an epizootic. N Engl J Med 1967;277:989-94.

157. Johnson KM, Vogel JE, Peralta PH. Clinical and serological response to laboratory-acquired human infection by Indiana type vesicular stomatitis virus (VSV). Am J Trop Med Hyg 1966;15:244-6.

158. Lim KI, Yin J. Computational fitness landscape for all gene-order permutations of an RNA virus. PLoS Comput Biol 2009;5:e1000283.

159. Rose NF, Marx PA, Luckay A, et al. An effective AIDS vaccine based on live attenuated vesicular stomatitis virus recombinants. Cell 2001;106:539-49.

160. Lichty BD, Power AT, Stojdl DF, Bell JC. Vesicular stomatitis virus: re-inventing the bullet. Trends Mol Med 2004;10:210-6.

161. Schlegel R, Tralka TS, Willingham MC, Pastan I. Inhibition of VSV binding and infectivity by phosphatidylserine: is phosphatidylserine a VSV-binding site? Cell 1983;32:639-46.

162. Coil DA, Miller AD. Phosphatidylserine is not the cell surface receptor for vesicular stomatitis virus. J Virol 2004;78:10920-6.

163. Roche S, Albertini AA, Lepault J, Bressanelli S, Gaudin Y. Structures of vesicular stomatitis virus glycoprotein: membrane fusion revisited. Cell Mol Life Sci 2008;65:1716-28.

164. Gaudin Y, Tuffereau C, Durrer P, Flamand A, Ruigrok RW. Biological function of the low-pH, fusion-inactive conformation of rabies virus glycoprotein (G): G is transported in a fusion-inactive state-like conformation. J Virol 1995;69:5528-34.

165. Roche S, Gaudin Y. Characterization of the equilibrium between the native and fusion-inactive conformation of rabies virus glycoprotein indicates that the fusion complex is made of several trimers. Virology 2002;297:128-35.

166. Ahmed M, McKenzie MO, Puckett S, Hojnacki M, Poliquin L, Lyles DS. Ability of the matrix protein of vesicular stomatitis virus to suppress beta interferon gene expression is genetically correlated with the inhibition of host RNA and protein synthesis. J Virol 2003;77:4646-57.

167. Ahmed M, Mitchell LM, Puckett S, Brzoza-Lewis KL, Lyles DS, Hiltbold EM. Vesicular stomatitis virus M protein mutant stimulates maturation of Toll-like receptor 7 (TLR7)-positive dendritic cells through TLR-dependent and -independent mechanisms. J Virol 2009;83:2962-75.

168. Randall RE, Goodbourn S. Interferons and viruses: an interplay between induction, signalling, antiviral responses and virus countermeasures. J Gen Virol 2008;89:1-47.

169. Seo YJ, Hahm B. Type I interferon modulates the battle of host immune system against viruses. Adv Appl Microbiol;73:83-101.

170. Stark GR, Kerr IM, Williams BR, Silverman RH, Schreiber RD. How cells respond to interferons. Annu Rev Biochem 1998;67:227-64.

171. Nagano K, Masters JR, Akpan A, et al. Differential protein synthesis and expression levels in normal and neoplastic human prostate cells and their regulation by type I and II interferons. Oncogene 2004;23:1693-703.

172. Shou J, Soriano R, Hayward SW, Cunha GR, Williams PM, Gao WQ. Expression profiling of a human cell line model of prostatic cancer reveals a direct involvement of interferon signaling in prostate tumor progression. Proc Natl Acad Sci U S A 2002;99:2830-5.

173. Balachandran S, Barber GN. Defective translational control facilitates vesicular stomatitis virus oncolysis. Cancer Cell 2004;5:51-65.

174. Honda K, Yanai H, Negishi H, et al. IRF-7 is the master regulator of type-I interferon-dependent immune responses. Nature 2005;434:772-7.

175. Tough DF. Type I interferon as a link between innate and adaptive immunity through dendritic cell stimulation. Leuk Lymphoma 2004;45:257-64.

176. Wu L, Huang TG, Meseck M, et al. rVSV(M Delta 51)-M3 is an effective and safe oncolytic virus for cancer therapy. Hum Gene Ther 2008;19:635-47.

177. pathway iI.

178. Kaplan-Lefko PJ, Chen TM, Ittmann MM, et al. Pathobiology of autochthonous prostate cancer in a pre-clinical transgenic mouse model. Prostate 2003;55:219-37.

179. Marker PC, Donjacour AA, Dahiya R, Cunha GR. Hormonal, cellular, and molecular control of prostatic development. Dev Biol 2003;253:165-74.

180. Garabedian EM, Humphrey PA, Gordon JI. A transgenic mouse model of metastatic prostate cancer originating from neuroendocrine cells. Proc Natl Acad Sci U S A 1998;95:15382-7.

181. Roy-Burman P, Wu H, Powell WC, Hagenkord J, Cohen MB. Genetically defined mouse models that mimic natural aspects of human prostate cancer development. Endocr Relat Cancer 2004;11:225-54.

182. Xue L, Yang K, Newmark H, Lipkin M. Induced hyperproliferation in epithelial cells of mouse prostate by a Western-style diet. Carcinogenesis 1997;18:995-9.

183. Dahia PL. PTEN, a unique tumor suppressor gene. Endocr Relat Cancer 2000;7:115-29.

184. Suzuki H, Freije D, Nusskern DR, et al. Interfocal heterogeneity of PTEN/MMAC1 gene alterations in multiple metastatic prostate cancer tissues. Cancer Res 1998;58:204-9.

185. Di Cristofano A, Pesce B, Cordon-Cardo C, Pandolfi PP. Pten is essential for embryonic development and tumour suppression. Nat Genet 1998;19:348-55.

186. Ahmad I, Sansom OJ, Leung HY. Advances in mouse models of prostate cancer. Expert Rev Mol Med 2008;10:e16.

187. Bhatia-Gaur R, Donjacour AA, Sciavolino PJ, et al. Roles for Nkx3.1 in prostate development and cancer. Genes Dev 1999;13:966-77.

188. Wu X, Wu J, Huang J, et al. Generation of a prostate epithelial cell-specific Cre transgenic mouse model for tissue-specific gene ablation. Mech Dev 2001;101:61-9.

189. Wang S, Gao J, Lei Q, et al. Prostate-specific deletion of the murine Pten tumor suppressor gene leads to metastatic prostate cancer. Cancer Cell 2003;4:209-21.

190. Mundy GR. Metastasis to bone: causes, consequences and therapeutic opportunities. Nat Rev Cancer 2002;2:584-93.

191. Greenberg NM, DeMayo F, Finegold MJ, et al. Prostate cancer in a transgenic mouse. Proc Natl Acad Sci U S A 1995;92:3439-43.

192. Gingrich JR, Barrios RJ, Kattan MW, Nahm HS, Finegold MJ, Greenberg NM. Androgen-independent prostate cancer progression in the TRAMP model. Cancer Res 1997;57:4687-91.

193. Winter SF, Cooper AB, Greenberg NM. Models of metastatic prostate cancer: a transgenic perspective. Prostate Cancer Prostatic Dis 2003;6:204-11.

194. Varghese S, Rabkin SD, Nielsen GP, MacGarvey U, Liu R, Martuza RL. Systemic therapy of spontaneous prostate cancer in transgenic mice with oncolytic herpes simplex viruses. Cancer Res 2007;67:9371-9.

195. Powell WC, Cardiff RD, Cohen MB, Miller GJ, Roy-Burman P. Mouse strains for prostate tumorigenesis based on genes altered in human prostate cancer. Curr Drug Targets 2003;4:263-79.

196. di Sant'Agnese PA. Neuroendocrine differentiation in human prostatic carcinoma. Hum Pathol 1992;23:287-96.

197. Yu D, Jia WW, Gleave ME, Nelson CC, Rennie PS. Prostate-tumor targeting of gene expression by lentiviral vectors containing elements of the probasin promoter. Prostate 2004;59:370-82.

198. Barton KN, Paielli D, Zhang Y, et al. Second-generation replication-competent oncolytic adenovirus armed with improved suicide genes and ADP gene demonstrates greater efficacy without increased toxicity. Mol Ther 2006;13:347-56.

199. Dilley J, Reddy S, Ko D, et al. Oncolytic adenovirus CG7870 in combination with radiation demonstrates synergistic enhancements of antitumor efficacy without loss of specificity. Cancer Gene Ther 2005;12:715-22.

200. Huang P, Watanabe M, Kaku H, et al. Direct and distant antitumor effects of a telomerase-selective oncolytic adenoviral agent, OBP-301, in a mouse prostate cancer model. Cancer Gene Ther 2008;15:315-22.

201. Drake CG. Immunotherapy for metastatic prostate cancer. Urol Oncol 2008;26:438-44.

202. Moinpour CM, Hayden KA, Unger JM, et al. Health-related quality of life results in pathologic stage C prostate cancer from a Southwest Oncology Group trial comparing radical prostatectomy alone with radical prostatectomy plus radiation therapy. J Clin Oncol 2008;26:112-20.

203. Moore CM, Pendse D, Emberton M. Photodynamic therapy for prostate cancer--a review of current status and future promise. Nat Clin Pract Urol 2009;6:18-30.

204. Klotz L. Active surveillance for prostate cancer: trials and tribulations. World J Urol 2008;26:437-42.

205. Balachandran S, Barber GN. Vesicular stomatitis virus (VSV) therapy of tumors. IUBMB Life 2000;50:135-8.

206. Balachandran S, Roberts PC, Brown LE, et al. Essential role for the dsRNA-dependent protein kinase PKR in innate immunity to viral infection. Immunity 2000;13:129-41.

207. Fraser MM, Bayazitov IT, Zakharenko SS, Baker SJ. Phosphatase and tensin homolog, deleted on chromosome 10 deficiency in brain causes defects in synaptic structure, transmission and plasticity, and myelination abnormalities. Neuroscience 2008;151:476-88.

208. Homma T, Fukushima T, Vaccarella S, et al. Correlation among pathology, genotype, and patient outcomes in glioblastoma. J Neuropathol Exp Neurol 2006;65:846-54.

209. Breitbach CJ, Paterson JM, Lemay CG, et al. Targeted inflammation during oncolytic virus therapy severely compromises tumor blood flow. Mol Ther 2007;15:1686-93.

210. Hadaschik BA, Zhang K, So AI, et al. Oncolytic vesicular stomatitis viruses are potent agents for intravesical treatment of high-risk bladder cancer. Cancer Res 2008;68:4506-10.

211. Moussavi M, Assi K, Gomez-Munoz A, Salh B. Curcumin mediates ceramide generation via the de novo pathway in colon cancer cells. Carcinogenesis 2006;27:1636-44.

212. Suzuki A, Yamaguchi MT, Ohteki T, et al. T cell-specific loss of Pten leads to defects in central and peripheral tolerance. Immunity 2001;14:523-34.

213. Oliere S, Arguello M, Mesplede T, et al. Vesicular stomatitis virus oncolysis of T lymphocytes requires cell cycle entry and translation initiation. J Virol 2008;82:5735-49.

214. Tumilasci VF, Oliere S, Nguyen TL, Shamy A, Bell J, Hiscott J. Targeting the apoptotic pathway with BCL-2 inhibitors sensitizes primary chronic lymphocytic leukemia cells to vesicular stomatitis virus-induced oncolysis. J Virol 2008;82:8487-99.

215. Margiotti K, Wafa LA, Cheng H, Novelli G, Nelson CC, Rennie PS. Androgen-regulated genes differentially modulated by the androgen receptor coactivator L-dopa decarboxylase in human prostate cancer cells. Mol Cancer 2007;6:38.

216. Hadaschik BA, Zhang K, So AI, et al. [Oncolytic vesicular stomatitis viruses as intravesical agents against non-muscle-invasive bladder cancer.]. Urologe A 2008;47:1145-51.

217. Ireland DD, Reiss CS. Gene expression contributing to recruitment of circulating cells in response to vesicular stomatitis virus infection of the CNS. Viral Immunol 2006;19:536-45.

218. Parato KA, Senger D, Forsyth PA, Bell JC. Recent progress in the battle between oncolytic viruses and tumours. Nat Rev Cancer 2005;5:965-76.

219. Kirn D, Martuza RL, Zwiebel J. Replication-selective virotherapy for cancer: Biological principles, risk management and future directions. Nat Med 2001;7:781-7.

220. Nelson WG, Simons JW, Mikhak B, et al. Cancer cells engineered to secrete granulocyte-macrophage colony-stimulating factor using ex vivo gene transfer as vaccines for the treatment of genitourinary malignancies. Cancer Chemother Pharmacol 2000;46 Suppl:S67-72.

221. Nguyen TL, Abdelbary H, Arguello M, et al. Chemical targeting of the innate antiviral response by histone deacetylase inhibitors renders refractory cancers sensitive to viral oncolysis. Proc Natl Acad Sci U S A 2008.

222. Stojdl DF, Lichty B, Knowles S, et al. Exploiting tumor-specific defects in the interferon pathway with a previously unknown oncolytic virus. Nat Med 2000;6:821-5.

223. Diaz RM, Galivo F, Kottke T, et al. Oncolytic immunovirotherapy for melanoma using vesicular stomatitis virus. Cancer Res 2007;67:2840-8.

224. Lun X, Senger DL, Alain T, et al. Effects of intravenously administered recombinant vesicular stomatitis virus (VSV(deltaM51)) on multifocal and invasive gliomas. J Natl Cancer Inst 2006;98:1546-57.

225. Ahmed M, Cramer SD, Lyles DS. Sensitivity of prostate tumors to wild type and M protein mutant vesicular stomatitis viruses. Virology 2004;330:34-49.

226. Maggini J, Raiden S, Salamone G, Trevani A, Geffner J. Regulation of neutrophil apoptosis by cytokines, pathogens and environmental stressors. Front Biosci 2009;14:2372-85.

227. Stevens JG, Cook ML. Restriction of herpes simplex virus by macrophages. An analysis of the cell-virus interaction. J Exp Med 1971;133:19-38.

228. Belardelli F, Vignaux F, Proietti E, Gresser I. Injection of mice with antibody to interferon renders peritoneal macrophages permissive for vesicular stomatitis virus and encephalomyocarditis virus. Proc Natl Acad Sci U S A 1984;81:602-6.

229. de Weerd NA, Samarajiwa SA, Hertzog PJ. Type I interferon receptors: biochemistry and biological functions. J Biol Chem 2007;282:20053-7.

230. Shelley MD, Kumar S, Wilt T, Staffurth J, Coles B, Mason MD. A systematic review and meta-analysis of randomised trials of neo-adjuvant hormone therapy for localised and locally advanced prostate carcinoma. Cancer Treat Rev 2009;35:9-17.

231. Chang G, Xu S, Watanabe M, Jayakar HR, Whitt MA, Gingrich JR. Enhanced oncolytic activity of vesicular stomatitis virus encoding SV5-F protein against prostate cancer. J Urol;183:1611-8.

232. Huang B, Sikorski R, Kirn DH, Thorne SH. Synergistic anti-tumor effects between oncolytic vaccinia virus and paclitaxel are mediated by the IFN response and HMGB1. Gene Ther.

233. Lun X, Chan J, Zhou H, et al. Efficacy and Safety/Toxicity Study of Recombinant Vaccinia Virus JX-594 in Two Immunocompetent Animal Models of Glioma. Mol Ther.

234. Touchefeu Y, Harrington KJ, Galmiche JP, Vassaux G. Review article: gene therapy, recent developments and future prospects in gastrointestinal oncology. Aliment Pharmacol Ther;32:953-68.

235. Gingrich JR, Barrios RJ, Morton RA, et al. Metastatic prostate cancer in a transgenic mouse. Cancer Res 1996;56:4096-102.

236. Greenberg NM, DeMayo FJ, Sheppard PC, et al. The rat probasin gene promoter directs hormonally and developmentally regulated expression of a heterologous gene specifically to the prostate in transgenic mice. Mol Endocrinol 1994;8:230-9.

237. Foster BA, Gingrich JR, Kwon ED, Madias C, Greenberg NM. Characterization of prostatic epithelial cell lines derived from transgenic adenocarcinoma of the mouse prostate (TRAMP) model. Cancer Res 1997;57:3325-30.

238. Ottolino-Perry K, Diallo JS, Lichty BD, Bell JC, McCart JA. Intelligent design: combination therapy with oncolytic viruses. Mol Ther;18:251-63.

239. Moussavi M, Fazli L, Tearle H, et al. Oncolysis of prostate cancers induced by vesicular stomatitis virus in PTEN knockout mice. Cancer Res 2010

70:1367-76.

240. Carey BL, Ahmed M, Puckett S, Lyles DS. Early steps of the virus replication cycle are inhibited in prostate cancer cells resistant to oncolytic vesicular stomatitis virus. J Virol 2008;82:12104-15.

241. Ozduman K, Wollmann G, Piepmeier JM, van den Pol AN. Systemic vesicular stomatitis virus selectively destroys multifocal glioma and metastatic carcinoma in brain. J Neurosci 2008;28:1882-93.

242. Ebert O, Harbaran S, Shinozaki K, Woo SL. Systemic therapy of experimental breast cancer metastases by mutant vesicular stomatitis virus in immune-competent mice. Cancer Gene Ther 2005;12:350-8.

243. Hu X, Jiao X, Narayanan S, et al. Resonantly enhanced off-specular X-ray scattering from polymer/polymer interfaces(small star, filled). Eur Phys J E Soft Matter 2005;17:353-9.

244. Thirukkumaran CM, Nodwell MJ, Hirasawa K, et al. Oncolytic viral therapy for prostate cancer: efficacy of reovirus as a biological therapeutic. Cancer Res;70:2435-44.

245. van der Velden AW, Thomas AA. The role of the 5' untranslated region of an mRNA in translation regulation during development. Int J Biochem Cell Biol 1999;31:87-106.

246. Manzella JM, Blackshear PJ. Regulation of rat ornithine decarboxylase mRNA translation by its 5'-untranslated region. J Biol Chem 1990;265:11817-22.

247. Grens A, Scheffler IE. The 5'- and 3'-untranslated regions of ornithine decarboxylase mRNA affect the translational efficiency. J Biol Chem 1990;265:11810-6.

248. Panwalkar A, Verstovsek S, Giles FJ. Mammalian target of rapamycin inhibition as therapy for hematologic malignancies. Cancer 2004;100:657-66.

249. Vishnu P, Tan WW. Update on options for treatment of metastatic castration-resistant prostate cancer. Onco Targets Ther;3:39-51.

250. Cozzi PJ, Burke PB, Bhargav A, et al. Oncolytic viral gene therapy for prostate cancer using two attenuated, replication-competent, genetically engineered herpes simplex viruses. Prostate 2002;53:95-100.

251. Shatkin AJ. mRNA cap binding proteins: essential factors for initiating translation. Cell 1985;40:223-4.

252. Gingras AC, Raught B, Sonenberg N. eIF4 initiation factors: effectors of mRNA recruitment to ribosomes and regulators of translation. Annu Rev Biochem 1999;68:913-63.

253. Zimmer SG, DeBenedetti A, Graff JR. Translational control of malignancy: the mRNA cap-binding protein, eIF-4E, as a central regulator of tumor formation, growth, invasion and metastasis. Anticancer Res 2000;20:1343-51.

254. Puli S, Jain A, Lai JC, Bhushan A. Effect of combination treatment of rapamycin and isoflavones on mTOR pathway in human glioblastoma (U87) cells. Neurochem Res;35:986-93.

255. Ghayad SE, Cohen PA. Inhibitors of the PI3K/Akt/mTOR pathway: new hope for breast cancer patients. Recent Pat Anticancer Drug Discov;5:29-57.

256. Bianchini A, Loiarro M, Bielli P, et al. Phosphorylation of eIF4E by MNKs supports protein synthesis, cell cycle progression and proliferation in prostate cancer cells. Carcinogenesis 2008;29:2279-88.

257. Tasseff R, Nayak S, Salim S, Kaushik P, Rizvi N, Varner JD. Analysis of the molecular networks in androgen dependent and independent prostate cancer revealed fragile and robust subsystems. PLoS One;5:e8864.

258. Balakumaran BS, Porrello A, Hsu DS, et al. MYC activity mitigates response to rapamycin in prostate cancer through eukaryotic initiation factor 4E-binding protein 1-mediated inhibition of autophagy. Cancer Res 2009;69:7803-10.

259. Shinozaki K, Ebert O, Woo SL. Treatment of multi-focal colorectal carcinoma metastatic to the liver of immune-competent and syngeneic rats by hepatic artery infusion of oncolytic vesicular stomatitis virus. Int J Cancer 2005;114:659-64.

260. Ciavarra RP, Taylor L, Greene AR, et al. Impact of macrophage and dendritic cell subset elimination on antiviral immunity, viral clearance and production of type 1 interferon. Virology 2005;342:177-89.

261. Coffey MC, Strong JE, Forsyth PA, Lee PW. Reovirus therapy of tumors with activated Ras pathway. Science 1998;282:1332-4.